Frameworks for Effective Blind Source Separation of Ground Borne Signals and Their Applications

Ph.D Thesis submitted to

COCHIN UNIVERSITY OF SCIENCE AND TECHNOLOGY

in partial fulfilment of the requirements

for the award of the degree of

DOCTOR OF PHILOSOPHY

under the Faculty of Technology by

KRISHNAKUMAR M.

(Reg.No. 3958)

Under the guidance of

Dr K. V. PRAMOD

Department of Computer Applications
Cochin University of Science and Technology
Kochi - 682 022, Kerala, India

FEBRUARY 2018

Frameworks for Effective Blind Source Separation of Ground Borne Signals and Their Applications

Ph.D. thesis

Author:
Krishnakumar M.
Department of Computer Applications
Cochin University of Science and Technology
Kochi - 682 022, Kerala, India
Email: krishnanow@gmail.com

Supervising Guide:
Dr K. V. Pramod
Associate Professor
Department of Computer Applications
Cochin University of Science and Technology
Kochi - 682 022.
Email: pramodkv@gmail.com

Cochin University of Science and Technology
Kochi - 682 022, Kerala, India.
February 2018

Dr K.V. Pramod
Associate Professor
Department of Computer Applications
Cochin University of Science and Technology
Kochi - 682 022

12th February 2018

Certificate

Certified that the work presented in this thesis entitled "*Frameworks for Effective Blind Source Separation of Ground Borne Signals and Their Applications*" is based on the authentic record of research carried out by Mr Krishnakumar M under my guidance in the Department of Computer Applications, Cochin University of Science and Technology, Kochi- 682 022 and has not been included in any other thesis submitted for the award of any degree.

Dr K.V. Pramod

Phone : +91 484 2576253

Declaration

I hereby declare that the work presented in this thesis entitled "*Frameworks for Effective Blind Source Separation of Ground Borne Signals and Their Applications*" is based on the original research work carried out by me under the supervision and guidance of Dr K.V. Pramod, Associate Professor, Department of Computer Applications, Cochin University of Science and Technology, Kochi - 682 022 and has not been included in any other thesis submitted previously for the award of any degree.

Kochi– 682 022 Krishnakumar M.
12^{th} February 2018

Dr K.V. Pramod
Associate Professor
Department of Computer Applications
Cochin University of Science and Technology
Kochi - 682 022, Kerala, India

12th February , 2018

Certificate

Certified that the work presented in this thesis entitled "Frameworks for Effective Blind Source Separation of Ground Borne Signals and Their Applications" submitted to **Cochin University of Science and Technology by Mr Krishnakumar M. for the award of the degree of Doctor of Philosophy under the Faculty of Technology**, contains all the relevant corrections and modifications suggested by the audience during the pre-synopsis seminar and recommended by the Doctoral Committee.

Dr K. V. Pramod

Phone : +91 484 2576253

Abstract

Ground Borne Vibration (GBV) signals are produced by various vibration sources and are propagated through ground. The ground vibrations usually propagate through the soil or rocks as waves. The source separation of GBV signals refers to the task of estimating the signals produced by the individual vibration sources and are propagated through the ground. Blind Source Separation (BSS) is a technique, which recovers both the unknown sources and unknown mixing matrix systems from the measured mixtures of signals, the only known quantities.

In many situations, difficulty in getting the exact measurements of the distance between vibration sources and the sensors and little knowledge on mixing systems makes the method of BSS as the best option for the source separation problem of GBV signals. In the case of BSS no information is needed on the source positions or the mixing systems.

The general algorithms for BSS fail to give good results due to the complexity of the captured signals and due to the heterogeneity of vibration propagation medium. This limitation necessitates new frameworks or modifications of existing methods for effective source separation of the targeted signals.

The main objective of the research was to study the BSS of signals and to develop new frameworks for effective BSS of GBV signals, which contribute to a major portion of ground borne signals.

This research work also aimed to study the major challenges in source separation of the target signals, propose applications based on the new frameworks and validate the proposed frameworks. The application of BSS of GBV is manifold. For example, the idea can be employed in developing a technology to trace lives buried in the cadaver following a landslide or earthquakes.

The GBV were modeled based on a semi-analytical approach and the selected BSS algorithms were extended to use for GBV based on this model. The extension of algorithms WASOBI, SYMWHITE and FastICA were presented in the thesis. The thesis included analytical proofs of extension of BSS for the problem. This is a straightforward approach and considers the problem of damping which is very crucial in GBV.

We developed new frameworks based on modified BSS algorithms. The various modified BSS algorithms, which forms the heart of the new frameworks; WASOBI-DECONV, SYMWHITE-DECONV and FastICA-DECONV were presented in the thesis. The performances were evaluated and superiority of our frameworks was established with benchmarked and the real world ground borne vibration signals.

Acknowledgements

I am grateful to my supervisor Dr K.V. Pramod for the helpful inputs and patient explications during this research work. I thank him for his passion towards this topic and his constant willingness to offer advice and encouragement throughout my research.

I express my gratitude to Dr B. Kannan, Head, Department of Computer Applications, Cochin University of Science and Technology for his help, advices and support, as well as for the confidence he placed on me.

Thanks should definitely go to distinguished experts, Dr P. Venkat Rangan, Dr K. B. M. Namboodirippad, Dr P.S. Chandramohan, Dr Balakrishnan Shankar, Dr M.R. Kaimal, Dr Sebastian George, Dr J Suresh Kumar, Er P. N. Biju, Er Binu P. Ulahannan, Dr Binu Sankar and Sri Jithesh V for their help, advice and encouragement during my PhD research.

I sincerely thank Dr M. Jathavedan, Dr A. Sreekumar , Dr Sabu M.K., Dr Judy M.V. and Ms Malathi S. of the Department of Computer Applications for supporting this work with valuable suggestions. I also wish to extend my special thanks to Sri Vijith T. K., Sri Vinu V. S., Sri Jino P. J. and all my fellow researchers and the non-teaching staff of the department.

I would like to acknowledge the considerable patience of my family that made this work possible. Thanks especially to my parents for their help and encouragement. Thanks to my wife Ms Geethu R.S. for her patience, moral support and confidence in my work. I would like to express my gratitude to my daughter Vyshnavi Krishna K. and son Vishnu Madhavan K. for their support and patience.

I would like to express my gratitude to all the people who walked with me during this adventure. All of you are contributors of this work and part of these few years of my life.

Beyond all, I bow before Almighty, who gave the wisdom and strength to make this a reality.

Krishnakumar M.

trust in the sound of universe..

Contents

List of Figures

List of Tables

Chapter 1

Introduction

1.1 Motivation and Scope of the work

Blind Source Separation (BSS) techniques were initially investigated in the early 80's for signal processing in the context of neural network modeling. During the last three decades, numerous studies were accomplished on this topic on various application fields[1][2][3][4]. The separation of a set of signals from a set of observed signal mixtures, without the information about the source signals or the mixing process is known as Blind Source Separation (BSS)[5][6][7]. The blind source separation of Ground Borne Vibration (GBV) signals refers to the task of blindly estimating the signals produced by the individual vibration sources and are propagated through the ground. The captured signals are complex mixtures of the individual sources. These signals have intrinsic reverberation, delayed mixing etc. Ground vibrations usually propagate through the soil or rock as waves. The parameters like frequency, amplitude, phase etc are affected during the propagation of vibration signals through the ground. The non-homogeneity of the vibration propagation medium makes the estimation extremely difficult[8][9]. In many cases it is not easy to measure the dis-

tance of the exact vibration sources and the mixing system is hidden due to the non-homogeneity of earth crust or propagation medium. This make the method of BSS as the best candidate for source separation problem of GBV signals where exact source-sensor distance remain unknown. In the case of BSS no information is needed on the source positions or the mixing systems.

The source separation problem of speech signals is well studied and was a blistering topic of research during the last decade. But only a few work appeared on the source separation of ground vibrations. To solve the source separation problems, a large selection of techniques are available in the scientific literature, each of them possessing its own features, advantages and limitations. Most of the methods concern the problem of air borne acoustic signals. The ground borne vibrations are subjected to adverse conditions such as high reverberation, ill-conditioning and occurrence of permutations. These general frame works are not robust for source separation of GBV. This demand for new frameworks and modifications of existing methods for effective source separation of the studied signals. This research work aims to study the major challenges in source separation of ground borne vibrations signals, propose and validate frameworks for blind source separation of vibration signals. The application of blind source separation of ground borne vibrations are manifold. For example the idea can be employed in developing a technology to trace lives buried in the cadaver following a landslide or earthquakes. The source localisation and identification, calibration methods and ground coupling efficiency are not included in the scope of our study

1.2 Objective of the thesis

The research work described in the thesis focused on the Blind Source Separation (BSS) of Ground Borne Signals(GBS), mainly on BSS of Ground

Borne Vibration (GBV) signals. BSS is a technique which recovers both the unknown sources and unknown mixing matrix systems from the only known quantities, measured mixtures of signals.As mentioned earlier the source separation of GBV signals refers to the task of estimating the signals produced by the individual vibration sources and are propagated through the ground.

Although the problem of BSS has been studied for three decades and is well explored [10], there are still areas require more research attention.

The objectives of the research are as follows:

The main aim of the research was to study the blind source separation of signals and propose new frameworks for the effective blind source separation of ground borne vibration signals

The aim can be further structured as:

- Identify the major challenging issues in blind source separation of ground borne vibration signals
- Study and identify suitable models for the propagation of ground borne vibration signals
- Develop new frameworks for the effective blind source separation of ground borne vibration signals

- Develop a system and procedure for field data collection for the evaluation of proposed algorithm

- Apply the developed frameworks for the blind source separation of ground borne vibration signals

The main challenges here are the separation in a highly reverberant environment, heterogeneous channel and the presence of background noise[11].

The BSS of GBV has considerable practical applications. One among them is to utilize the framework in developing a technology to track human lives buried in the debris following a landslide or collapse of building [12].

1.3 Contributions

We studied and identified appropriate models for propagation of ground borne vibration. These models were validated and justified. Algorithms based on higher order statistics were studied. Various new frameworks for the effective BSS of GBV were presented, evaluated and compared. The superiority of the proposed methods was established based on the real world data.

We considered semi-analytical approach for wave propagation and seismic convolution model for wave propagation through ground as the basis for developing frameworks.

1.3.1 New Frameworks based on Extended BSS algorithms

The GBV were modeled based on a semi-analytical model and the selected BSS algorithms were extended to use for GBV. The thesis justifies how

BSS model fits into the ground borne vibration separation problem. The results of source separation using extended BSS algorithms as the core are included in the *chapter 5*. We considered compression waves only for this study as the source sensor distance was small. This is a simple and straight forward approach.

1.3.2 New Frameworks based on Modified BSS algorithms

We developed new frameworks based on 'Convolution Model' and modified BSS algorithm. The "convolution model" proposed by Enders Robinson et al. and approximates the earth by a linear system. The convolution model seems to be much more realistic for representing seismic vibration. The various modified BSS algorithms,WASOBI-DECONV, SYMWHITE-DECONV and FastICA-DECONV which forms the heart of the new frameworks are discussed below. The SYMWHITE-WASOBI, a hybrid algorithm, developed for GBV is also included in the thesis. We considered mainly surface waves for these frameworks.

WASOBI-DECONV

In this framework, the signal is preprocessed to obtain a noiseless, (at least theoretically) signal. The signal is subjected to de reverberation (de convolution) to an optimal level using spectral subtraction, a computationally efficient method [13] without affecting the direct signals. The signals are then source separated using famous WASOBI algorithm, which uses a second order statistics[14]

SYMWHITE-DECONV

This algorithm is an effective steps to achieve spatio-temporal de-correlation In the proposed framework the signal is subjected to noise reduction and

de-reverberation (de convolution) to an optimal level using spectral subtraction, a computationally efficient method [13] [15] without affecting the direct signals. The signals are then processed using SYMWHITE algorithm[16].

FastICA-DECONV

The signal is subjected to noise reduction and de-reverberation. These processed signals are source separated using a computationally efficient method, FastICA[17].

SYMWHITE-WASOBI

In this algorithm SYMWHITE-WASOBI algorithm is derived by combining two algorithms: SYMWHITE algorithm [16] and WASOBI algorithm[14]. This combination makes the BSS of signals considered in a more effective way in many cases.

1.4 Thesis overview

The thesis focused on the Blind Source Separation (BSS) of Ground Borne Vibration (GBV) signals. Thesis include an overview of the various methods of source separation, instantaneous mixing model, principles of BSS, acoustic BSS models, extension of BSS in noisy environment, a BSS framework for reverberant environment and performance measures. A system and method for field data collection for the evaluation of proposed algorithms are elucidated in the thesis.

The thesis besides contains an overview of the various models of vibration sources, models of vibration propagation, extended models and the application of BSS in GBV. The new methods and authors improvements of algorithms for more effective source separation of ground borne

vibration; WASOBI-DECONV, SYMWHITE-WASOBI and SYMWHITE-DECONV and FastICA-DECONV are presented in the thesis. Validation and performance analysis of proposed algorithms, evaluations of the proposed methods and discussions are also included.

For the purpose of comparison, three benchmarked signals [18] were considered. New frameworks and extended algorithms were compared for benchmarked signals. The performances were evaluated and compared using the real world ground borne vibration signals. The applicability of proposed methodology for practical cases is discussed. When evaluating the performances of the algorithms our focus were mainly on the quality of separation and discussion on computation efficiency was mostly superficial.

1.5 Structure and chapter wise contribution of the thesis

Chapter 1. Introduction

This chapter gives an overview of the entire research work. Provides the research background, problem identification, motivation, objectives of the thesis, research contributions, thesis overview and summary of publications related to the research work

Chapter 2. Review of Blind Source Separation and Its Applications

Provides the review of the related works and narrates a brief review of some important publications which are related to our work. Comprehensive reviews of different topics which are relevant to our study are included in the review. The review includes earlier works and advancement in the

area of Principal Component Analysis(PCA), Factor Analysis(FA), Projection Pursuit(PP), Independent Component Analysis(ICA), Single-Channel Deconvolution(SCD), Single-Channel Blind Deconvolution, Multichannel Blind Deconvolution, Ground Borne Vibration(GBV) and Vibration Application problems of Blind Source Separation.

Chapter 3. Blind Source Separation Models and Ground Borne Vibrations

Provides an overview of the various methods of source separation, Instantaneous mixing model, Principles of Blind Source Separation (BSS), Acoustic BSS models, Convolute Mixing model, Extension of BSS in noisy environment. An overview BSS framework for reverberant environment, various models of vibration sources, models of vibration propagation, various relevant BSS algorithms and performance measures are also included.

Chapter 4. Blind Source Separation of Ground Borne Vibration: The New Frameworks

Presents extended models and new frameworks for more effective BSS of GBV. The chapter discusses the following new algorithms such as WASOBI-DECONV, SYMWHITE-DECONV, SYMWHITE-WASOBI and FastICA-DECONV

Chapter 5. Blind Source Separation with the New Frameworks

This chapter discusses, methods of evaluation, performance evaluation and the results, analysis of BSS performed using new frameworks in the case of benchmarked signals as well as real world signals. The theory and standard procedures which forms the base of data collection the seismic

refraction methods is explained and experimental setup and procedures for field data collection are narrated towards in the chapter.

Chapter 6. Comparative Analysis and Discussion

This chapter presents comparison of various new frameworks.

Chapter 7. Applications of the New Frameworks

This chapter discusses proposed targeted application of the research; detection of lives buried in debris using the new methods. The chapter also discusses an application development, source separation of heartbeat sounds using these frameworks. The fault detection of machine and other application are also briefed.

Chapter 8. Conclusion and Future Direction

This chapter concludes the thesis with a narration on contributions made in this research and brief discussion on the possible future extension of the work.

1.6 List of publications related to the thesis

Journal Publications

- Krishna Kumar M., Geethu R. S., Pramod K. V., Extension of Blind Source Separation Model for Near Field Ground Borne Vibrations, Hydel Journal, ISSN 0970-4582 Volume 63, pp 23-28, 2017.

- Krishna Kumar M., Geethu R. S., Pramod K. V., New Method for Source Separation of Ground Borne Vibration Signals, Hydel Journal, ISSN 0970-4582 Volume 62, pp 48-54, 2016.

- Krishna Kumar M, Geethu R S, Sudhish N. George, Pramod K.V, Source Separation of Heartbeat Sounds for Effective e-Auscultation, Journal of IE(I): Series B, IEI-Springer Journal Series, PISSN 2250-2106, VOL 97(1), PP 69-75, 2016- *SCOPUS indexed*

- Krishna Kumar M., Geethu R. S., Pramod K. V., Performance of Source Separation Algorithm on Ground Borne Low Level Vibration Signals, Hydel Journal, ISSN 0970-4582 Volume 60, pp 48-54, June 2014.

- Krishna Kumar M, Pramod K.V, Geethu R S, A scheme to improve the effectiveness of Auscultation, International Journal of Science, Technology and Management, ISSN 0974-8334, Vol 07 No.01, pp 35-41, March 2014.

- Krishna Kumar M., Pramod K. V., Geethu R. S., A Low Cost Scheme for Tracking the Lives Buried in Landslides, International Journal of Computer Applications Special Issue on Computational Science - New Dimensions and Perspectives (2), pp. 44-49, 2011.

- Krishna Kumar M., Pramod K. V., Geethu R.S., Source Separation of Heartbeat Sounds, MES Journal of Technology and Management, ISSN 0976-3724, Vol 1, No 02 PP-65-71,2011

Conference Proceedings

- Geethu R S, Krishna Kumar M, Sudhish N George, A Proposal for source separation of low level vibration signals and its FPGA Implementation, IEEE International Conference on VLSI Systems, Architecture, Technology and Applications (VLSI-SATA 2015) ,8-10 Jan 2015, IEEE, *SCOPUS indexed*

- Krishna Kumar M., Geethu R S, Pramod K V, A Scheme for Source Separation of Ground Borne Vibrations , 2014 IEEE International Conference on Communication and Network Technologies, Sivakasi, Tamilnadu, India ,December 18-19, 2014, IEEE, *SCOPUS indexed*

- Krishna Kumar M., Geethu R S, Pramod K V, Source Separation of Ground Borne Low Level Vibration Signals Using Statistical Methods, International Conference on Advances in Computing, Communication and Information Science (ACCIS-14), *Elsevier Publications* 2014, pp (389-403) ISBN: 9789351072478

- Geethu R.S., Sudhish N. George, M. Krishna Kumar, A Proposal for Source Separation of Heartbeat Sounds and Its FPGA Implementation, CSNT2012, pp.755-758, 2012 IEEE International Conference on Communication Systems and Network Technologies, 2012. Published by IEEE Computer Society. IEEE, *SCOPUS indexed*

- Krishna Kumar M., Pramod K. V., Geethu R.S., A Life Tracking System based on Audio Source Separation. Proceedings of the IETE Zonal seminar on Networking Paradigms and Cyber Security, Coimbatore 2010.

Chapter 2

Review of Blind Source Separation and Its Applications

2.1 Introduction

The topic of research in this thesis rooted in the area of blind source separation and the ground borne vibration. Only a few papers appeared on this application area- blind source separation of ground borne vibration. We discuss various pioneer works appeared in the related fields like blind source separation, ground borne vibrations etc. in the proceeding sessions. Blind Source Separation (BSS) is a signal processing technique initially emerged in the early 80s [19]. The aspiration of any BSS technique is to reveal the underlying structure of a set of observed phenomena. Recovering unobservable signals from measured data is a generic problem in many domains. During the last three decades, it attracted many researchers from various fields. It finds application in separation of artifacts in MEG data,

finding hidden factors in financial data, reducing noise in natural images, telecommunications and audio signal processing

BSS was first appeared in the article [19]. This was during 1980's. The theory was further developed in the 1990s where researchers came with proposals to solve the (over)determined problem using natural gradient methods, maximum likelihood estimation , higher order statistics , information maximization, mutual information , and non-stationarity. For under determined problems the use of sparse sources were exploited and another approach was proposed, that is, the mixing matrix was estimated using a clustering algorithm. Estimating the sources and mixing matrix using Expectation-Maximization (EM) was also appeared. A brief description of the related works in the closely related areas is given below.

2.2 Principle Component Analysis

Principal Component Analysis (PCA) is one of the conventional techniques in multivariate statistical data analysis and data processing. The concept of PCA was introduced in the article [20] and further development can be seen in the works [21] [22]. Many papers were published in the area of PCA since 1960, with application in many disciplines such as Agriculture, Biology, Chemistry, Climatology, Demography, Ecology, Economics, Food research, Geology, Meteorology, Psychology and Quality control etc. [23] [24]

2.3 Factor Analysis

Factor analysis is a generative model method that has the same mathematical expression as the model of ICA. However, Factor Analysis (FA) has a different goal in the analysis, as described in [25], [26], [27], [28]. Various

techniques are available such as the Varimax, Quartimax and Oblimin algorithms in [29]. Other approaches, such as Bayesian factor analysis are available in [30].

2.4 Projection Pursuit

Projection Pursuit (PP) is also called exploratory projection pursuit data analysis. It aims to find useful structure by projecting the data onto a 2-D plane, spanned by two orthogonal axes. Useful structure is defined as departure from normality and includes such things as clusters, linear structures, holes, outliers etc. Thus the objective is to find a projection plane that provides a 2-D view of data such that the structure is maximized over all possible 2-D projections. Details of PP can be found in the following papers: [31], [32], [33], [34]. The Central Limit Theorem (CLT) which is the basis states that linear combination of independent data leads to normal or Gaussian distribution. This result in lower dimensional projection, which is closer to a Gaussian distribution and the few projections that are far away from Gaussian distribution will have the most meaningful structures. Note that PP is not a generative model.

2.5 Blind Source Separation

The objective of any Blind Source Separation(BSS) technique is to reveal the underlying structure of a set of observed phenomena[5]. Blind source separation techniques are based on statistical concepts. Various work in the field of BSS and related field are reviewed in the proceeding session. The work described in [35] investigates the application of blind source separation methods to extract independent components from signals recorded at the output of detectors used in spectrometry. The classification of these algorithms according to their performance index of separability showed that

the symmetric pre-whitening algorithm is the most efficient one to achieve the separation task. Blind source separation of convolutive mixtures is used as a preprocessing stage in many applications as in[36] . In enclosed spaces, due to reverberation, audio signal mixtures are considered to be convolutive ones. Time domain algorithms (as neural network based blind source separation) are not suitable for signal recovery from convolutive mixtures, thus the need of frequency domain or sub-band processing arise. The article propose a sub-band approach: the mixtures are split to several sub-bands, and time-domain blind source separation is carried out in each sub-band. The paper [37] presents a technique that exploits the intensity vector statistics to achieve a nearly closed-form solution for the separation of the convolutive mixtures as recorded with a coincident microphone array. Here no assumptions were made on the signals, but it was assumed that the source directions are known a priori. Numerical evaluation results were presented for various speech and instrument sounds and source positions. The performance of blind source separation algorithms is commonly measured by the output interference-to-signal ratio (ISR) [38]. This paper proposes an asymptotic bound on the attainable ISR for the case of Gaussian parametric auto-regressive (AR), moving-average (MA), or auto-regressive moving-average (ARMA) processes. [39] Proposes an algorithm FCOMBI computationally efficient method with to combined the strengths of non-Gaussianity based Blind Source Separation (BSS) and cross correlations-based BSS. This is done by fusing the separation abilities of two well-known BSS algorithms: EFICA and WASOBI.

The [40] paper presents a general broadband approach to blind source separation (BSS) for convolutive mixtures based on second-order statistics. This avoids several known limitations of the conventional narrow-band approximation, such as the internal permutation problem. In contrast to traditional narrow-band approaches, the new framework simultaneously exploits the non-whiteness property and non-stationarity property

of the source signals. The paper [41], discuss BSS algorithms for static models (instantaneous mixtures), extension of BSS and ICA incorporating with sparseness or non-negativity constraint sand BSS algorithms for dynamic models (convolutive mixtures). This article [42] considers the problem of simultaneous blind signal extraction of arbitrary group sources from a rather large number of observations. The work described in [43] addresses a method of blind source separation that jointly exploits the non-stationarity and temporal structure of sources. The method needs only multiple time-delayed correlation matrices of the observation data, each of which is evaluated at different time-windowed data frame, to estimate the de-mixing matrix. [44] Discuss set of experiments designed to evaluate and compare the performances of three well known blind source separation algorithms . The specific algorithms studied are two group of neural networks algorithms, Bell and Sejnowskis infomax algorithm and Hyvarinens fixed-point family, and J. F. Cardosos joint approximate diagonalization of Eigen-matrices algorithm. In this paper, the algorithms are quantitatively evaluated and compared using the three measures, MAT LAB flops (floating point operations), the difference between the mixing and separating matrices and the signal-to-noise ratios of the separated signals. In [45] the application of the symmetric prewhitening algorithm for the separation of overlapping pulses is presented. Most of the widely used performance indexes or methods for BSS are mentioned and discussed in [46]. This paper gives many examples to show limitations or drawbacks of some performance indexes or methods.

2.6 The Independent Component Analysis

The Independent Component Analysis (ICA) deals with the same model as in factor analysis which was explained in the previous section. ICA has originated from BSS problems such as in telecommunication and brain

imaging. In FA the components in s are assumed to be uncorrelated Gaussian factors but in ICA they are assumed to be non-Gaussian independent components. ICA aims at extracting interesting features or structures of data. The Gaussian distribution corresponds to the mixture of an infinite number of sources. Hence Gaussian distribution property for any real world source or data component is a kind of approximation. From this viewpoint, the assumption of non-Gaussian sources in ICA is more appropriate, and the non-Gaussian property can be taken for granted as true for most real world sources. According to [10] ICA could be considered as non-Gaussian factor analysis. Algorithms such as JADE, FastICA, Infomax, etc belong to the class of ICA algorithms. They are based on the different properties of independent sources. One of them is the maximally non-Gaussian property which leads to the family of algorithms that finds ICs in the direction of maximum non-Gaussianity, such as FastICA. Another property of independent sources based on the definition of independence which states that independence means decorrelation at every order of statistics. This leads to the family of algorithms that do higher order decorrelation. The JADE algorithm proposed in [47] does decorrelation of fourth order cumulants. The Bussgang-type algorithms that do nonlinear decorrelation also belong to this family. An ICA algorithm based on the ubiquitous maximum likelihood method begins its derivation directly from the fundamental property of independent sources which states that the joint probability of independent variables equals the product of the probabilities of each variable[48] [49]. By assuming proper probability distribution functions or the derivative function of their logarithm in the algorithm can be derived [50]. It was first derived using Infomax principle. Pre-whitening and adopting natural gradient adaptation is proposed in[51] for fast convergence of algorithms such as the Infomax algorithm . The concept of applying the natural gradient is proposed in [52] . The concept of relative gradient proposed in[53] was also the same concept. The Kullback-Leibler Divergence (KLD) or

Relative Entropy is another important approach to derive ICA/BSS algorithms. Other algorithms utilizing different properties of the ICA model or sources are also available such as Geometric ICA which explores the geometric transformation of data space [54] and the SOBI, RSOBI, SONS algorithms which explore the continuous wave form structure of independent sources in the form of second order de-correlations [55] [56].

Note that there is another slightly different topic called Blind Signal Extraction (BSE),which refers to a process extracting signals of interest one by one. There are several algorithms, among which FastICA is one. Along with aiming to find more robust and efficient algorithms for the basic ICA model, researches on more challenging problems of ICA are being conducted. These include the case of reducing noise (noisy ICA) such as described in [10] and [52], over complete base ICA, when there are more sources s_i than observations x_j [10]. More works in the domain worth considering are described below.

The article [57] proposes a method of mapping real signals into a complex vector space that takes into account the temporal order of signals and enforces certain mixing stationarity constraints. This Pairwise Complex Independent Component Analysis (PWC-ICA), performs the ICA in a complex setting and then reinterprets the results in the original observation space. Performance evaluation of several existing ICA algorithms for the blind source separation (BSS) problem on both real and simulated EEG data are presented. The paper [58] attempts to cover the fundamental concepts involved in ICA techniques and review its applications. A thorough discussion of the applications and ambiguities problems of ICA has been carried out. The article [59]discusses various models and applications of ICA and [60] discuss the application of ICA on short-time Fourier transforms of EEG/MEG signals, in order to find more 'interesting'sources than with time-domain ICA, and to more meaningfully sort the obtained components. The method is especially useful for finding sources of rhythmic

activity. It also discusses other biological applications of ICA. The paper[61] presents a spatio-temporal extension of the well-known FastICA algorithm of Hyvárinen and Oja that is applicable to both convolutive blind source separation and multichannel blind deconvolution tasks. This time-domain algorithm combines multichannel spatio-temporal pre-whitening via multi-stage least-squares linear prediction with a fixed-point iteration involving a new adaptive technique for imposing paraunitary constraints on the multichannel separation filter. The technique also allows for efficient reconstruction of individual signals as observed in the sensor measurements for single-input, multiple-output (SIMO) BSS tasks. Analysis and simulations verify the utility of the proposed methods. Study of the applicability of ICA in EEG is presented in [62], The study proves that ICA is a powerful tool when the biomedical analysis. The analysis of biological signals and The applications of Independent Component Analysis (ICA) to biomedical signals and medical diagnosis is discussed in [63].

The work [64] review complexities of classical ICA algorithms and present an ICA algorithm based on accelerated kernel entropy estimation. It achieves both high separation performance and low computational complexity. The work [65] present the basic theory and applications of ICA and various alos various models of ICA.

2.7 Single-Channel Deconvolution

Single-channel deconvolution is also called the supervised adaptive filtering theory. Filtering theory is helpful in dealing problems in communication channel [66]. A typical example in the case of a mechanical problem, a dynamic force applied to a mechanical structure at one location and vibration acceleration being measured at another location on the structure. Adaptive filtering is an estimation method for recovering the original message in the form of deconvolution. For the deconvolution equation to work properly,

the key issue is to find an appropriate inverse filter. In the supervised filtering process, there is a section of the training message available to help to find the process. In the case of the batch approach, the well-known Wiener filter can be employed. In the case of the on-line adaptive approach, the least mean square error principle is adapted as a least squares principle and a stochastic gradient adaptation algorithm is used. For fast implementation, the recursive least squares (RLS) algorithm is developed, which is later shown to be a special case of Kalman filtering algorithms described in state space concepts. Other filter structures are also available such as frequency domain filters, order-recursive adaptive filters and infinite impulse response filters.

2.8 Blind Deconvolution

If no training signal $s(k)$ is available, the problem model becomes Single Channel Blind Deconvolution, which seeks to find both the inverse system impulse response and the source $s(k)$ by means of only the observed system output. Blind deconvolution algorithms can be classified into Second Order Statistics (SOS) algorithms [66] and Higher Order Statistics (HOS) approach. The explicit HOS approach uses higher order cumulants or their corresponding polyspectra to achieve blind deconvolution [67] [68]. However this method is computationally very complex. The implicit HOS methods are usually called the Bussgang-type algorithms because they exploit the Bussgang property. This method adapts a nonlinear function to produce the desired signal resembling that used in the LMS algorithm, in supervised filtering. Different Bussgang-type algorithms are the Godard algorithm [69], the Constant Modulus Algorithm (CMA) [70] and the Sato algorithm [71].

Practical SBD problems arise in multi-point data networks, wireless communication, reflection seismology etc. Mechanical examples can be

such as the gear meshing force or shaft transmission torque in a single stage gearbox that cannot be measured directly, yet vibration signals of the gearbox can be measured. Limited mechanical applications only explored for SBD techniques [72].

Multichannel Blind Deconvolution (MBD) deals with the general problem of mixing multiple sources both temporally and spatially. The simplest MBD model is the case of two input sources and two output mixtures. The MBD model is much more complicated to solve than the two simple models. The most real world problems, such as in audio application e.g. the cocktail party problem [30], and in radio communication problems, mechanical vibration problems and many others are very complicated. This topic is still under intensive research for finding efficient and robust solutions.

2.9 BSS and Vibration Application Problems

The first mechanical application of BSS methods can be seen in[73], where they applied frequency domain BSS method to signals of a rotating machine. The instantaneous mixing model algorithms, such as JADE, to be applied in the frequency domain for each frequency bin. The BSS method described in [74] is carried out by means of two iterative procedures: The first procedure is to estimate the coefficients of the filters. The independence criterion is used and the unknown filters are obtained by a back propagation procedure by means of simplifying the coefficients of filters. The second procedure is to estimate the source vibration signals. The coupled vibration signals are obtained by means of the filters obtained from the former procedure and the estimation sources are obtained through decoupled procedure. Simulation and experiment results show that the method can be used to separate convolutive mixtures with non-stationary mechanical vibrations. The article [75] discusses low level vibrations and its control. The paper also describes models of vibration sources. The paper [76]

presents a new approach for machine vibration analysis and health monitoring, combining blind source separation (BSS) and change detection in source signals. The assessment of the approach on a real machine is presented in this paper. In the paper [77] a comparison study is presented. Some widely used BSS and BE algorithms have been compared to evaluate their performance in the separation of mechanical vibrations. Both simulated signals and real vibrations generated by industrial machines were used to verify the effectiveness of BSS and BE. Their deficiencies have also been identified and improvements are proposed in the paper. Various application of algorithms are discussed. The paper [78] proposes application of BSS to more realistic goals, and in particular to separate vibration signal into contributions of (1) periodic, (2) random stationary, and (3) random non-stationary sources.The paper claims that the separation can provide substantial information in many practical cases of interest. The work proposed two robust separation techniques for convolute mixtures based on the short-time Fourier transform. Many papers appeared on mechanical applications but are beyond the scope of our work. The paper 'Blind separation of vibration components: principles and demonstrations' [78] is a good paper in describing characteristics of mechanical vibration signals.

2.10 Vibration Propagation through Ground

The simplest soil model is the linear isotropic homogeneous half space described as a continuous elastic solid medium. The governing partial differential equations of this ground model has been laid down in the beginning of the 19-th century. Some specific effects of wave propagation in the homogeneous half space has been discovered by Rayleigh, Lamb and Love [79] [80] . All three types of waves (P-, S-,and R-waves) are non-dispersive. This means that their wave speeds are each independent of the excitation frequencies. As P and S-waves spread with hemispherical wavefronts in the

ground, their decay rate is inversely proportional to the distance from the source. R-waves on the surface spread on a circular wavefront and with a decay rate inversely proportional to the square root of distance from the source. This reduction in amplitude with distance is called geometric decay. Material damping will also influence the rate at which energy decays with distance from the source, and to estimate this material decay it is necessary to use a model for damping. The paper [81] describes elastic moduli and body waves, P- and S-wave velocities, waveforms and polarization.

The work described in [82] is designed to offer realistic approaches to solve ground vibration problems by anticipation, identification, analysis, design and test. The discussion includes wave propagation of the soil, vibration of foundations, isolation of seismic masses, design trade-offs, and vibration survey field measurements by recent techniques. Additional subjects such as vibration generated by machinery and human factor engineering are discussed. In order to predict the field vibrations caused by new railway lines in the project stage, which will be useful to design appropriate counter measures, in the work a ground-borne vibration model for rail systems at-grade developed by the authors described in [83] is validated with experimental measurements in an existing commuter railway line. It checked that this model is a very useful tool to predict the vibration field that will be caused by a railway infrastructure in the planning stage of the project. The basic features of wave propagation in the half-space with soil medium are discussed in [84]. A review is presented of the various methods used in investigating the soil vibrations, including the analytical methods, field measurements, empirical prediction models, and numerical methods of simulation. Particular emphasis is placed on the vibrations induced by trains moving on the ground or through underground tunnels. The article also summarized are the methods of isolation for ground-borne vibrations and the evaluation criteria adopted by different countries. This article [85] shows that ICA is a suitable technique to separate a volcanic

source component from ocean microseisms background noise in a seismic dataset recorded at the Mt. Merapi volcano, Indonesia. The encouraging results obtained with this methodology in the presented case study support their wider applicability in seismology. The paper [86] introduces a new model that captures the spike added to the geophones and models the effect of geophone burial. The geophones is modeled as a rigid, movable cylinder embedded in a half-space near or at the surface. The coupling problem is then tackled by a scattering approach using the elastic form of reciprocity. The potential application of the work in [87] is the detection and imaging of buried objects using acoustic methodology. This paper [88] aims to evaluate and compare avalanche safety equipment for downhill and off-piste skiers on the basis of published rescue data. A new classification for avalanche rescue devices is proposed. Safety devices for rescue operation of buried lives are classified and presented in the paper based on different mechanisms of action.

2.11 Spectral Subtraction

Spectral subtraction is a method for restoration of the power or the magnitude spectrum of a signal observed in additive noise, through subtraction of an estimate of the average noise spectrum from the noisy signal spectrum. This idea can be used in dereverberation of convolute signals. Dereverberation using spectral subtraction removes reverberant energy by canceling the energy of preceding phonemes in the current frame. This energy is only an estimation, and does not offer a perfect reconstruction, but does indeed remove the effect of reverberation. The paper[89] discuss a blind dereverberation method based on generalized spectral subtraction (GSS), which has been shown to be effective for noise reduction, instead of power SS. The extension of missing feature theory (MFT), to dereverberation also proposed. A one-stage dereverberation and denoising method based on GSS

is presented to simultaneously suppress both the additive noise and non-stationary multiplicative noise (reverberation). The work in [90] proposed a robust distant-talking speech recognition method based on spectral subtraction (SS) employing the multi-channel least mean square (MCLMS) algorithm. The article also investigates the robustness of the power SS-based dereverberation under various reverberant conditions for large vocabulary continuous speech recognition (LVCSR) and also describes the outline of blind dereverberation based on spectral subtraction. [91] Gives an introduction to spectral subtraction and its relation to Wiener filters. The main attraction of spectral subtraction is its relative simplicity, in that it only requires an estimate of the noise power spectrum. Proposal for improving computation efficiency of Discrete Fourier Transform (DFT) can be seen in [92].

2.12 Summary

This chapter presented snapshots of the origin and growth in related field of our research work. We discussed various associated works in the area of BSS and ground borne vibrations. Literature in the area of PCA, FA,PP, ICA, deconvolution,vibration applications of BSS and vibration propagations were reviewed thoroughly. Pioneer works which are relevant to our area and recent developments in the field were briefed in the chapter

Chapter 3

Blind Source Separation Models and Ground Borne Vibrations

3.1 Introduction

Blind Source Separation techniques are based on statistical concepts. BSS aim at revealing the independent components hidden within a set of measured signal mixtures [5].

The aspiration of any BSS technique is to reveal the underlying structure of a set of observed random variables, measurements or signals. Recovering non discernible signals from measured data has numerous applications many domains. In other words, the blind source separation (BSS) aims to recover the multiple source signals from multiple mixtures which are acquired by an array of sensors. The general goal of BSS is to recover a set of unobserved signals or sources from a set of observed mixtures. The observations can be obtained at the output of a set of sensors, where

each sensor receives a different combination of the source signals. The term blind stresses the facts that the source signals are not observed and no information is available about the mixing system. In other words the term 'blind'means that the source signals are extracted from the rough data without the knowledge of nature of those initial components. These methods are said to be versatile in the sense that the data can originate from various domains, and that no apriori knowledge is required about the physical phenomenon of interest[5].

The lack of prior knowledge about the source signals and the mixing system obligated to have some assumptions on unknown sources. The common assumptions are that the sources are statistically independent, the sources are statistically orthogonal; the sources are non stationary or can be generated by finite dimensional model space[6]. The BSS problem is modeled in the figure (3.1)

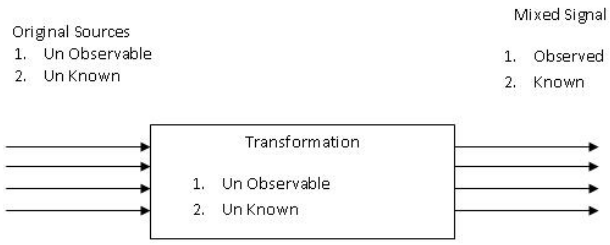

Figure 3.1: The Blind Source Separation problem

The concepts of Blind Source Separation(BSS), Independent Component Analysis(ICA), FastICA, Weight Adjusted Second Order Blind Identification (WASOBI) and SYMWHITE algorithm are discussed in the proceeding sessions. The concepts ground borne vibration and, its propagation are also discussed. The effect of sensor imperfections and performance measures are included in the chapter

3.2 The Principles of Blind Source Separation

Blind source separation (BSS) is an approach for estimating source signals $s_i(n)$ using only the information of mixed signals $x_j(n)$ observed at each input channel[93]. Typical examples of such source signals include mixtures of simultaneous speech signals that have been picked up by several microphones, brain waves recorded by multiple sensors, interfering radio signals arriving at a mobile station and vibration signals picked up by multiple sensors.

A simple two channel BSS system is shown in the figure (3.2). The source signals are denoted by s_i, which are unknown quantity and are unobservable. The measured signals, which are weighted mixtures of the source signals represented by x_j. These mixtures are observable quantity but are corrupted version of the original source signals. The separated signals y_i are obtained as a result of the blind source separation. The mixing system is denoted by A and un-mixing system by W [93]

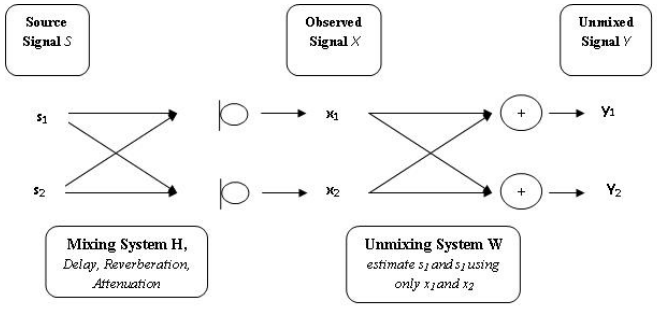

Figure 3.2: The BSS system configuration [93]

In the real-world situations we can assume that if different signals originate from different physical processes, they are unrelated. This is physically justifiable. Mathematically, the property of *un-relatedness* can be coined in terms of statistical independence. Two random variables x_1 and x_2 are

said to be independent if the value of any one of them cannot be inferred from the value of the other one.

The key strategy for separating the signal mixtures is based on the fact that:

if different physical sources lead to statistically-independent signals then the signals extracted from the mixtures that verify the statistical independence property should be issued from different physical processes [65] [5].

This assumption, which sets the foundation of all BSS methods, is not mathematically demonstrated but works in practice. By way of clarification, BSS techniques aim at separating signal mixtures into statistically independent signals, and each of them is a desired interpretable signal because it is generated by a different physical process.

3.3 Blind Source Separation Model

Consider a situation where there are multiple number of signals from physical sources and several sensors which are located at different positions capable to capture the signals. Therefore, each sensor acquires a slightly different mixture of the original source signals. The goal of blind source separation is to recover the original source signals from the acquired signals. The term 'blind'stresses the fact that the source signals and the mixing system are not known. The fundamental assumption necessary for applying many BSS methods is that the original source signals are mutually statistically independent[65] [94]. In reality this assumption holds for a variety of signals, such as multiple speakers. Therefore, the problem of BSS refers to finding a demixing system whose outputs are statistically independent. The following sessions describe the different mixing models which are encountered in various applications.

Consider a simple arrangement as given in the figure (3.3). For simplicity we considered the number of sensors equal to the number of mixtures.

The problem as it is depicted in figure (3.3) is similar to cocktail party problem [95]. The cocktail party effect is the phenomenon of being able to focus one's hearing attention on a particular stimulus while filtering out a range of other stimuli, much the same way that a number of people are talking simultaneously in a room and one is trying to follow one of the discussions.

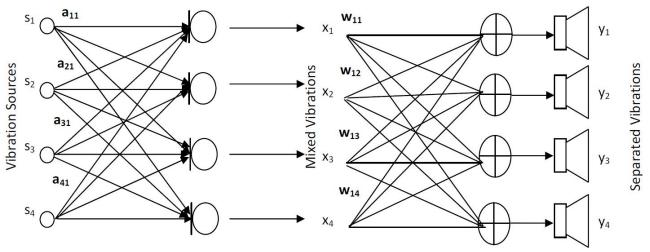

Figure 3.3: Schematic of BSS

Therefore the source separation can be stated into (3.1) to (3.4) ; given the source signals s_1, s_2, s_3 and s_4, the captured signals x_1, x_2, x_3 and x_4 at sensor $P1$ to $P4$ as [94]:

$$x_1 = a_{11}s_1 + a_{12}s_2 + a_{13}s_3 + a_{14}s_4 \tag{3.1}$$

$$x_2 = a_{21}s_1 + a_{22}s_2 + a_{23}s_3 + a_{24}s_4 \tag{3.2}$$

$$x_3 = a_{31}s_1 + a_{32}s_2 + a_{33}s_3 + a_{34}s_4 \tag{3.3}$$

$$x_4 = a_{41}s_1 + a_{42}s_2 + a_{43}s_3 + a_{44}s_4 \tag{3.4}$$

a_{11} to a_{44} are constant coefficients that give the mixing weights and are assumed to be unknown, since the properties of the physical mixing system are not known. The source signals s_1, s_2, s_3 and s_4 are also unknown. The original source signals are required to be found from the mixtures x_1 to x_4.

This is the blind source separation problem. The equations (3.1) to (3.4) can be written as:

$$X = A \cdot S \tag{3.5}$$

Assumed that the coefficients a_{ij} are different enough to make the matrix that they form invertible. Thus, there exists a matrix W with coefficients w_{ij}, such that we can separate s_i as

$$Y = W \cdot X \tag{3.6}$$

where y is as close to s as possible. W is the inverse of A [4] [11].

3.4 Instantaneous Mixing Model

At the discrete time index t, a mixture of N source signals
$s(t) = s_1(t), ..., s_N(t)$ are received at an array of M sensors. The received signals are denoted $x(t) = x_1(t), ..., x_M(t)$. The simplest BSS model is an instantaneous mixing model where no delayed versions of the source signals appear can be expressed as [4][6][94]

$$x_m(t) = \sum_{n=1}^{N} a_{mn} s_n(t), \text{ where } m = 1, 2, .., M \tag{3.7}$$

The captured signal is a linear mixture of filtered versions of each of the source signals and a_{mn} corresponding mixing filter coefficients or scalar weight. Consider an additive noise, $V_m(t)$. Then the Equation (3.7) can be expressed as

$$x_m(t) = \sum_{n=1}^{N} a_{mn} s_n(t) + V_m(t), \text{ where } m = 1, 2, .., M \tag{3.8}$$

In this instantaneous BSS case we are interested in finding a corresponding demixing system with the weights w_{pk}, which recover estimates $y_p(t)$, where $p = 1, ..., P$ of the original sources $s_n(t)$ from

$$y_p(t) = \sum_{k=1}^{N} w_{pk} x_k(t) \tag{3.9}$$

There are several applications where the instantaneous mixing model can be employed. For example to identify underlying components of brain activity from recordings of brain or in econometrics where BSS is used to find hidden factors from parallel financial time series and in image processing. The source separation of heartbeat sounds, described as an application based on the instantaneous model[96] [97]. In the case of BSS for GBV the instantaneous mixing model is not appropriate as delayed versions of the source signals were considered. Therefore, we will extend this model to suit for our application in the next chapter

3.5 Convolute Mixing Model

In the convolute mixing model with multiple source-multiple sensor frameworks the observation at each sensor contains the convoluted and mixed signals from different sources. At the discrete time index t, a mixture of N source signals $s(t) = (s_1(t), ...s_N(t))$ are received at an array of M sensors. The received signals are denoted $x(t) = (x_1(t), ..., x_M(t))$, The basic model of convolute mixtures can be given as follows [4].

$$x_m(t) = \sum_{n=1}^{N} \sum_{k=0}^{K-1} a_{mnk} s_n(t-k) + V_m(t) \tag{3.10}$$

where $V_m(t)$ is the additive noise.
The captured signal is a linear mixture of filtered versions of each of the

source signals and a_{mnk} corresponding mixing filter coefficients and in practical case $k < \infty$.
In matrix form [4] the equation can be expressed as:

$$x(t) = \sum_{k=0}^{K-1} A_k s(t-k) + V(t) \tag{3.11}$$

A_k is an MXN matrix which contains k^{th} filter coefficient and $V(t)$ is the $MX1$ noise vector. The de-convoluted and de-noised model, theoretically can be considered as the instantaneous model which is given as;

$$x(t) = As(t) \tag{3.12}$$

The coefficients a_{ij} of matrix A are assumed different enough to make the matrix that they form invertible. Thus, there exists a matrix W with coefficients w_{ij}, such that we can separate $s(t)$ as

$$y(t) = Wx(t) \tag{3.13}$$

where $y(t)$ is as close to $s(t)$ as possible[4] [11].
Similar to instantaneous BSS, we are interested in finding a corresponding de-mixing system whose output signals $y_p(t)$ are described by

$$y_p(t) = \sum_{m=1}^{M} \sum_{l=0}^{L-1} w_{pml} x_m(t-l) \tag{3.14}$$

where $p = 1, 2, .., P$
in the matrix form [4] the equation can be expressed as:

$$y(t) = \sum_{l=0}^{L-1} w_l x(t-l) \tag{3.15}$$

The BSS techniques are not restricted to time variables. Any random

distribution can be considered as a generalisation

The assumptions over the system and the sources are minimum. This makes the methodology very attractive, The objective function, the so-called *contrast function*, representing the independence of the identified sources and, on the algorithm used to optimize this function are the fundamental differences seen in different BSS algorithms.

The principle of non-Gaussianity forms the basis of many BSS algorithms. The statistical concepts such as kurtosis and neg-entropy (or any approximate of them) can estimate the non-Gaussianity. The gradient methods or fixed point algorithms can be used to maximize the latter. Maximum likelihood estimation, a fundamental method of statistical estimation, is a popular approach for estimating the BSS model. Maximization techniques such as the Bell-Sejnowski or the natural gradient algorithms can be used for the minimization of mutual information which is a measure of dependence. BSS models may also be obtained by making zero the higher-order cumulants. Cumulant tensors used in this case can be considered as generalizations of the covariance matrix and then leads to higher-order de-correlation of the signals. The Second-Order Blind Identification (SOBI), the BSS problem may be simplified by taking into account the time structure of the data[55]. SOBI is based on a joint diagonalization of time-lagged covariance matrices. Methods for noisy data or convolute mixtures have also been developed in the scientific literature. Detailed discussions of the various approaches were included in the preceding chapter. This work focuses on the extension and modification of the various algorithms like FastICA, Weight Adjusted Second Order Blind identification and Symmetrical Whitening for the targeted signals.

3.6 The FastICA Algorithm

The FastICA algorithm is a computationally efficient method for performing the estimation of ICA [98]. It uses a fixed-point iteration scheme. In some cases it is 100 times faster than conventional gradient descent methods for ICA. The data input to the FastICA is assumed to be preprocessed by centering and whitening as discussed below. The following sections describes the FastICA algorithm, different normalization approaches of algorithm and its properties[17].

3.6.1 Data Pre-processing for ICA

In the previous sections, the statistical principles underlying ICA methods were discussed. Before applying ICA algorithm on the data, it is worthy to do some preprocessing. The preprocessing techniques make the problem of ICA estimation simpler and better conditioned.

3.6.2 Centering

The most basic preprocessing step is to center$x$, i.e. subtract its mean vector $m = E\{x\}$ so as to make x a zero-mean variable. This is an essential step for FastICA. This preprocessing is made solely to simplify the ICA algorithms. After estimating the mixing matrix A with centered data, we can complete the estimation by adding the mean vector of s back to the centered estimates of s. The mean vector of s is given by $A^{-1}m$, where m is the mean that was subtracted in the preprocessing.

3.6.3 Whitening

Another useful preprocessing strategy in ICA is to first whiten the observed variables. This means that after centering, we transform the observed vector x linearly so that we obtain a new vector $\tilde{x}$ which is white, i.e. its

components are uncorrelated and their variances equal unity. In other words, the covariance matrix of $\tilde{x}$ equals the identity matrix:

$$E\{\tilde{x}\tilde{x}^T\} = I \tag{3.16}$$

This process reduces the number of parameters to be estimated. Instead of having to estimate the n^2 parameters that are the elements of the original matrix A, we only need to estimate the new, orthogonal mixing matrix $\tilde{A}$. An orthogonal matrix contains $n(n-1)/2$ degrees of freedom. For example, in two dimensions, an orthogonal transformation is determined by a single angle parameter. In larger dimensions, an orthogonal matrix contains only about half of the number of parameters of an arbitrary matrix. Thus one can say that whitening solves half of the problem of ICA. Because whitening is a very simple and standard procedure, much simpler than any ICA algorithms, it is a good idea to reduce the complexity of the problem this way.

3.6.4 Further Pre-processing

The success of ICA for a given data set may depend crucially on performing some application-dependent pre-processing steps. For example, if the data consists of time-signals, band-pass filtering may be very useful. Note that if we filter linearly the observed signals $x_i(t)$ to obtain new signals, say $\hat{x}_i(t)$,the ICA model still holds for $\hat{x}_i(t)$,with the same mixing matrix.

3.6.5 Uncertainties of ICA

In the ICA model the following ambiguities will hold:

- *We cannot determine the variances (energies) of the independent components.*

- *We cannot determine the order of the independent components.*

3.6.6 FastICA for One Computational Unit

One computational unit, here means an artificial neuron, having a weight vector w and the neuron is able to update by a learning rule. The FastICA learning rule finds a direction, i.e. a unit vector w such that the projection $w^T x$ maximizes non-gaussianity. Non-gaussianity can be measured by kurtosis or the approximation of neg-entropy. The FastICA is based on a fixed-point iteration scheme for finding a maximum of the nongaussianity of $w^T x$, The standard basic form of FastICA is as follows:

Step 1. Choose an initial (e.g. random) weight vector w

Step 2. Let $w^+ = E\{xg(w^T x)\} - E\{g^{'}(w^T x)\}w$

Step 3. Let $w = w^+/||w^+||$

Step 4. If not converged, go back to Step 2.

When the old and new values of w point in the same direction, we call it as convergence. It is not necessary that the vector converges to a single point, since w and $-w$ define the same direction. This is because the independent components can be defined only up to a multiplicative sign [17]. Here it is assumed that the data is pre whitened. There are four different nonlinearities used for the fixed point algorithm: *pow3, tanh, gauss and skew.*

Nonlinearity

pow3 $g(u) = u^3$

tanh $g(u) = tanh(a_1 * u)$

gauss $g(u) = u * exp(-a_2 * u^2/2)$

skew $g(u) = u^2$

3.6.7 FastICA for Several Independent Components

The one-unit algorithm of the preceding subsection estimates just one of the independent components, or one projection pursuit direction. To estimate several independent components, we need to run the one-unit FastICA algorithm using several units (e.g. neurons) with weight vectors $w_1, ..., w_n$. ie. to estimate n independent components, run these algorithm n times and to ensure that each time a different independent component is estimated, add a simple orthogonalising projection inside the loop. To prevent different vectors from converging to the same maxima we must de-correlate the outputs $w_1^T x, ..., w_n^T x$ after every iteration. There are three methods for achieving this. A simple way of achieving decorrelation is a deflation scheme based on a Gram-Schmidt like de-correlation. This means that the independent components are estimated one by one. When we have estimated k independent components, or k vectors $w_1, .., w_{(k)}$ we run the one-unit fixed-point algorithm for $w_{(k+1)}$, and after every iteration step subtract from $w_{(k+1)}$ the projections $w_{(k+1)}^T w_j w_j, j = 1, k$ of the previously estimated k vectors, and then re normalize $w_{(k+1)}$:

$$Let\ w_{k+1} = w_{k+1} - \sum_{j=1}^{k} w_{k+1}^T w_j w_j \tag{3.17}$$

$$Let\ w_{k+1} = w_{k+1} / \sqrt{w_{k+1}^T w_{(k+1}} \tag{3.18}$$

In certain applications, however, it may be desired to use a symmetric de-correlation, in which no vectors are privileged over others. This can be accomplished, e.g., by the classical method involving matrix square roots,

$$Let\ W = (WW^T)^{-1/2} W \tag{3.19}$$

where W is the matrix $(w_1, .., w_n)^T$ of the vectors, and the inverse square root $W = (WW^T)^{-1/2}$ is obtained from the eigen value decomposition of

$WW^T = FDF^T$ as $(WW^T)^{(-1/2)} = FD^{(-1/2)}F^T$. A simpler alternative is the following iterative algorithm

$$Step\ 1.\ Let\ W = W/\sqrt{(||WW^T||)} \tag{3.20}$$

Repeat Step 2. Until convergence:

$$Step\ 2.\ Let\ W = \frac{3}{2}W - \frac{1}{2}WW^TW \tag{3.21}$$

The norm in Step 1 can be almost any ordinary matrix norm.

3.6.8 Ortho-normalization of FastICA Algorithm

The algorithm is an iterative method to find the local maximum of a cost function defined by

$$J_G = \sum_{I=1}^{n} E\{Gw_i^T Z\} \tag{3.22}$$

With G an even symmetrical function. The symbol E stands for expectation, which in practice would be estimated by sample mean over the whitened vectors z. A widely used cost function is the *fourth-order cumulant* or *kurtosis*, defined for any random variable v as

$$kurt(v) = E\{v^4\} - 3(E(\{v^2\})^2 \tag{3.23}$$

With the constraint that the argument $w_i^T z = y_i$ has unit variance the cost function becomes

$$J_G^{kurt} = \sum_{i=1}^{n} E\{(w_i^T z)^4\} \tag{3.24}$$

For the one-unit case, in which only one of the rows of W is considered and orthogonalization is reduced to just normalization of the vector to unit

length after each iteration step, the FastICA algorithm for the general cost function, the updating step is

$$\overline{w_i} = E\{zg(w_i^T z)\} - E\{g'(w_i^T z)\}w_i \tag{3.25}$$

with function g the derivative of G and g' the derivative of g. For the kurtosis cost function, the corresponding updating step is

$$\overline{w_i} = E\{z(w_i^T z)^3\} - 3 \times w_i \tag{3.26}$$

To obtain the full matrix W, we need to run the one-unit algorithm n times and the vector $\overline{w_i}$ must be re-orthonormalized after the update. This is to compensate the of lose their ortho-normality in the updating step. The ortho-normalization can be accomplished basically in two ways: deflationary approach and symmetric approach

3.6.9 Deflationary Approach

The estimated components are obtained one by one in the FastICA algorithm with deflation ortho-normalization. Deflationary ortho-normalization is given by

$$w_p = w_p - \sum_{j=1}^{p-1}(w_p^T w_j)w_j \tag{3.27}$$

with p the previously estimated vectors numbers.

3.6.10 Symmetric Approach

In certain situations it is more appropriate to use a symmetric de-correlation, in which no vectors are "privileged"over others; this means that the vectors w_i are not estimated one by one; instead, they are estimated in parallel. The deflationary method has the drawback that estimation errors in the first

vectors are cumulated in the subsequent ones by the ortho-normalization. This can be overcome in the symmetric method. Another one is that the symmetric orthonormalization methods enable parallel computation of independent components.

3.6.11 Properties of FastICA

The FastICA algorithm and the underlying contrast functions have a number of desirable properties when compared with existing methods for ICA.

- Fast Convergence: The convergence is quadratic to cubic , under the assumption of the ICA data model. In the case of ordinary ICA algorithms based on (stochastic) gradient descent methods, where the convergence is only linear. This implies a very fast convergence.

- Ease of Use: There are no step size parameters to choose. This means that the algorithm is easy to use.

- No need of External Parameter Settings: The algorithm finds directly independent components of (practically) any non-Gaussian distribution using any nonlinearity g. This is in contrast to many algorithms, where some estimate of the probability distribution function has to be first available, and the nonlinearity must be chosen accordingly.

- Ease of Optimization: The performance of the method can be optimized by choosing a suitable nonlinearity g. In particular, one can obtain algorithms that are robust and/or of minimum variance.

- Reduced Computational Complexity: The independent components can be estimated one by one, which is roughly equivalent to doing projection pursuit. This is useful in exploratory data analysis, and decreases the computational load of the method in some cases.

- Other Advantages: The FastICA has most of the advantages of neural algorithms: It is parallel, distributed, computationally simple, and requires little memory space. Stochastic gradient methods seem to be preferable only if fast adaptivity in a changing environment is required.

Computational Complexity

The computational complexity of FastICA is $O(d(d+1)nm)$, where d number of variable/dimensions, n-number of samples and m- number of iterations [99]

3.7 Weight Adjusted Second Order Blind Identification

Blind separation of gaussian sources with different spectra can be attained using second-order statistics. The second-order blind identification (SOBI) algorithm, proposed by Belouchrani et al in [55]., uses approximate joint diagonalization. Weight Adjusted Second Order Blind Identification (WASOBI) provide that substantial improvement over SOBI [14]. This is attained when the joint diagonalization is transformed into a properly weighted nonlinear least squares problem. Optimal weights for weights-adjusted SOBI (WASOBI) algorithm is obtained by an iterative procedure. When the signals are either non-stationary or stationary with different spectra, second-order statistics may be used to attain consistent estimates of the observations correlation matrices

$$R_x[\tau] \triangleq E[x[t+\tau]x^H[t]] \quad satisfy\ R_x[\tau] = AR_s[\tau]A^H \quad \forall\tau \tag{3.28}$$

Where

$$R_s[\tau] \stackrel{\Delta}{=} E[s[t+\tau]s^H[t]] \tag{3.29}$$

are the unknown source signals'diagonal correlation matrices. Thus, A is a joint diagonalizer of any set of K matrices $\{R_x[\tau_1], R_x[\tau_2], .., R_x[\tau_K]\}$. In addition, it can be shown that if all the source signals have different spectra (differing by more than scale), then a set of lags can be found such that the joint diagonalizer is unique, up to irrelevant scaling and permutation of columns. It is therefore proposed in[55] to estimate A as the joint diagonalizer of a set of estimated correlation matrices , $\{\hat{R}_x[\tau_1], \hat{R}_x[\tau_2], .., \hat{R}_x[\tau_1]\}$. While A the set of true correlation matrices admits exact diagonalization, it is most likely impossible to jointly diagonalize the set of estimated matrices. It is still possible, however, to obtain consistent estimators for by resorting to approximate joint diagonalization, attained in two phases as described below.

In the first phase, a whitening matrix $\hat{W}$ is found such that $\hat{W}\hat{R}_x[0]\hat{W}^H$ equals the identity matrix. All the other matrices are then similarly transformed

$$\tilde{\hat{R}}[\tau_k] = \hat{W}\hat{R}_x[\tau_k]\hat{W}^H \quad k = 1, 2, .., K \tag{3.30}$$

In the second phase, the unitary approximate joint diagonalizer of the transformed set is found using successive Jacobi rotations, which iteratively minimize the off-diagonal entries of the transformed matrices (The desired estimate is then given by $A = \hat{W}^{\#}\hat{U}$ where $\hat{W}^{\#}$ denotes the pseudo-inverse of $\hat{W}$) .

The second phase optimizes a least-squares (LS) fit of the $\tilde{\hat{R}}[\tau_k] - s$ with respect to $\hat{U}$. However, this LS criterion is not optimized with respect to $\hat{A}$, since the non unitary part $\hat{W}$ is chosen to attain exact diagonalization of $\hat{R}_x[0]$, possibly at the expense of poor diagonalization of the other matrices. As noted in such a 'hard-whitening'operation bounds the attainable performance. Furthermore, the errors in estimating the correlations are

strongly correlated. It is therefore expected that an unweighted LS criterion might yield inferior performance relative to an optimally weighted LS (WLS) criterion.

WASOBI algorithm addresses the two shortcomings of the SOBI algorithm. First, it reformulate the approximate diagonalization problem as a nonlinear WLS problem and outline an iterative algorithm for minimization with respect to an arbitrary (not necessarily unitary) matrix $\hat{A}$. It then find the optimal weight matrix under the assumption of Gaussian source signals with finite-length correlations such as moving average (MA) processes. The problem is focused in the case of $M = N = 2$, real valued signals and mixing system. Extension to complex system and higher dimensions is straight forward.

3.7.1 Formulating as a Weighted LS Problem

It is assumed that $\hat{R}_x[\tau_k]$ are estimated using

$$\hat{R}_x[\tau_k] = \frac{1}{T}\sum_{t=1}^{T} x[t]x^T[t+\tau_k] \tag{3.31}$$

(assuming $T + \tau_k$ samples are available). A 2 x 2 matrix and A and K diagonal matrices $A_1, A_2, .., A_K$ such that $\hat{R}_x[\tau_k]$ are 'best fitted' by $AA_KA^T for\ k = 1, 2.., K$. Thus, there are $four$ parameters of interest, denoted $a \stackrel{\Delta}{=} vec\{A\} = [A^{(1,1)}A^{(2,1)}A^{(1,2)}A^{(2,2)}]^T$, and $2K$ nuisance parameters, which are the K 2×1 vectors $\lambda_k \stackrel{\Delta}{=} diag\{A_K\} \quad k = 1, 2, .., K$. However, due to the inherent scaling ambiguity (which enables one to commute scales between $A\ and\ A_K$), we may arbitrarily fix, for example, A_1, reducing the true number of nuisance parameters to $2(K-1)$.

Note that the estimated $R_x[\tau_k]$ are not necessarily symmetric ($for\ \tau_k \neq 0$) *in contrast to* AA_KA^T. We shall thus attempt to fit each AA_KA^T to

a symmetric variant of the respective $\hat{R}_x[\tau_k]$, obtained by substituting its off-diagonal terms with their arithmetic average.

We therefore define $\hat{r}_k \triangleq vec\{\hat{R}_x[\tau_k]\}$ and

$$y_k \triangleq \begin{bmatrix} 1 & 0 & 0 & 0 \\ 0 & \frac{1}{2} & \frac{1}{2} & 0 \\ 0 & 0 & 0 & 1 \end{bmatrix} \cdot \hat{r}_k \triangleq C\hat{r}_k \quad k = 1, 2..., K$$

The desired fit for each k can be expressed as

$$Y_k \approx \begin{bmatrix} a_1^2 & a_3^2 \\ a_1 a_2 & a_3 a_4 \\ a_2^2 & a_4^2 \end{bmatrix} \cdot \lambda_k \triangleq G(a)\lambda_k \tag{3.32}$$

Concatenating all y_k *into* $y \triangleq [y_1^T y_2^T ... y_k^T]^T$,
will give $y \approx [I_K \bigotimes G(a)]\lambda \triangleq \tilde{G}(a)\lambda$, where I_K denotes the $K \times K$ identity matrix, $\bigotimes$ denotes Kroneckerś product, and $\lambda = [\lambda_1^T \lambda_2^T ... \lambda_K^T]^T$ is the concatenation of λ_K.Let $\bar{\lambda} = [\lambda_2^T \lambda_3^T ... \lambda_K^T]^T$, the vector of free parameters in λ . Given any $3K \times 3K$ symmetric weight matrix W, we may now define the WLS criterion as

$$C_{WLS}(a, \lambda) \triangleq [y - \tilde{G}(a)\lambda]^T W [y - \tilde{G}(a)\lambda] \tag{3.33}$$

to be minimized with respect to a and $\bar{\lambda}$,with λ_1, set arbitrarily. This is linear in $\bar{\lambda}$, , and is nonlinear in a. Differentiating $\tilde{G}(a)\lambda$ with respect to a, obtaining

$$H(a, \lambda) \triangleq \frac{\partial(\tilde{G}(a)\lambda)}{\partial a} = \begin{bmatrix} \lambda_1^{(1)} D_1(a) & \lambda_1^{(2)} D_2(a) \\ \lambda_2^{(1)} D_1(a) & \lambda_2^{(2)} D_2(a) \\ \vdots & \vdots \\ \lambda_k^{(1)} D_1(a) & \lambda_k^{(2)} D_2(a) \end{bmatrix} \tag{3.34}$$

where $\lambda_k^{(i)}$ denotes the i^{th} element of λ_k , and where

$$D_1(a) \triangleq \begin{bmatrix} 2a_1 & 0 \\ a_2 & a_1 \\ 0 & 2a_2 \end{bmatrix} \tag{3.35}$$

$$D_2(a) \triangleq \begin{bmatrix} 2a_3 & 0 \\ a_4 & a_3 \\ 0 & 2a_4 \end{bmatrix} \tag{3.36}$$

Differentiating $\tilde{G}(a)\lambda$ with respect to $\bar{\lambda}$ is

$$\bar{G}a \triangleq \tilde{G}a[Z : I_{2(k-1)}]^T \tag{3.37}$$

here Z denotes a $2(K-1) \times 2$ all-zeros matrix. The iterative Gauss algorithm thus assumes the following form:

$$\begin{bmatrix} a^{[l+1]} \\ \lambda^{[l+1]} \end{bmatrix} = \begin{bmatrix} a^{[l]} \\ \lambda^{[l]} \end{bmatrix} + \begin{bmatrix} H^T W H & H^T W \bar{G} \\ \bar{G}^T W H & \bar{G}^T W \bar{G} \end{bmatrix}^{-1} \cdot \begin{bmatrix} H^T W \\ \bar{G}^T W \end{bmatrix} \left[y - \tilde{G}\lambda^{[l]} \right] \quad l = 1, 2, \ldots \tag{3.38}$$

where, $H^T, \bar{G} and\ \tilde{G}$ are $H(a^{[l]}, \lambda^{[l]}), \bar{G}a^{[l]}$ and $\tilde{G}a^{[l]}$ respectively. An initial value for $a^{[0]}\ and\ \lambda^{[0]}$ can be obtained from the SOBI algorithm.

The sparse structure of $\tilde{G}(a)$ is used to reduce the computational load. Alternating between linear minimization (with respect to λ) and nonlinear minimization (with respect to a) is also helpful in reducing computational load. Note only that the computational load of the minimization depends only on and is independent of the number of observations T.

3.7.2 Optimal Weighting

To apply optimal weighting, the covariance matrix of y denoted by ϕ. Assuming Gaussian signals, from eq.3.31

$$\begin{aligned} E\left[\hat{R}_x^{(i,j)}[\tau_k]\hat{R}_x^{(m,n)}[\tau_l]\right] &= \frac{1}{T^2}\sum_{t=1}^{T}\sum_{s=1}^{T} E\Big[x_i[t]x_j[t+\tau_k]x_m[s]x_n[s+\tau_1]\Big] \\ &= R_x^{(i,j)}[\tau_k]R_x^{(m,n)}[\tau_1] \\ &+\frac{1}{T}\sum_{p=-(T-1)}^{T-1}(1-\frac{|p|}{T})(R_x^{(i,m)}[p]R_x^{(j,n)}[p+\tau_l-\tau_k] \\ &+R_x^{(i,n)}[p+\tau_1]R_x^{(j,m)}[p-\tau_k]) \end{aligned} \tag{3.39}$$

which implies that the covariance of $\hat{R}_x^{(i,j)}[\tau_k]$ *and* $\hat{R}_x^{(m,n)}[\tau_l]$ is given by the expression of the last three rows. Assume that the source signals are MA processes of orders $\leqslant Q$, whereas the selected lags are $\tau_k = k-1, k = 1, 2, \ldots Q+1$. The summation over p can then be reduced from $-Q$ *to* Q $for 1 \leqslant k, l \leqslant K = Q+1$, which implies that estimating the correlation matrices up to lag Q is also sufficient for consistently estimating ϕ.

Eq.3.39 can be reformulated in matrix form, such that

$$\begin{aligned} Cov[\hat{r}_k, \hat{r}_l] = \frac{1}{T}\sum_{p=-Q}^{Q}\left(1-\frac{|q|}{T}\right)(R_x[p+\tau_1-\tau_k]\otimes R_x[p] \\ +(R_x[p-\tau_k]\otimes R_x[p-\tau_1])P) \end{aligned} \tag{3.40}$$

Where P is a permutation matrix that swaps the second and third columns of the matrix to its left. Recalling the linear transformation eq.3.32 from $\bar{r}_k$ *to* y_k, we conclude that the $(k.l)^{th}$ 3×3 block of ϕ is given by

$$\phi_{k,l} \triangleq Cov[y_k, y_i] = C\ Cov[\hat{r}_k, \hat{r}_l]C^T \tag{3.41}$$

The optimal weight matrix is then given by $W_{opt} = \phi^{-1}$. In practice, estimated correlations would replace true correlations , providing a consistent estimate of W_{opt}. A more computationally efficient implementation can be found in [100]

Computational Complexity

The computational complexity of SOBI is $O(d^4M)$ and WASOBI is $O(d^6 + d^3m^3)$, where d-no signal, M- no of covariance matrix [100].

3.8 SYMWHITE Algorithm

The SYMWHITE algorithm presented in[16] is revisited in the proceeding sessions. The temporal, spatial or temporal-spatial de-correlation is very important in BSS. Pre-whitening is often a necessary condition for the stronger stochastic independence criteria. After pre-whitening the BSS become somewhat easier and less ill conditioned, because the subsequent separating system is described by an orthonormal matrix for real valued signals. The de-correlation technique can be used to identify the mixing matrix and perform blind signal separation for colored signals[16].

3.8.1 A Pre-whitening Algorithm

A random, zero mean vector $y \subset R^n$ of dimension n is said to be white if its covariance (correlation) matrix is an identity matrix, ie.,

$$R_{yy} = E\{yy^T\} = 1_n \tag{3.42}$$

The white signals form the correlation matrix which is diagonal. It means that such signals are not correlated with each other. Any set of vectors $x \subset R^m$ can be de-correlated (whitened) by applying some preprocessing stage. The whitening procedure is equivalent to the linear transformation of the vector x. The whitened vector y is described by the relation

$$y = Wx \tag{3.43}$$

where W is an $n \times m$ whitening matrix. If $n < m$ the matrix W simultaneously reduces the dimension of the data vectors from m *to* n. If $n = m$ the size of the whitened vector is the same as original one. The vectors y are mutually uncorrelated and have unit variance. It means that

$$R_{yy} = E\{yy^T\} = E\{W_{xx}^T W^T\} = W R_{xx} W^T = 1_n \tag{3.44}$$

Usually the the measured sensor signals are mutually correlated, i.e., the covariance matrix Rxx is not diagonal one. However it is always symmetric and usually positive definite. It means that it can be decomposed using the eigenvalue decomposition as follows

$$Rxx = V_x L_x V_x^T = V_x L_x^{1/2} L_x^{1/2} V_x^T \tag{3.45}$$

where V_x is an orthogonal matrix and L_x is a diagonal matrix with all non-negative eigenvalues λ_i, that is $L_x = diag\{\lambda_1, \lambda_2, \ldots, \lambda_m\}$. The columns of the matrix V_x are the eigenvectors corresponding to the appropriate eigenvalues. Thus, assuming that the covariance matrix is positive definite, the required de-correlation matrix W can be computed as follows

$$W = L_x^{1/2} V_x^T \tag{3.46}$$

If some eigenvalues of R_{xx} are zero we can take only positive eigenvalues and the eigenvectors associated with them. We use a modified version of the basic algorithms as explained below. This method is more robust in the practical case [35] [101].

3.8.2 Bias Removal

The main problem of whitening is due to the noise that is usually contained in the captured signal. Let us assume the noisy signal $x = s + n$, where s is the signal and n the random white noise of the standard deviation σ_n. The eigenvalues corresponding to the noise are usually very small, so their inverse very high. It means that the whitening algorithm described by the relations above amplifies the noise in the transformed signals. To process the noisy data we need some modifications of the whitening procedure as follows

The most important point in this approach is removing the estimated noise components of the signal. Let us denote the noise variance in the system by σ_n^2 . It is easy to show that at random white noise, uncorrelated with the signal s, the autocorrelation matrix R_{xx}, calculated in a standard way (without delays) may be presented in the form

$$R_{xx} = R_{vv} + R_{nn} \tag{3.47}$$

where R_{vv} is the autocorrelation matrix of signal $v = As$ (A the mixing matrix) and R_{nn} the autocorrelation matrix corresponding to the noise n, ie., $R_{nn} = E\{nn^T\}$. Taking into account the uncorrelated character of the noise, we can estimate the autocorrelation matrix of the signal as

$$R_{vv} = R_{xx} - \sigma_n^2 1 \tag{3.48}$$

where in this equation σ_n^2 represents the estimation of the noise variance. It is straightforward to note that the matrix L_v is equal

$$L_v = diag\{\lambda_1 - \sigma_n^2, \ldots, \lambda_m - \sigma_n^2\} \tag{3.49}$$

where $\lambda_j \ \ (j = 1, 2, ..., m)$ are the eigenvalues of the correlation matrix R_{xx} of measured signals x. In such case we can apply the standard eigenvalue decomposition to the matrix R_{vv}

$$R_{vv} = V_V L_V V_V^T \tag{3.50}$$

and define the whitening matrix W on the basis of this decomposition

$$W = L_V^{-1/2} V_V^T \tag{3.51}$$

The key point in this approach is the accurate estimation of the noise variance. Generally this value is not known apriori and should be estimated on the basis of measurement of the noisy signal. The most straightforward way to perform such estimation is to calculate the autocorrelation matrix R_{xx} of the observations and to analyze the distributions of the eigenvalues of this matrix. Irrespective of the noise level there is a visible knee point in this distribution. The eigenvalues corresponding to the signals are relatively high. The other small values represent the noise. The variance of the noise may be estimated as the mean of all these insignificant eigenvalues. If only K eigenvalues of the autocorrelation matrix are considered, the remaining last $(m-K)$ eigenvalues represent the noise. The variance of the noise may be then estimated as

$$\sigma_n^2 = \frac{\sum_{j=K+1}^{m} \lambda_1}{m - K} \tag{3.52}$$

3.9 Ground Borne Vibration

Vibration is a phenomenon which exists and presents itself in many ways, such as heartbeat, car travel or earthquakes etc. Ground Borne Vibration (GBV) are signals produced by some vibration sources and are propagated through ground. It propagates through ground as waves. GBVs may be categorized into the microseism range which is ever present in the earth's crust and the induced vibrations which are caused by man and nature such as earthquakes, wind, water and storms[102]. Microseisms appears at the earth's surface as a result of motion from within the earth. Seismological centers around the world record such ground vibrations from a period of $16.67 seconds$ to frequencies of approximately $10Hz$ [9].

3.9.1 Vibration Measurement

Vibration measurement establishes the degree and magnitude of a vibratory environment. Usually vibration surveys are performed in various locations, so portable equipment should be used [82]. The details of equipments used in this experiment are discussed separately later.

Seismic vibration sensors used in field vibration surveys should be rugged velocity transducers or accelerometers. Velocity transducers are normally larger than accelerometers in size and produce a greater output (1 to 2 v/mm/sec) without using amplifiers. Accelerometers have less of a voltage output in volt/g. Accelerometers are smaller, and since they have a small voltage output, amplification is required to raise the signal output from the diagnostic instrumentation noise levels.

3.10 Descriptors of Ground-Borne Vibration

3.10.1 Vibratory Motion

Vibration is an oscillatory motion which can be described in terms of the displacement, velocity, or acceleration. There is no net movement of the vibration element. The average of any of the motion descriptors is zero. The displacement of a vibrating area is simply the distance of that area moves away from its static position[103]. The velocity represents the instantaneous speed of the movement and acceleration is the rate of change of the speed. The ground borne vibration is usually described in terms of velocity and acceleration. Most transducers used for measuring ground-borne vibration use either velocity or acceleration as the parameters of the measurement.

3.10.2 Amplitude Descriptors

Vibration consists of rapidly fluctuating motions with an average motion of zero. Several descriptors can be used to quantify vibration amplitude, as shown in figure (3.4)[103]. The raw signal is the lighter curve and this curve shows the instantaneous vibration velocity which fluctuates positive and negative about the zero point. The Peak Particle Velocity (PPV) is defined as the maximum instantaneous positive or negative peak of the vibration signal. The root mean square (rms) amplitude is used to describe the smoothed vibration amplitude. The root mean square of a signal is the square root of the average of the squared amplitude of the signal. The average is typically calculated over a one-second period. The rms amplitude is shown superimposed in the figure (3.4)[103]. The PPV and rms velocity are normally described in meters per second. Decibel notation is also for vibration. Decibel notation acts to compress the range of numbers required to describe vibration. The accepted reference quantities for

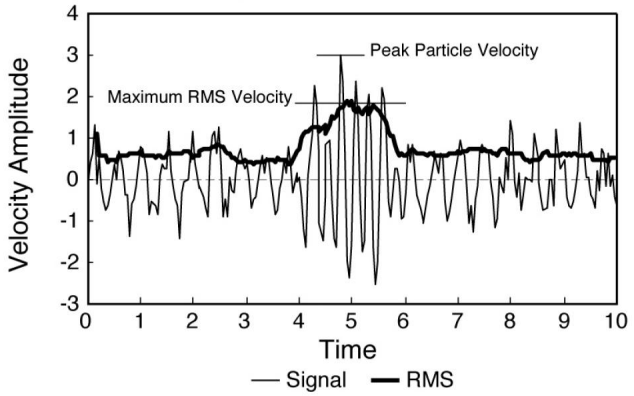

Figure 3.4: Representation of vibration signals [103]

vibration velocity are either 1 times 10-8 meters/second or 5 times 10-8 meters/second.

3.11 Modes of Propagation

Vibration waves in the ground are almost like sound waves in air. In solids many different kinds of waves exist depending on the nature of the medium and its boundaries. In an isotropic elastic full space, two kinds of waves can propagate, and these are called the body waves. These are moving spherically away from the point of excitation. The first is a dilatational wave, or a pressure wave (known as the P-wave). This is a wave similar to compressive waves in air where the particles within the medium oscillate parallel to the direction of propagation of the wavefront. The second is the equi-voluminal wave, or the shear wave (known as the S-wave). This is a transverse wave where particle motion is perpendicular to the direction of travel of the wavefront. Air has no stiffness so there is no equivalent to the S-wave in air. In an elastic half-space model where a third kind of wave appears, confined to the free surface. This is the Rayleigh wave, also known

as the R-wave, and the motion of particles is elliptical in a plane perpendicular both to the free surface and to the wavefront. Rayleigh waves are superficially similar to surface waves in water, but, whereas water waves are controlled by the action of gravity or surface tension, the Rayleigh wave is controlled by the elastic properties of the solid. This leads to very different characteristics. For instance, the particle motion for Rayleigh waves is retrograde while for waves in water particle motion is pro-grade, which means that the particles orbit in opposite directions. Also unlike water waves the vertical component of particle motion in a solid is greater than the horizontal component. Both components decay exponentially with depth so that most of the energy associated with Rayleigh waves is confined near the surface to a depth roughly equal to the wavelength. This has got many practical implications. R-waves will not be attenuated by barriers (natural or man-made) that are small compared with the wavelength. Pioneering work of Lamb on the response of an isotropic elastic half space to different kinds of impulsive and harmonic loads forms the basis of all contemporary understanding of wave propagation in elastic half space. All three types of waves (P-, S-, and R-waves) are non-dispersive This means that their wave speeds are each independent of the excitation frequencies[104] [105] [106]. In the ground, the P-wave speed is the highest, typically 400 to 800 m/s. The S-wave is somewhat slower than the P-wave and only slightly faster than the R-wave, typically 200 to 300 m/s [87]. For the frequency range of interest, the distribution of energy between the three different kinds of waves are calculated by Miller and Pursey in [107] for an elastic half space excited by a vertically oscillating rigid disk on the surface. Of the total input energy, 67% radiates as R-waves, 26% as S-waves, and 7% P-waves. As P and S-waves spread with hemispherical wavefronts in the ground, their decay rate is inversely proportional to the distance from the source. R-waves on the surface spread on a circular wavefront and with a decay rate inversely proportional to the square root of distance from the source.

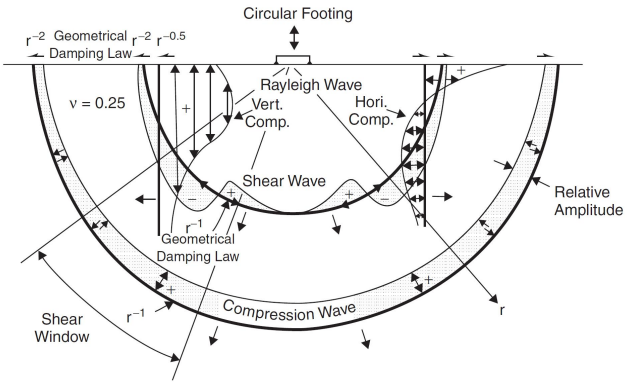

Figure 3.5: Wave propagation
[104]

The geometric decay is defined as reduction in amplitude with distance. The rate at which energy decays with distance from the source is also influenced by material damping. The other kinds of waves like the Stoneley wave,, appears at the discontinuous interface within an infinite solid formed by bonding two different half spaces. The Love wave moves within a surface layer bonded to a half space. The motion of particles is in a horizontal plane parallel to the free surface. Love waves can cause vibration to travel long distances from a source of disturbance. It is the fastest of all surface waves. The real ground conditions are typified by continuous variation of soil properties with depth, and geological layers are generally inclined or discontinuous. The transfer of energy at the various rock-soil and soil-soil interfaces will cause all wave types to be excited. The depth of the water table is a further complicating and seasonally varying factor. It is useful to know that surface waves are of significance because they carry most of the energy and their geometric decay rate is low [8]. For propagation over long distances it is necessary to include a realistic model for damping. The most common damping model is based on material loss factor. Wave propagation in an elastic half space is shown in figure(3.5) [102] [104].

3.11.1 Fundamental Equations of GBV

The ground behavior, is described through the use of the Naviers elastodynamics equations. This is based on a semi space model. If we consider a body where the volumetric forces are negligible, the displacement governing equation is [83] [84]:

$$(\lambda + \mu) \cdot \bigtriangledown \cdot \bigtriangledown \cdot \ u + \mu \cdot \bigtriangledown^2 \cdot u = \rho \cdot u \tag{3.53}$$

From this displacement expression it is possible to obtain the equations of the primary and secondary body waves as follows;

$$\frac{\partial^2 \varphi}{\partial t^2} = v_p^2 \cdot \bigtriangledown^2 \cdot \varphi \tag{3.54}$$

and

$$\frac{\partial^2 \psi}{\partial t^2} = v_s^2 \cdot \bigtriangledown^2 \cdot \psi \tag{3.55}$$

respectively and their velocity expressions are given by:

$$v_p = \left(\frac{\lambda + 2\mu}{\rho} \right)^{1/2} \tag{3.56}$$

and

$$v_s = \left(\frac{\mu}{\rho} \right)^{1/2} \tag{3.57}$$

Where μ is the shear modulus G and ρ is the material density, λ *and* μ are *Lamé* constant given by

$$\lambda = \frac{\nu E}{(1+\nu)(1-2\nu)}$$

and

$$\mu = \frac{E}{2(1+\nu)}$$

where E is Youngs modulus and ν is Poission's ratio.

From these equations it is possible to obtain the integral solution of the superficial displacement for a punctual source placed on the ground surface. The horizontal displacement, w, and the vertical displacement,q, represented by the potentials $\varphi \; and \; \psi$ are shown in the expressions below

$$q = \frac{\partial \varphi}{\partial r} + \frac{\partial^2 \psi}{\partial r \partial z} \tag{3.58}$$

for horizontal displacement and

$$w = \frac{\partial \varphi}{\partial z} - \frac{\partial^2 \psi}{\partial r^2} - \frac{1}{r} \cdot \frac{\partial \Psi}{\partial r} = \frac{\partial \varphi}{\partial z} + \frac{\partial^2 \psi}{\partial z^2} - \frac{1}{\beta^2} \cdot \frac{\partial^2 \psi}{\partial r^2} \tag{3.59}$$

for vertical displacements
Given that the potentials $\varphi \; and \; \psi$ have to satisfy the previous wave equations, one can develop the expressions for displacements in order to obtain the integral solution of the horizontal and vertical displacements, when this is evaluated by boundary and line integrals, we obtain the final expressions of the displacement. Thus, the time dependent equation of the vertical displacement can be written as a function of the distance, r, the Lamé constant, μ the wave-numbers, k, k_α, k_β, the force applied to the ground surface, L, and the frequency, ω, $K = f(k, k_\alpha, k_\beta)$

$$\begin{aligned} w_0 = \frac{LKk}{\mu} \cdot \sqrt{\frac{1}{2\pi kr}} \cdot e^{j(wt - kr - \frac{\pi}{4})} \\ - \frac{Lk_\alpha}{2\pi^2 \mu} \cdot \frac{\sqrt{2\pi}}{(k_\alpha r)^2} \cdot \frac{k_\alpha^2 \cdot k_\beta^2}{(k_\beta^2 - 2k_\alpha^2)^2} \cdot e^{j(wt - k_a r - \frac{\pi}{4})} \\ - \frac{Lk_\beta}{2\pi^2 \mu} \cdot \frac{4\sqrt{2\pi}}{(k_\beta r)^2} \cdot \left(1 - \frac{k_\alpha^2}{k_\beta^2}\right) \cdot e^{j(wt - k_\beta r - \frac{\pi}{4})} \end{aligned} \tag{3.60}$$

here the first term refers to the Rayleigh surface waves rest two terms refers to the primary body waves, P and secondary body wave, S.

3.11.2 Vibration Propagation through Ground

Ground vibration decay has many variables, but is primarily a function of soil pressure, frequency and amplitude of vibration, degree of saturation and granular characteristics of the soil. The papers[108] [83] , suggests that Rayleigh waves dominate at a distance from the source; while body waves are significant within the first 20 m, approximately. The paper[82] [84], present equation for propagation attenuation of waves in linear elastic half space. The Rayleigh wave is considered important, especially at greater distances from the source, since the body waves decay more rapidly by geometric spreading than the Rayleigh wave. In other words, in close proximity to the source, compression waves dominate the ground vibration excitation. However, at large distances from sources, Rayleigh waves dominate the received vibration amplitudes due to a combination of geometrical spreading and frequency dependence of attenuation[82] [102]. Particle velocity at a point is given by[109],

$$v = v_0 \left(\frac{r}{r_0} \right)^{-n} e^{-\alpha(r-r_0)} \tag{3.61}$$

v_0: particle velocity at source

r: the distance from source to the receiver

r_0: the distance from the source to the reference point on the ground

n: the power of geometric attenuation. See the table (3.1)

α: the factor of material damping. See the table (3.2)

Wave Type	Point Source
Shear Waves	1
Compression Waves	1
Rayleigh Waves	0.5
Love Wave	0.5

Table 3.1: Geometric attenuation n for various wave types [110]

Soil Type	Soil Attenuation $[\alpha][m^{-1}]$
Water Saturated Clay	0.04 -0.12
Loess and Loessial Soil	0.1
Sand and Slit	0.04

Table 3.2: Soil attenuation factor for various soil types

3.12 Speed of Waves

The speed of $P-waves$ is given by [87] [102]

$$v_p = \sqrt{\frac{\lambda + 2\mu}{\rho}} \tag{3.62}$$

$\lambda + 2\mu$ is the bulk modulus The speed of $S-waves$ is given by

$$v_s = \sqrt{\frac{\mu}{\rho}} \tag{3.63}$$

μ is the shear modulus G and speed of Rayleigh waves is given by

$$c_R \approx c_s \frac{0.86 + 1.14\ \nu}{1+\nu}, \tag{3.64}$$

ρ is the material density, $\lambda\ and\ \mu$ are Lamé constant given by

$$\lambda = \frac{\nu E}{(1+\nu)(1-2\nu)}$$

and

$$\mu = \frac{E}{2(1+\nu)}$$

where E is Youngs modulus and ν is Poission's ratio. For soil or rock compressional (dilatational) waves travels at wave speeds of $2.5 - 4$ *times* the speed of shear or Rayleigh waves.

3.13 Effects of Sensor Imperfections and Positioning

In this research we used omni directional sensors as it was assumed that no prior information on the spatial locations of the desired sources were available. These sensors are generally considered to be perfect point receivers with ideal omni-directional properties and the frequency response is shown in *chapter 5*. It was assumed that all sensors in the array have smiler characteristics. These assumptions were necessary for the some conventional methods where sensor imperfections will have a detrimental effect. However, in reality the assumption of ideal and equal characteristics are usually not fulfilled. This work was based on the semi analytical approach and a convolute model which allows reverberant environments. As BSS algorithms have the advantage that no distinction between the component caused by the mixing environment and the component caused by the sensor characteristics. There is no much harm in avoiding calibration of sensors. The sensor imperfections can be incorporated with the mixing systems. So the influence on results were minimal.

The sensors can be positioned in different array configurations. The positioning of the sensors can be interpreted as a spatial sampling of the vibration wave field. To avoid ambiguities in the representation of the vibrations, i.e., to avoid spatial aliasing the distance d between two sensors

has to fulfill

$$d \leqslant \frac{\lambda_{min}}{2} \tag{3.65}$$

for the minimum wavelength λ_{min} [111]. This is the spatial analog on to the temporal sampling theorem. For discrete-time signals with sampling frequency f_s, this leads to the condition $d \leqslant c/f_s$. In this thesis $fs = 16\ KHz$ is chosen which would correspond to a maximum sensor spacing of $d \leqslant 2.1\ cm$. This is an important aspect in the design of fixed and adaptive beam-formers. On the other hand, the concept of BSS does in general not constrain the positioning of the sensors as these methods are assumed to be blind and therefore no information about the mixing system and the location of the sources and sensors are needed. The BSS algorithms do not rely on fulfilling the spatial sampling theorem and thus are applicable to arbitrary array configurations.

3.14 Ambiguities in Instantaneous and Convolute Blind Source Separation

As the concept of BSS is solely based on the assumption of mutual independence of the source signals there arise some ambiguities. In instantaneous BSS the following indeterminacies appear[6] [7]

Ambiguity on Scaling: The estimated independent components can only be determined up to a scalar factor.

Ambiguity on Permutation : The order of the independent components cannot be determined.

Due to the impossibility to distinguish if the scaling and permutation occurred in the source signals or in the mixing system, these ambiguities

cannot be resolved without using additional a-priori information if only the sensor signals are observed. Thus, the original sources can only be recovered up to an unknown scaling and permutation.
In the convolute BSS case the indeterminacies translate to:

Ambiguity on Filtering: The estimated independent components can only be determined up to an arbitrary filtering operation.

Ambiguity on Permutation: The order of the independent components cannot be determined.

3.15 Methods of Performance Measures

The performance measures of signal processing methods can be subjective and objective tests [112] [113] [114] [115]. In subjective testing, listening tests are conducted with a number of test persons which implies a considerable effort for the team. To reduce the large effort of subjective evaluations it is desirable to substitute the listening tests by instrumental measuring methods (also termed objective measures) which usually compare processed and unprocessed signal in the time or frequency domain. However, as this is still an active research area, we used established objective measures to assess the performance of BSS algorithms. To evaluate the BSS performance appropriately it has to be pointed out that the perceived quality of the BSS output signals is determined by three factors which have to be addressed individually:
Suppression of interfering point sources
Attenuation of background noise
Distortion of the desired signal
In general, BSS algorithms focus on the suppression of interfering point sources and have only a limited capability of attenuating background noise.

3.16 Summary

The chapter discussed theoretical foundations of the work. The concepts of BSS, ICA, FastICA, WASOBI and whitening algorithm with bias removal were discussed in detail. The concepts ground borne vibration, its propagation were discussed. The effect of sensor imperfections and methods of performance measures were included in the chapter

Chapter 4

Blind Source Separation of Ground Borne Vibrations: The New Frameworks

4.1 Introduction

A Framework is a schema of interlinked subsystem which supports a particular approach to a specific objective and can be modified as required by adding or deleting items. The BSS algorithms forms the core of our frameworks. We made two approaches for the frameworks, extending the basic BSS algorithms and modifying the existing algorithms. Aiming to have a simple direct method, at the outset we extended the basic BSS algorithms for the problem. We expressed the complex problem in elastodynamics as a simple acoustics problem using a semi analytical approach using the general vibration propagation formula, which includes the effect of internal damping losses in the soil. This direct adaptation is discussed in the proceeding sessions. The problem of vibration propagation through the ground

is a very complex problem. The nature and properties of various kinds of waves created because of the vibration source in the ground were detailed in *chapter 3*. In the case of the vibrations in the ground, many different kinds of waves exist depending on the nature of the medium and its boundaries. Based on this fact, looking for more effective methods for tackling the problem, we considered vibration propagation as a 'convolution model' proposed by Enders Robinson et.al[116]. This model is widely accepted as a practical model for describing the ground vibration. The algorithms are modified based on this concept of GBV. We studied the performance of 20 BSS algorithms with the real world data. The most performing algorithms in these cases were considered for further study and improvement. The proposed algorithm SYMWHITE-DECONV can be an effective preprocessing step to achieve spatio-temporal de-correlation. The algorithms WASOBI-DECONV, and FastICA-DECONV were proved as effective candidate for the BSS of the targeted signals. The The algorithms are modified based on this concept of GBV. The proposed SYMWHITE-WASOBI is obtained by combining two well-known algorithms, SYMWHITE and WASOBI.

4.2 The Extension of BSS Algorithms for GBV

Consider *four* (for simplicity) vibration sources v_1, v_2, v_3 *and* v_4, producing stable vibrations. Let these exist as simultaneous vibration sources and stimulate ground waves. Let $s_1,\ s_2,\ s_3$ *and* s_4 are the vibration produced by these sources. These vibrations were captured using *four* sensors $P1, P2, P3$ *and* $P4$. The captured signals $x_1,\ x_2,\ x_3$ *and* x_4 are weighted mixtures of the *four* vibration sources. We can represent the constant coefficients that give the mixing weights as a_{11} *to* a_{44}. Later we prove that these mixing weights only depend on the distances between the sources and the sensors. Therefore, the BSS can be stated into equation 4.1 to 4.4; given

the source signals $s_1,\ s_2,\ s_3\ and\ s_4$ the captured signals $x_1,\ x_2,\ x_3\ and\ x_4$ at sensor $P1\ to\ P4$ as [10]:

$$x_1 = a_{11}s_1 + a_{12}s_2 + a_{13}s_3 + a_{14}s_4 \tag{4.1}$$

$$x_2 = a_{21}s_1 + a_{22}s_2 + a_{23}s_3 + a_{24}s_4 \tag{4.2}$$

$$x_3 = a_{31}s_1 + a_{32}s_2 + a_{33}s_3 + a_{34}s_4 \tag{4.3}$$

$$x_4 = a_{41}s_1 + a_{42}s_2 + a_{43}s_3 + a_{44}s_4 \tag{4.4}$$

The mixing weights were assumed to be unknown, since the properties of the physical mixing system were not known. The source signals were also unknown. The original source signals are required to be found from the mixtures $x_1\ to\ x_4$ This is the BSS problem. The equation 4.1 to 4.4 can be written in matrix form as [10]:

$$X = A \cdot S \tag{4.5}$$

The coefficients a_{ij} are assumed different enough to make the matrix that they form invertible [10]. Thus, there exists a matrix W with coefficients w_{ij} , such that we can separate y_i as

$$y_1 = w_{11}x_1 + w_{12}x_2 + w_{13}x_3 + w_{14}x_4 \tag{4.6}$$

$$y_2 = w_{21}x_1 + w_{22}x_2 + w_{23}x_3 + w_{24}x_4 \tag{4.7}$$

$$y_3 = w_{31}x_1 + w_{32}x_2 + w_{33}x_3 + w_{34}x_4 \tag{4.8}$$

$$y_4 = w_{41}x_1 + w_{42}x_2 + w_{43}x_3 + w_{44}x_4 \tag{4.9}$$

The above equation can be written as

$$Y = W \cdot X. \tag{4.10}$$

If we knew coefficients a_{ij}, matrix W could be found as the inverse of the matrix that consists of the mixing coefficients a_{ij} where y is as close to s as possible. W is the inverse of A [4] [11].

4.2.1 Semi-Analytical Model

When the ground vibration propagates through the soil or rock as waves, the amplitude of the waves generally decreases with distance from the source. The compressional waves or primary or $P-waves$, shear waves or secondary or $S-waves$, and Rayleigh waves or $R-waves$ are the significant ground vibration waves, which propagate through different means and exhibit different behaviors. In the case of semi-analytical model we consider the problem as two cases depending on which the type of waves dominate, namely a near field problem and as a far field problem [117] [118] [119].

Semi-Analytical Model-Near Field Problem

The near field is the area very close to the source where vibration pressure level may vary significantly with small change in position. The area extends to a distance less than wavelength of the lowest frequency emitted from the source or at less than twice the greatest dimension of the source, which ever distance is greater. In close proximity to the source, the compression waves dominate and the effect of $R-wave$ is not considered[108]. In the case of ground borne vibration; the effect of signal damping is considerable and cannot be ignored as in the case of acoustic models. The vibration propagation through the ground is an intricate problem as noted earlier. We express this by a simple acoustics problem using a semi analytical approach using the general vibration propagation formula, which includes the effect of internal damping losses in the soil. A general formula for vibration

propagation with damping in semi-analytical approach[102] can be written as

$$S(r) = S(r_0)\ e^{-\omega\eta r/2c} \tag{4.11}$$

where $S(r)$ is the vibration signal at source-receiver distance of r, $S(r_0)$ is the vibration signal at source-receiver distance of r_0 , ω is the frequency in $rads^{-1}, \eta$ is the soil loss factor (which can be frequency-dependent) and c is the compressional or dilatational wave speed. This method is referred as *'Ungar and Bender approach'*[102][84]. This method predicts the attenuation of vibration through soil with a simplified formula by neglecting all wave types except compressional waves. A complex problem in elastodynamics is reduced to a simple acoustics problem. The method does not allow any modification to account for unusual or complex situations. It is essentially a flat-ground model, which assumes only simplistic changes in soil type in the direction of propagation. This method is not ideally suited for use in situations where the soil is saturated, because the method neglects Biot waves. As noted in the case of near field problem, we consider only compression waves and ω, η, c are assumed to be constants. The equation can be re- written as

$$S(r) = S(r_0)e^{k.r} \tag{4.12}$$

where $k = -\omega\eta/2c$

From the equation (4.12) given above it is clear that the mixed signal depends only on the source-sensor distance in this case also. Hence, the BSS problem of ground borne vibration in this case can be given by

$$x_1 = e^{k.r_{11}}s_1 + e^{k.r_{12}}s_2 + e^{k.r_{13}}s_3 + e^{k.r_{14}}s_4 \tag{4.13}$$

$$x_2 = e^{k.r_{21}}s_1 + e^{k.r_{22}}s_2 + e^{k.r_{23}}s_3 + e^{k.r_{24}}s_4 \tag{4.14}$$

$$x_3 = e^{k.r_{31}}s_1 + e^{k.r_{32}}s_2 + e^{k.r_{33}}s_3 + e^{k.r_{34}}s_4 \tag{4.15}$$

$$x_4 = e^{k.r_{41}} s_1 + e^{k.r_{42}} s_2 + e^{k.r_{43}} s_3 + e^{k.r_{44}} s_4 \tag{4.16}$$

The original source signals are required to be found from the mixtures x_1 *to* x_4 . The equation can be rewritten in the matrix form as

$$X = K \cdot S \tag{4.17}$$

The element $e^{k.r_{ij}}$ of matrix K are assumed different enough to make the matrix that they form invertible. We can see that this is just the basic BSS model, $X = A \cdot S$ with modified mixing matrix. We can estimate the independent component using any basic BSS algorithm.

We assume that the mixture is instantaneous. This is valid as the source-sensor distances are small. In practical cases we cannot neglect signal as well as sensor noise. The noise is assumed to be additive. Thus, the noisy ICA model can be expressed as,

$$X = AS + n \tag{4.18}$$

where n is the noise vector, and assuming zero-mean and uncorrelated Gaussian noise $n \sim N(0, diag(\Sigma))$. We can neglect the source noise in the case of near field problem. The sensor noise can be filtered to an extend by using a noise filter. A noise filter by the method of spectral subtraction is detailed later in this chapter and can be used for noise filtering. It should be noted that we get only damped estimates of the independent component.

Semi-Analytical Model-Far Field Problem

The displacement amplitude decays with $\frac{1}{\sqrt{r}}$, at large distance from source where r is the distance from source. This is the behavior in the so called far-field[117] [120]. Vibrations propagate from a source through the ground to a distant receiver predominantly by means of Rayleigh (surface) waves

and secondarily by body (shear and compressional) waves. The far-field boundary, r_f is obtained by

$$r_f \propto \lambda_R \tag{4.19}$$

where λ_R is the wave length of $R-Wave$ [117]. In the far-field assumption, the surface response is dominated by the Rayleigh wave; and as shown in[104] the Rayleigh waves account for 67.4% of the total energy radiated from the point of excitation. Rayleigh waves are formed within a few meters of the point on the surface directly above the source. The amplitude of these waves diminishes with distance from the source. This attenuation is due to two factors: expansion of the wave front (geometrical attenuation) and dissipation of energy within the soil itself (material damping). The rate of geometrical attenuation depends upon the type of wave and the shape of the associated wave front. One of the key points that established in[80] (Lamb pioneered the classical theory of elastic wave propagation in homogeneous ground) research is the amplitude geometric damping rates for each of the types of wave. This is widely used by researchers, as a basis for developing empirical prediction models. For instance, at the far-field when considering a homogeneous half-space the geometric spreading can be described by the following equation:

$$S(r_1) = S(r_0)\left(\frac{r_0}{r_1}\right)^n \tag{4.20}$$

where $S(r_0)$ and $S(r_1)$ represents the vibration signal at distance from the source r_0 and r_1 respectively, n is *Lamb's coefficient*. Lamb's predicated geometric attenuation coefficient at surface for $R-waves$ is $n = 1/2$

Material damping is generally thought to be attributable to energy loss due to hysteresis, perhaps caused by internal sliding of soil particles. In addition to other factors, the amount of material damping that occurs as a function of the vibration amplitude. Material damping in soil is a function of many parameters, including soil type, moisture content and temperature. Clays tend to exhibit higher damping than sandy soils. Wet sand attenuates

less than dry sand because the pore water between sand particles carries a significant portion of compressional energy. Propagation of Rayleigh waves is insensitive to the presence or absence of water [109].

The geometric spreading and material damping attenuation effect can be combined through the general equation [121] [110] of ground vibration as

$$S(r_1) = S(r_0)\left(\frac{r_0}{r_1}\right)^n e^{-\alpha(r_1-r_0)} \tag{4.21}$$

where α is the attenuation coefficient due to material damping. The paper [110] [122], suggests an α ranging from 0.01 m^-1 to 0.13 m^-1 to be used as material damping coefficient. In reality, the propagating medium is usually stratified, and possesses discontinuities forming layers. In layered ground, some energy is refracted through to adjacent layer(s) and some is reflected. Depending on the density ratio between materials and the angle of incidence at the boundary, the velocity of reflected and refracted waves can be greater than that of the incident wave. Our discussion is limited to the general equation of ground vibration stated above. Considering R wave in the case of far-field problem the equation can be written as:

$$S(r_1) = S(r_0)\left(\frac{r_0}{r_1}\right)^{1/2} e^{-\alpha(r_1-r_0)} \tag{4.22}$$

$$S(r_1) = S(r_0)\left(\frac{\sqrt{r_0}}{\sqrt{r_1}}\right) e^{(-\alpha r_1+\alpha r_0)} \tag{4.23}$$

$$S(r_1) = S(r_0)\left(\frac{\sqrt{r_0}}{\sqrt{r_1}}\right) e^{-\alpha r_1} e^{\alpha r_0} \tag{4.24}$$

Let us assume at a negligibly small distance r_0 from the source, the amplitude is finite and the effect of damping is negligible and hence the equation becomes

$$S(r_1) = S(r_0) k e^{-\alpha r_1}/\sqrt{r_1} \tag{4.25}$$

where, constant, $k = e^{\alpha r_0}\sqrt{r_0}$
In general, the signal at a distance r_1 from the i^{th} source

$$S_i(r_1) = S_i(r_0)ke^{-\alpha r_1}/\sqrt{r_1} \tag{4.26}$$

This shows that damping depends only on the distance from source to sensor, r_1

The BSS problem of ground borne vibration in the case of far field problem can be written as

$$x_1 = k \cdot \frac{e^{-\alpha r_{11}}}{\sqrt{r_{11}}} s_1 + k \cdot \frac{e^{-\alpha r_{12}}}{\sqrt{r_{12}}} s_2 + k \cdot \frac{e^{-\alpha r_{13}}}{\sqrt{r_{13}}} s_3 + k \cdot \frac{e^{-\alpha r_{14}}}{\sqrt{r_{14}}} s_4 \tag{4.27}$$

$$x_2 = k \cdot \frac{e^{-\alpha r_{21}}}{\sqrt{r_{21}}} s_1 + k \cdot \frac{e^{-\alpha r_{22}}}{\sqrt{r_{22}}} s_2 + k \cdot \frac{e^{-\alpha r_{23}}}{\sqrt{r_{23}}} s_3 + k \cdot \frac{e^{-\alpha r_{24}}}{\sqrt{r_{24}}} s_4 \tag{4.28}$$

$$x_3 = k \cdot \frac{e^{-\alpha r_{31}}}{\sqrt{r_{31}}} s_1 + k \cdot \frac{e^{-\alpha r_{32}}}{\sqrt{r_{32}}} s_2 + k \cdot \frac{e^{-\alpha r_{33}}}{\sqrt{r_{33}}} s_3 + k \cdot \frac{e^{-\alpha r_{34}}}{\sqrt{r_{34}}} s_4 \tag{4.29}$$

$$x_4 = k \cdot \frac{e^{-\alpha r_{41}}}{\sqrt{r_{41}}} s_1 + k \cdot \frac{e^{-\alpha r_{42}}}{\sqrt{r_{42}}} s_2 + k \cdot \frac{e^{-\alpha r_{43}}}{\sqrt{r_{43}}} s_3 + k \cdot \frac{e^{-\alpha r_{44}}}{\sqrt{r_{44}}} s_4 \tag{4.30}$$

Where r_{ij} is the distance from j^{th} source to i^{th} sensor. The original source signals are estimated from the mixtures x_1 *to* x_4 without knowing any other parameters. This is the blind source separation problem. The equation can be rewritten in the matrix foam as

$$X = K \cdot S \tag{4.31}$$

The element $\frac{e^{-\alpha r_{ij}}}{\sqrt{r_{ij}}}$ of matrix K are assumed different enough to make the matrix that they form invertible. We can see that this is just the basic ICA model, $X = A \cdot S$ with modified mixing matrix. We can estimate the independent component using any basic BSS algorithm.

We assume that the mixture is instantaneous. The effect of reverberation is not considered. In practical cases, we cannot neglect signal as well as sensor noise. The noise is assumed to be additive. Thus, the noisy model can be expressed as, $X = AS+n$ where n is the noise vector, and assuming zero-mean and uncorrelated Gaussian noise $n \sim N(0, diag(\Sigma))$, In the case of the far field problem the source noise cannot be neglected. The source noise can be modeled with equation $X = A(S+n)$ where covariance of the noise is diagonal, noisy independent component is given by

$$\check{S}_i = S_i + n_i \tag{4.32}$$

and equation can be rewritten as

$$X = K\check{S} \tag{4.33}$$

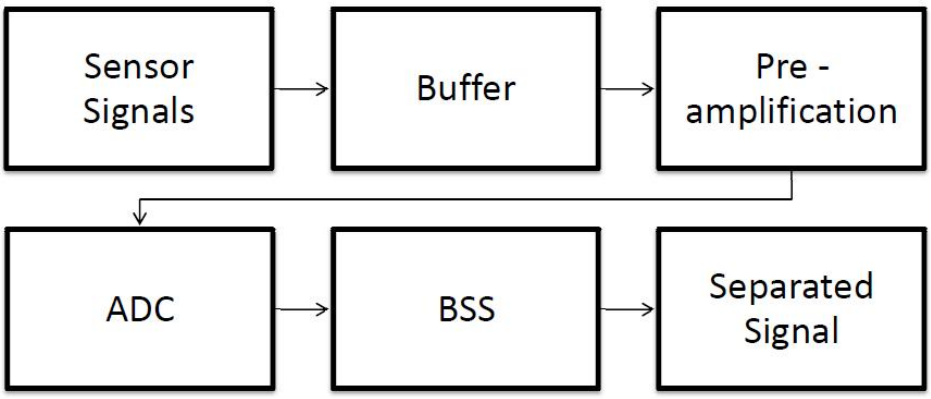

Figure 4.1: A general arrangement of the new frameworks using extended BSS

We see that this is also the basic BSS model, with modified independent components and mixing matrix. We can estimate the model by any method for basic BSS. It should be noted that we only get damped, noisy

estimates of the Independent Component. Eliminating complete noise and obtaining original Independent Component(IC) is not completely feasible in this situation. So we can use wiener filter or Kalman filter get an optimal IC, $\hat{s}i$. A general arrangement of the new-frameworks based on extended BSS algorithms as the core is shown in the figure(4.1)

4.3 Modification of BSS Algorithms

Many of the BSS frameworks already exist are seem to be not much effective or even fail to separate the real world signal. It is observed that the presence of noise and the reverberation is the major reason for this drawback. The modified algorithms which form the core of the new frameworks improve the effectiveness of the separation by amalgamating an adaptive noise gate and noise reduction based on spectral subtraction followed by a de- reverberation process using amplitude spectral subtraction method. The concept is based on the 'convolution model'[116] , which is a widely accepted practical model for representing the ground borne vibrations. A part from these modification as noted earlier a hybrid algorithm is proposed by combining two algorithms.

4.3.1 The Convolution Model

The primary waves, P, and shear waves, S, and Rayleigh surface waves, R, propagate through different means. These three waves exhibit different behaviors. The Rayleigh waves are elliptically retrograde waves, which propagate in normal direction to excitation source, in surface and also into the semi-space. The rate of attenuation is more in this later direction [8]. Rayleigh surface waves have lower geometric attenuation ratio than body waves so they transport vibration energy to higher distances from the excitation source. In the ground, the $P - wave$ speed is the highest,

typically 400 to 800 m/s. The $S - wave$ travel typically at 200 to 300 m/s. As discussed earlier due to the higher contribution to the energy transportation and the lower decaying rate, Rayleigh surface waves are considered in the development of the ground borne vibration propagation model[102]. The level of vibration considered for the experiment is low and the measurement distance is only a few meters [103], This assumptions also justifies considering $R - waves$ as the major component of propagation of waves.

The convolution model assumes that the recorded seismic signals $s(t)$ is the convolution of an earth-reflectivity function $e(t)$ and a seismic wavelet $w(t)$ from a point source, where t represents recording time. The convolution model approximates the earth by a linear system[9]. According to this model, the seismic trace $s(t)$ is given by:

$$s(t) = w(t) * e(t) + v(t) \tag{4.34}$$

where $v(t)$ is an additive noise. The de convolution is used to compute the earth's reflectivity $e(t)$ given the seismic trace $s(t)$. The convolution model of the seismic trace is widely accepted because it agrees well with the observed seismic traces. We principally focus at $R - waves$, the effect of $P - waves$ with multi-path reflections are not ignored completely. The following assumptions will hold for use of convolution model as the base

- Our experiments and application are restricted to few meters and the vibrations considered were low level.

- It is assumed that the earth is composed of various layered media

- The phenomena reflection, refraction and dispersion were present in the captured signals and occurs at the boundaries of the layered media

- The vibration source produces all typical waves in ground irrespective of the level of excitation.

These assumptions are valid for the system under consideration and the use of convolution model as a base for developing our model can well justified. The proposed model is a multiple source-multiple sensor model based on the single source 'convolution model'. In the multiple source-multiple sensor model the observation at each sensor contains the convoluted and mixed signals from different sources. At the discrete time index t , a mixture of N source signals $s(t) = s_1(t), \cdots s_n(t)$ are received at an array of M sensors. The captured signals are denoted $x(t) = x_1(t), \cdots x_n(t)$, The basic model of convolute mixtures can be given as follows[4];

$$x_m(t) = \sum_{n=1}^{N} \sum_{k=0}^{K-1} a_{mnk}\ s_n(t-k) + v_m(t) \tag{4.35}$$

where $v_m(t)$ is the additive noise. The captured signal is a linear mixture of filtered versions of each of the source signals and 'a_{mnk}' corresponding mixing filter coefficients and in practical case $k < \infty$. Re writing the equation (4.35)

$$x(t) = \sum_{k=0}^{K-1} A_k s(t-k) + V(t) \tag{4.36}$$

A_k is an $M \times N$ matrix which contains k^{th} filter coefficient and $V(t)$ is the $M \times 1$ noise vector. The captured signals $x(t)$ are complex mixtures of the individual sources. Our aim is to separate the mixtures into component signals. The only known quantities are the signal mixtures captured using the deployed sensors. Towards the solution domain, the separated

components can be estimated as follows. The two stage de-noised and de-convoluted signals are assumed to be instantaneous, and the instantaneous model which is given below is applicable.

$$x(t) = As(t) \tag{4.37}$$

The coefficients a_{ij} of matrix A are assumed different enough to make the matrix that they form invertible[6]. Thus, there exists a matrix W with coefficients w_{ij}, such that we can separate $s(t)$ as

$$y(t) = W \cdot x(t) \tag{4.38}$$

where $y(t)$ is as close to $s(t)$ as possible [4][11]. In the proceeding section, we introduce frameworks for achieving separation based on the convolution model discussed in this section.

4.3.2 Noise Reduction Based on Adaptive Noise Gating

The noise is any random fluctuations of data that makes the perception of an expected signal more difficult. De-noising or noise reduction is any signal processing method, which reconstructs a signal from a noisy one. Its goal is to remove noise and preserve useful information. Discretion between sound and noise are subjective. Any sound may be considered noise depending on the perceiver or application. Noise is indistinguishable from sound as both are vibrations through a medium, like air or ground.

Noise Gate or Audio Gate

Noise Gate [123] is the control of when and to what degree audio passes through a channel. Its based on factors including the signal level strength.

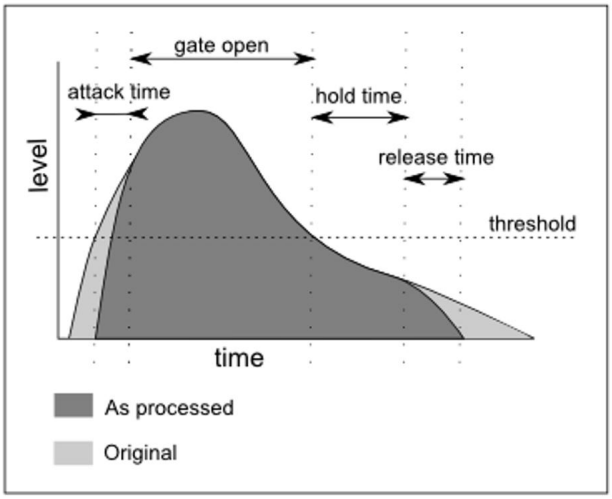

Figure 4.2: Various control parameters

It can be mainly used to control the reduction of unwanted external sounds and reduction of natural channel noise. The noise gate allows only the signals above the desired threshold to pass-through. We take the threshold as a function of amplitude spectrum. The threshold is decided from a statistical estimate of mixed signal. It is computed for each mixed source signal or channel and is decided in such a way that the unwanted noise and a portion of the late reflection are only filtered out and the required signals including signals from far sources should not be blocked. A detailed discussion of control parameters are included below. Gates are controlled through setting five parameters; threshold, attack, release, range, and hold as shown in the figure (4.2). The output of a typical gate is included in the figures(4.3)(4.4) for reference.

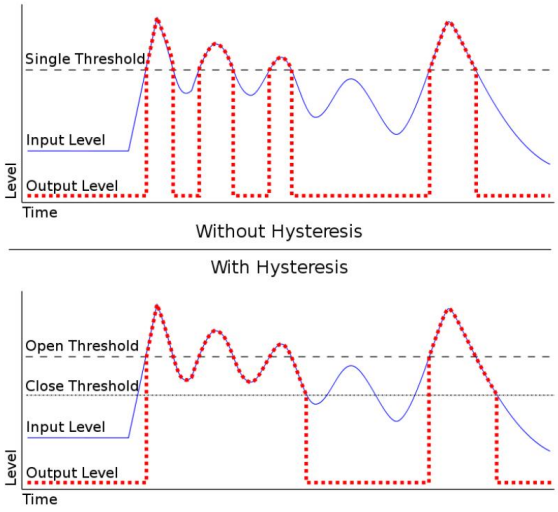

Figure 4.3: Noise gate and hysteresis
[124]

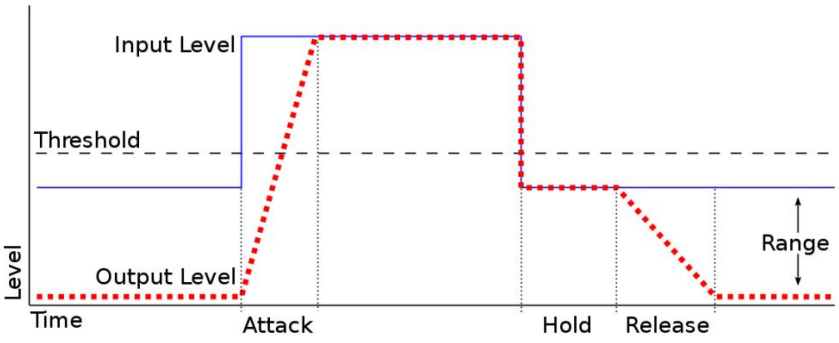

Figure 4.4: Output of a typical noise gate
[124]

Threshold

When the input level reaches the threshold, the gate is opened, its held open after dropping below the threshold, and then the gate is closed during the release time. Its the decibel level in which the gate opens or closes. The higher the threshold, the louder the sound (stronger the signal) must be to open the gate. The lower the threshold, the more sound that will pass through when the gate is open.

Attack and Release

Audio gating, which seems like an on-or-off control, creates a better sound when the speed of the opening and closing varies based on the need. The attack time controls the speed of the gate opening. The time is in milliseconds. A gate that opens too quickly on a slower signal attack can produce an impulse sound. The release (decay) time is the key to a natural sounding audio decay. Its measured in microseconds to seconds. Setting these time is critical in noise elimination.

Range

The range is the amount of decibel reduction to the signal once its gated.

Hold

The hold time is the minimum time the gate is held open. The hold time is typically set to a minimum of 20-30 milliseconds to prevent chatter. Chatter is the constant opening and closing of a gate due to a high-speed fluctuating signal level. Another type of chatter-control is called hysteresis. In this case, the threshold automatically increases for subsequent gate openings and decreases a few decibels for closing the gate.

Adaptive Noise Gate

Adaptive noise gate is primarily introduce to increase the signal to noise ratio (SNR) and to avoid signal distortion due to non linear rectification process used in the Noise Reduction (NR) using spectral subtraction. The adaptive noise gate proposed in this experiment allows the signal to pass through (Gate Open), when the signal reaches a threshold value and it is held open after dropping below the threshold, and then the gate is closed during the release time. This threshold is decided based on the signal amplitude spectrum estimate $\hat{A}(f)$ and is related to the expected signal spectrum $E[|A(f)|]$ which is usually calculated using time averaged signal spectrum $\bar{A}(f)$ taken from the parts of the signal where the early and late reflection are present. The signal estimate is given by:

$$\hat{A}(f) = E[|A(f)|] \cong \bar{A}(f) = \frac{1}{K}\sum_{i=0}^{K-1}|A_i(f)| \tag{4.39}$$

Where $|A_i(f)|$ is the amplitude spectrum of the i_{th} of $frames$ of signal and the threshold value is obtained as

$$A_{threshold} = \alpha \cdot \hat{A}(f) \tag{4.40}$$

where α is the threshold adjustment parameter and is empirically estimated based on the strength of the signals. The limiting values of $\alpha = 0.5$ for *signals with good strength* and $\alpha = 0.75$ for *low level signals*. It can vary between these limits. The gating is performed for the entire frequency range. A level reduction of $-12dB$ is applied and the attack/decay time is taken as 250 ms. The value were found to be optimum in our independent experiments.

4.3.3 Noise Reduction Based on Spectral Subtraction

Spectral subtraction is a method for restoration of the power spectrum or the magnitude spectrum of a targeted signal from observed noisy signal. This is achieved through subtraction of an estimate of the average noise spectrum from the noisy signal spectrum. The noise spectrum is usually estimated from the periods when the signal is absent and only the noise is present. We assume that the noise is a stationary or a slowly varying process, and that the noise spectrum does not change significantly in between the update periods.

In the case where noisy signal and the noise is accessible on a separate channel, it may be possible to retrieve the signal by subtracting an estimate of the noise from the noisy signal. In many situations including the one examined, the only signal that is available is the noisy signal. In these cases, it is possible to reduce the average effects of the noise on the signal spectrum. The effect of additive noise on the magnitude spectrum of a signal is to increase the mean and the variance of the spectrum. The increase in the variance of the signal spectrum results from the random fluctuations of the noise, and cannot be canceled out. The increase in the mean of the signal spectrum can be removed by subtraction of an estimate of the mean of the noise spectrum from the noisy signal spectrum.

The noise reduction was implemented based on the methodology depicted in [125], which is as follows. The noisy signal model in the time domain is given by

$$x(t) = s(t) + n(t) \tag{4.41}$$

where $s(t), n(t), x(t)$ are the original signal, the additive noise and the noisy signal respectively, and m is the discrete time index. In the frequency domain, the equation can be expressed as

$$X(f) = S(f) + N(f) \tag{4.42}$$

where $S(f), X(f)$ *and* $N(f)$ are the Fourier transforms of the original signal $s(t)$, the noisy signal $x(t)$ and the noise $n(t)$ respectively, and f is the frequency variable. In spectral subtraction, the incoming signal $x(t)$ is buffered and divided into segments of N samples length. Each segment is windowed, using a Hanning window, and then transformed via discrete Fourier transform (DFT) to N spectral samples. The windows alleviate the effects of the discontinuities at the endpoints of each segment. The windowed signal is given by

$$x_w(t) = w(t)x(t) = w(t)[s(t) + n(t)] = s_w(t) + n_w(t) \tag{4.43}$$

The windowing operation can be expressed in the frequency domain as

$$X_w(f) = W(f) * X(f) = S_w(f) + N_w(f) \tag{4.44}$$

where the operator $*$ denotes convolution. Throughout this chapter signals are assumed to be windowed and hence for simplicity we avoid subscript. The statistical parameters of the noise are not known thus the noise and vibration signals are replaced by their estimates

$$\hat{S}(f) = X(f) - \hat{N}(f) \tag{4.45}$$

The noise spectrum estimate $\hat{N}(f)$ is related to the expected noise spectrum $E[|N(f)|]$ which is usually calculated using time averaged noise spectrum $\bar{N}(f)$ taken from parts of the signal where only noise is present. The noise estimate is given by:

$$\hat{N}(f) = E[|N(f)|] \cong \bar{N}(f) = \frac{1}{K}\sum_{i=0}^{K-1} |N_i(f)| \tag{4.46}$$

where $|N_i(f)|$ is the amplitude spectrum of the i^{th} of K frames of noise.

Noise estimate in k^{th} frame can be obtained by filtering the noise using first order low pass filter

$$\hat{N_k}(f) = |\tilde{N_k}(f)| = \lambda_n \cdot |\check{N}_{k-1}(f)| + (1 - \lambda_n)|N_k(f)| \tag{4.47}$$

where $\tilde{N_k}(f)$ is the smoothed noise estimate in the i^{th} frame, λ_n is the filtering coefficient and $0.5 \leqslant \lambda_n \leqslant 0.9$. We considered $50\ to\ 100\ ms$ duration for obtaining noise estimate

The spectral subtraction error may be defined as $\epsilon_{def} = \hat{S}(f) - S(f)$ The error degrades the signal quality, introducing the distortions known as residual noise. The error is a function expected $E[|N(f)|]$ or average $\bar{N}(f)$

Noise spectrum estimate:

$$\epsilon = N(f) - E[|N(f)|] \cong |\bar{N}(f)| - E[|N(f)|] \tag{4.48}$$

Therefore longer noise spectrum is used for analysis the more accurate the result is.Time-domain signal can be obtained by combining the magnitude spectrum estimate $\hat{X}(f)$ with the phase of the noisy signal, and then transformed into the time domain via the Inverse Discrete Fourier Transform (IDFT)

$$\hat{s}(m) = \sum_{k=0}^{N-1} |\hat{S}(k)| e^{j\theta_X(k)} e^{-j\frac{2\pi}{N}km} \tag{4.49}$$

where $\theta_Y(k)$ is the phase of the noisy signal $X(k)$. The signal restoration equation(4.49) is based on the assumption that the audible noise is mainly

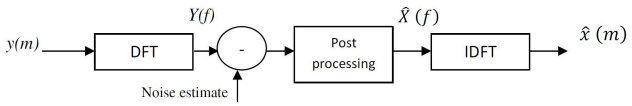

Figure 4.5: Block diagram of the spectral subtraction method [125]

due to the distortion of the magnitude spectrum, and that the phase distortion is largely inaudible. This assumption is valid in most cases. The figure (4.5) illustrates a block diagram configuration of the spectral subtraction method

The spectral subtraction can result in negative estimates of the power or the magnitude spectrum. This is most likely in the case of low signal-to-noise ratio (SNR). To avoid negative magnitude estimates the spectral subtraction output is post-processed using a mapping function $T[\cdot]$. This nonlinear rectification process can distorts the distribution of the restored signal. The processing distortion becomes more noticeable for low signal-to-noise ratio. We used an earlier noise gating to increase SNR

$$T[|\hat{S}(f)|] = \begin{cases} |\hat{S}(f)| & if\ |\hat{S}(f)| > \beta[|X(f)|] \\ f_n[|X(f)|] & otherwise \end{cases} \tag{4.50}$$

We may choose a rule such that if the estimate $|\hat{S}(f)| > 0.01[|X(f)|]$ (in magnitude spectrum 0.01 is equivalent to 40 dB) then $|\hat{S}(f)|$ should be set to some function of the noisy signal $f_n[|X(f)|]$. In its simplest form, $f_n[X(f)] = noisefloor$, where the noise floor is a positive constant. An alternative choice is $f_n[|X(f)|] = \beta|X(f)|$. In this case,

$$T[|\hat{S}(f)|] = \begin{cases} |\hat{S}(f)| & if\ |\hat{S}(f)| > \beta[|X(f)|] \\ \beta[|X(f)|] & otherwise \end{cases} \tag{4.51}$$

Spectral subtraction may be implemented in the power or the magnitude spectral domains. The two methods are similar, although the performances are different. It is noted that a better performance is obtained in magnitude spectral domain.

Magnitude Spectrum Subtraction

The magnitude spectrum subtraction is defined

$$|\hat{S}(f)| = |X(f)| - |\overline{N(f)}| \tag{4.52}$$

Where $|\overline{N(f)}|$ is the time averaged magnitude spectrum of noise. Taking Expectation on both sides

$$\begin{aligned} E[|\hat{S}(f)|] &= E[|X(f)|] - E[\overline{|N(f)|}] \\ = E[|S(f) + N(f)|] - E[\overline{|N(f)|}] &= E[|S(f)|] \end{aligned} \tag{4.53}$$

For signal restoration the magnitude estimate is combined with the phase of the noisy signal and then transformed into the time domain as discussed in the preceding session

In terms of computational complexity, spectral subtraction is relatively inexpensive. However, owing to random variations of noise, spectral subtraction can result in negative estimates of the short-time magnitude or power spectrum.

4.3.4 De-reverberation Based on Spectral Subtraction

Reverberation is an acoustical noise appearing in enclosed spaces through the multiple reflections and diffractions of the sound on different layers of obstructions. These multiple echoes add to the direct sound alter its temporal and spectral characteristics.

The process of reverberation can be modeled as a filtering process. The vibration signal is convolved with the impulse response of the propagation channel defined by the source, sensor and the surrounding environment. The impulse response referred is room impulse response (RIR) considering the reverberation happening in a closed chamber. The energy of a sound portion is smeared over time and overlaps the proceeding portions. This

results in the blur and masking of spectral features of the sound waves [126].

The reverberant energy decays exponentially with a time constant because of the absorption of the energy due to reflection and diffraction. The reverberant tails will have an exponential decay behavior. In a comparative study of different short time spectral attenuation algorithms concludes that the amplitude subtraction gives very good performance compared with other sophisticated methods.

We can express reverberation as the process of multi path propagation of an acoustic signal $s(n)$ from its source to one or more sensors. The observed signal at the m^{th} sensor can be written as [89]

$$x_m(n) = h_m^T(n)s(n) + V_m(n) \tag{4.54}$$

where $h_m = [h_{m1} + h_{m2} \cdots h_{mL}]^T$ is the impulse response of the acoustic channel from source to sensor m and $V_m(n)$ is the observation of the noise or in other words we can represent the medium as a filter g between the source and the sensor and that is modeled as in figure (4.6) This can be

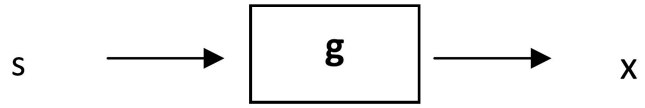

Figure 4.6: Representation of medium

represented as:

$$x_n = g(n) * s(n) + V(n) \tag{4.55}$$

n is the time index and $V(n)$ is the additive noise. Due to the effect of phenomenon of reverberation, sensors will receive not only the direct vibration signal but also various multi-path copies of it formed by reflections

on various layers of the ground and other objects. The multi-path signals are delayed and possibly attenuated as compared to the direct signal. A very simple scenario is illustrated in the figure(4.7) In time domain rever-

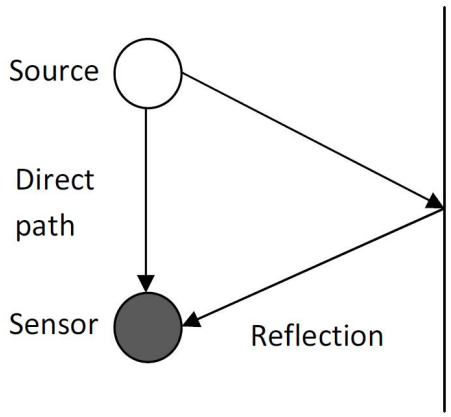

Figure 4.7: Simple reflection model

beration can be classified into early and late reflections. Early reflection can be defined as first 50-100 ms of reflection. The direct, early and late reflection in time domain is shown in figure (4.8). Consider a single source-

Figure 4.8: Direct and reflected sound

single sensor model. If signal $s[t]$ is corrupted by convolution noise $h[t]$ and

additive noise $n[t]$ the observed signal $x[t]$ becomes

$$x[t] = h[t] * s[t] + n[t] \tag{4.56}$$

where $*$ denotes the convolution operation. If we neglect the additive noise for simplicity the equation becomes

$$x[t] = h[t] * s[t] \tag{4.57}$$

For performing dereverberation we use the method described in [90]. The method is described in the following sections. We separate the impulse response $h[t]$ *two* parts $h_{early}[t]$ *and* $h_{late}[t]$

$$h_{early}[t] = \begin{cases} h[t], & t < T \\ 0, & otherwise \end{cases} \tag{4.58}$$

$$h_{late}[t] = \begin{cases} h[t+T], & t \geqslant T \\ 0, & otherwise \end{cases} \tag{4.59}$$

where T is the length of the spectral analysis window,

$$h[t] = h_{early}[t] + \delta[t-T] * h_{late}[t] \tag{4.60}$$

$\delta(\cdot)$ is a dirac delata function (that is , a unit impulse function). The equation (4.57) can be written as

$$x[t] = s[t] * h_{early}[t] + s[t-T] * h_{late}[t] \tag{4.61}$$

where the early effect is distortion within a frame (analysis window), and the late effect comes from previous multiple frames. When the length of impulse response is much shorter than analysis window size T used for Short-

Time Fourier Transform (STFT), STFT of distorted signal equals STFT of clean signal multiplied by STFT of impulse response $h[t] = h_{early}[t]$

In the case of multi source mixed signals, it is difficult to distinguish early reverberation signals and direct signals from other sources. Therefore, de-reverberation process of early reflection may lead to loss of useful information.

In the case of late reverberations, the length of impulse response is much longer than an analysis window size, STFT of distorted signal is usually approximated by

$$X(f,\omega) \approx S(f,\omega) * H(\omega) = S(f,\omega) * H(0,\omega) + \sum_{d-1}^{D-1} S(f-d,\omega)H(d,\omega) \tag{4.62}$$

where f is frame index, $H(\omega)$ is STFT of impulse response, $S(f,\omega)$ is STFT of clean signal s and $H(d,\omega)$ denotes the part of $H(\omega)$ corresponding to frame delay d . With long impulse response, the channel distortion is convolution in a linear spectral domain. We will apply a spectral subtraction method for the late term of equation(4.61). we treat $s[t-T]*h_{late}[t]$ similar to an additive noise $n[t]$ and apply a noise reduction technique based on spectrum subtraction. Assuming the noise $s[t-T]*h_{late}[t]+n(t)$ could be estimated from $x[t]$. The spectrum subtraction is performed as

$$|\hat{S}(f,\omega)| = max(|X(f,\omega)| - \alpha \cdot g(\omega)|X(f-1,\omega)|, \beta.|X(f,\omega)|) \tag{4.63}$$

Where α is the noise over estimation factor, β is the spectra; floor parameter to avoid negative or underflow values and $g(\omega) = |1-0.9e^{j\omega}|$ $\alpha = 1$ *and* $\beta = 0.1$ are typical empirically estimated value [89].

Computational Complexity

Computational complexity for finding Covariance matrix is $O(p^{2n})$. Computational complexity for finding Eigen value is $O(p^3)$ and computational complexity for finding DFT $O(nlogn)$, where n is the data points, p is the features [127].

4.3.5 Selection of Algorithms

There are many existing algorithms for BSS. They utilize different properties of the sources. The various properties exploited in different algorithms for BSS include non-Gaussian properties, properties of statistical independence, Maximum likelihood, info-max principle, Kullback-Leibler divergence, geometric transformation of data space and continuous waveform structure of independent sources in the form of second order de-correlation. The most methods of BSS are optimised for the acoustic problems or instantaneous mixtures. As discussed earlier these models are not robust for the BSS of GBV. Reverberation, ill conditioning, damping and low Signal to Noise Ratio (SNR) characterize the GBVs . We evaluated the performance of 20 existing algorithms for real world vibration signals. These algorithms were tested on simulated and real-world acoustic signals by various researchers. Many article citing these experiments [52][39][128][129] are available in scientific literature. So we confined our experiments of these algorithms using real world vibration signals. The performance was evaluated based on Performance Index of Separability (PI).
The **Performance Index (PI)**, is defined by (4.64) [115][52][129]

$$PI = \frac{1}{n(n-1)} \sum_{i=1}^{n} \left\{ \left(\sum_{k=1}^{n} \frac{|w_{tk}|}{max_j|w_{ij}|} - 1 \right) \left(\sum_{k=1}^{n} \frac{|w_{ki}|}{max_j|w_{ij}|} - 1 \right) \right\} \tag{4.64}$$

where w_{ij} is the $(i,j)^{th}$ element of the de-mixing matrix W. The term $max_j|w_{ij}|$ is the maximum value along the i^{th} row of W and $max_j|w_{ji}|$

is the maximum value of the i^{th} column of W. When perfect separation is achieved, PI is zero. In practice this is too optimistic. The table (4.1) shows the Performance Index of various algorithms for instantaneous mixing and for various source sensor distance for 40000 samples in each case. The table shows the performances of algorithms are utmost when the mixing is instantaneous. The performance of algorithms generally deteriorated with increase in distance. This is because of decrease SNR, damping and increased effect of reverberation.

Algorithm	PI of Instantaneous Mixing	Source- Sensor Distance in cm						Avg. PI
		20	40	60	80	100	120	
WASOBI	0.0096	0.0564	0.0643	0.2243	0.1753	0.1859	0.1683	0.1457
SYM-WHITE	0.0026	0.1263	0.1257	0.2050	0.2857	0.1436	0.1836	0.1783
MCOMBI	0.0032	0.0803	0.1323	0.2874	0.3034	0.1654	0.1423	0.1852
EVD 2	0.0461	0.2103	0.0704	0.3206	0.2044	0.1880	0.1737	0.1946
AMUSE	0.0558	0.2160	0.0666	0.2634	0.2442	0.2427	0.1510	0.1973
SOBI	0.0123	0.2836	0.0703	0.2978	0.1688	0.2097	0.2100	0.2067
COMBI	0.0016	0.2781	0.0672	0.2720	0.3083	0.2226	0.1669	0.2192
SOBI-BPF	0.0114	0.1908	0.1452	0.2760	0.2843	0.1977	0.2361	0.2217
NG-FICA	0.0000	0.2817	0.1261	0.2757	0.2782	0.2840	0.2884	0.2557
SANG	0.0053	0.2587	0.1183	0.2372	0.3164	0.3322	0.3010	0.2606
ERICA	0.0806	0.3369	0.1659	0.2204	0.3446	0.1575	0.2689	0.2490
SIMBEC	0.0082	0.2098	0.1902	0.2708	0.2663	0.2584	0.3712	0.2611
QJADE	0.0080	0.2657	0.2225	0.1801	0.2822	0.3338	0.3370	0.2702
UNICA	0.0806	0.3332	0.1656	0.2163	0.3446	0.2720	0.2679	0.2666
FPICA	0.0047	0.3071	0.2752	0.3849	0.3483	0.2320	0.1837	0.2885
FJADE	0.0022	0.2896	0.2455	0.3706	0.3204	0.2195	0.2907	0.2894
EFICA	0.0045	0.2914	0.2440	0.2903	0.4096	0.2346	0.2683	0.2897
POWERICA	0.1453	0.2371	0.2037	0.2924	0.2836	0.3235	0.2648	0.2675
ThinICA	0.0026	0.2919	0.2200	0.3862	0.3556	0.2571	0.2673	0.2964
SONS	0.1533	0.2814	0.3362	0.2614	0.3414	0.2743	0.2528	0.2912

Table 4.1: Performance Index of separability of different algorithms on real world data

The figure (4.9) shows the plot of average performance index of separability of different algorithms for real world data. The algorithms are listed on X-axis and average PI is plotted in Y-axis. The figure(4.10) shows the plot of the performance index of separability of different algorithms for real world data for various source-sensor distances. The algorithms are listed

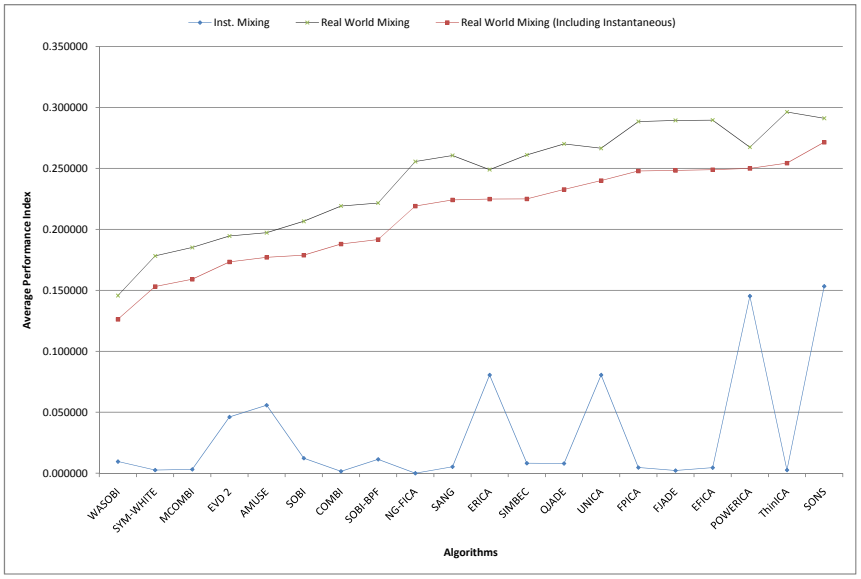

Figure 4.9: Average PI of different algorithms

on X-axis and PI is plotted in Y-axis. The figure (4.11) shows the plot of average time for convergence in the case of real world signals for various source-sensor distance. The algorithms are listed on X-axis and average

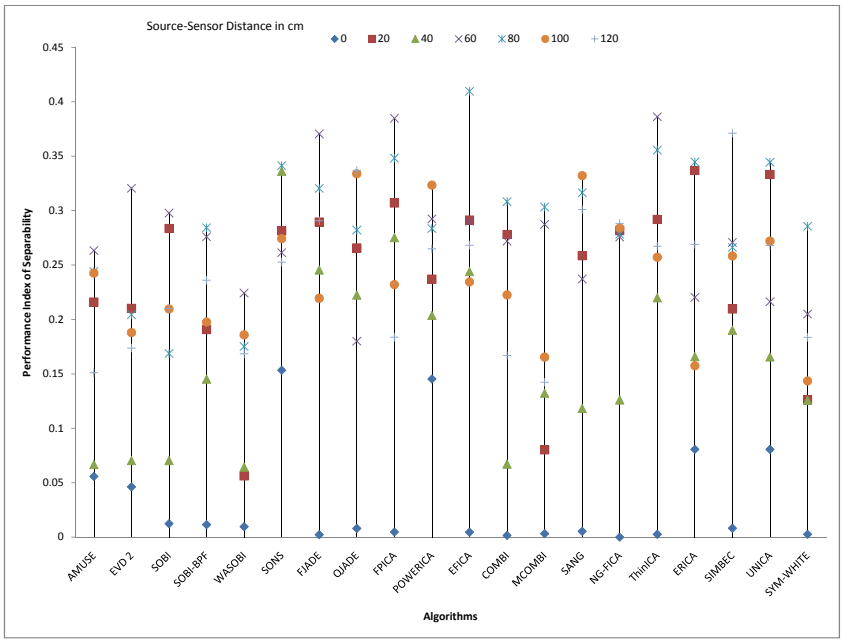

Figure 4.10: Performance Index of Separability of different algorithms on real world data for various source sensor distance

time in seconds is plotted in Y-axis.

From the figure (4.9)(4.10) and (4.11), we can infer that, the best performing algorithms in the case of real world vibrations signal separation are WASOBI and SYMWHITE.

We selected the FastICA also for further study because of the popularity of the FastICA algorithm and computational efficiency in certain class of signals. In this study, the consideration of time complexity is superficial and our concentration is on the improvement of performance of algorithms. It was noted that that even in the case of convergence time for a larger samples, the performances of WASOBI and SYMWHITE is acceptable.

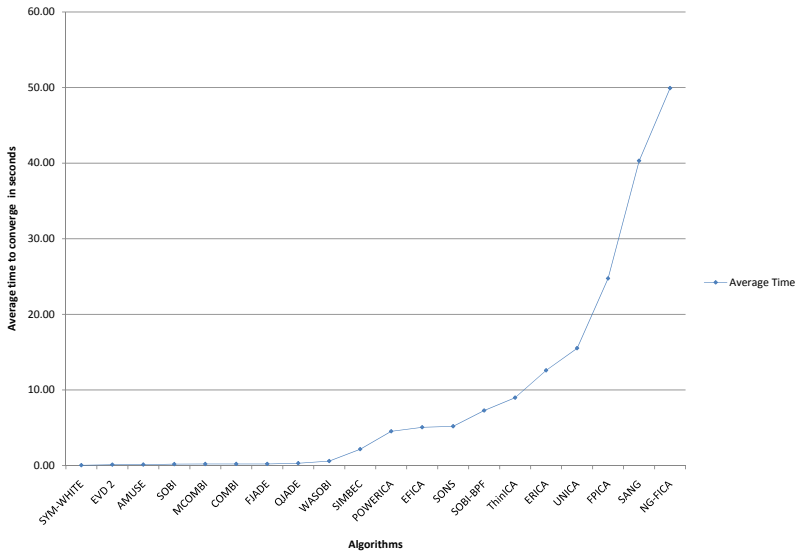

Figure 4.11: Average time for convergence

4.3.6 WASOBI-DECONV

The WASOBI algorithm is modified for the effective BSS of GVB signals. The modification is based on convolution model as discussed earlier. The modified algorithm is discussed below. The sensor signals are de-noised using an adaptive noise gate and amplitude spectrum subtraction method. The signals then subjected to deconvolution (de reverberate in the case of audio signals) to remove remaining reverberation traces using spectral method. The details of this process were explained in preceding sessions. These signals after deconvolution is assumed to be Gaussian and can be modeled as Autoregressive (AR) processes with distinct spectra. Weights-Adjusted Second Order Blind Identification (WASOBI) is asymptotically

optimal solution under these conditions. **The Noise reduction and deconvolution stage of the algorithm can be defined by the implementation Algorithm 1**

Algorithm 1: WASOBI-DECONV

1 Get signal estimate of $X(f)$ *as* $\hat{A}(f) = \frac{1}{K}\sum_{i=0}^{K-1}|A_i(f)|$ for a minimum of 50 ms

2 Perform Adaptive Noise Gating as follows: Calculate $A_{threshold} = \alpha \cdot \hat{A}(f)$, α varies between the limits 0.5 for *near field problems or signals with fairly good strength* and 0.75 for *far field problems or low level signals*, set level reduction to -12 dB attack/decay to 250 ms

3 Find the noise estimate of the gated signal in k^{th} frame by filtering the noise using first order low pass filter as

$$\hat{N_k}(f) = |\tilde{N_k}(f)| = \lambda_n \cdot |\tilde{N}_{k-1}(f)| + (1-\lambda_n)|N_k(f)|$$

where $\tilde{N_k}(f)$ is the smoothed noise estimate in the i^{th} frame, λ_n is the filtering coefficient and $0.5 \leqslant \lambda_n \leqslant 0.9$.

4 Obtain the magnitude spectrum subtraction by $|\hat{S}(f)| = |X(f)| - \overline{|N(f)|}$, where $\overline{|N(f)|}$ is the time averaged magnitude spectrum of noise

5 Perform the de-reverberation on the de-noised signal by spectrum subtraction as

$$|\hat{Y}(f,\omega)| = max(|S(f,\omega)| - \alpha \cdot g(\omega)|S(f-1,\omega)|, \beta.|S(f,\omega)|)$$

where α is the noise over estimation factor, β is the spectra; floor parameter to avoid negative or underflow values and $g(\omega) = |1 - 0.9e^{j\omega}|$ $\alpha = 1$ *and* $\beta = 0.1$ are typical empirically estimated value

6 Perform BSS using WASOBI on the mixed signal(de-reverberated and de noised) obtained from *step 5*, (*as explained below*)

Weight Adjusted Second Order Blind Identification (WASOBI) is a

weighted version of the Second Order Blind Identification (SOBI)[130][14] [100]. This BSS algorithm is based on second order statistics. WASOBI algorithm rely on time-structure in the sources correlation and based on approximate joint diagonalization of say$M$ time lagged signal, estimated correlation matrices

$$\hat{R}_X(\tau) = \frac{1}{N-\tau} \sum_{n=1}^{N-\tau} x[n]x^T[n+\tau], \tau = 0, \cdots M-1 \tag{4.65}$$

where $x[n]$ denotes the n^{th} column of x. In the approximate joint diagonalization process the algorithm incorporates proper weighting which is inversely proportional to the covariance in the correlation estimates

The Cramér-Rao Lower Bound (CRLB) on the (unbiased) estimation of W induces a different type of lower bound (on the attainable ISR, in the form of an ISR-like matrix with element-wise bounds. This is referred as 'Cramér-Rao-Induced Bound'(CRIB). A separation algorithm is said to be 'optimal'(for a specified mixing model) when its ISR matrix equals the respective CRIB. WASOBI have been shown to be asymptotically optimal (under some mild conditions) for their respective model-classes. If all sources are Gaussian AR of order$M-1$, then under asymptotic conditions the ISR matrix attained by WASOBI can be shown to equal CRIB

$$ISR_{kl} = \frac{1}{N} \frac{\phi_{kl}}{\phi_{kl}\phi_{lk} - 1} \frac{\sigma_k^2 R_l[0]}{\sigma_l^2 R_k[0]} \tag{4.66}$$

where σ_k^2, the variance of the innovation is sequence of the k^{th} source and ϕ_{kl} is given by

$$\phi_{kl} = \frac{1}{\sigma_k^2} \sum_{i,j=0}^{M-1} a_{il} a_{jl} R_k[i-j] \tag{4.67}$$

where $\{a_{il}\}_{i=0}^{M-1}$ are the AR coefficients of the l^{th} source with $a_{0l} = 1 \; for \; k, l = 1, \cdots d$ and $R_k[m]$ is the autocorrelation of the k^{th} source at time lag m and

assumed $R_k[0] = R_l[0] = 1$

4.3.7 SYMWHITE-DECONV

The SYMWHITE algorithm is modified for effective BSS of GBV. This algorithm has a framework similar to the WASOBI-DECONV. SYMWHITE algorithm can separate source under weak condition and when a mixing matrix H is symmetric and the covariance matrix of the original sources is supposed to be $R_{ss} = I_m$ *The algorithm can be defined by the implementation, Algorithm 2.*

4.3.8 FastICA-DECONV

The FastICA , a computationally efficient and popular algorithm is modified for effective BSS.The proposed algorithm is very similar to WASOBI-DECONV. Instead of WASOBI algorithm we use popular algorithm FastICA. The FastICA algorithm is detailed in chapter 3. **The Noise reduction and deconvolution stage of the algorithm can be defined by the implementation Algorithm 3** and FastICA has the following basic implementation.

Step 1. Choose an initial (e.g. random) weight vector w

Step 2. Let $w^+ = E\{xg(w^T x)\} - E\{g^{'}(w^T x)\}w$

Step 3. Let $w = w^+/||w^+||$

Step 4. If not converged, go back to Step 2.

Convergence means the old and new values of w point in the same direction. It is not necessary that the vector converges to a single point, since w and $-w$ define the same direction.

4.3.9 SYMWHITE-WASOBI

The proposed is SYMWHITE-WASOBI algorithm is derived by combining two algorithms: Symmetrical Whitening Algorithm and WASOBI algo-

Algorithm 2: SYMWHITE-DECONV

1 Get signal estimate of $X(f)$ *as* $\hat{A}(f) = \frac{1}{K}\sum_{i=0}^{K-1}|A_i(f)|$ for a minimum of 50 ms

2 Perform Adaptive Noise Gating as follows: Calculate $A_{threshold} = \alpha \cdot \hat{A}(f)$, α varies between the limits 0.5 for *near field problems or signals with fairly good strength* and 0.75 for *far field problems or low level signals*, set level reduction to -12 dB attack/decay to 250 ms

3 Find the noise estimate of the gated signal in k^{th} frame by filtering the noise using first order low pass filter as

$$\hat{N_k}(f) = |\tilde{N_k}(f)| = \lambda_n \cdot |\tilde{N}_{k-1}(f)| + (1-\lambda_n)|N_k(f)|$$

where $\tilde{N_k}(f)$ is the smoothed noise estimate in the i^{th} frame, λ_n is the filtering coefficient and $0.5 \leqslant \lambda_n \leqslant 0.9$.

4 Obtain the magnitude spectrum subtraction by $|\hat{S}(f)| = |X(f)| - \overline{|N(f)|}$, where $\overline{|N(f)|}$ is the time averaged magnitude spectrum of noise

5 Perform the de-reverberation on the de-noised signal by spectrum subtraction as

$$|\hat{Y}(f,\omega)| = max(|S(f,\omega)| - \alpha \cdot g(\omega)|S(f-1,\omega)|, \beta.|S(f,\omega)|)$$

where α is the noise over estimation factor, β is the spectra; floor parameter to avoid negative or underflow values and $g(\omega) = |1 - 0.9e^{j\omega}|$ $\alpha = 1$ *and* $\beta = 0.1$ are typical empirically estimated value

6 Compute a symmetric pre-whitening matrix W on the basis of the covariance matrix R_{xx} such that $W = inv\sqrt{(R_{xx})}$

Algorithm 3: FastICA-DECONV

1 Get signal estimate of $X(f)$ *as* $\hat{A}(f) = \frac{1}{K}\sum_{i=0}^{K-1}|A_i(f)|$ for a minimum of 50 ms

2 Perform Adaptive Noise Gating as follows: Calculate $A_{threshold} = \alpha \cdot \hat{A}(f)$, α varies between the limits 0.5 for *near field problems or signals with fairly good strength* and 0.75 for *far field problems or low level signals*, set level reduction to -12 dB attack/decay to 250 ms

3 Find the noise estimate of the gated signal in k^{th} frame by filtering the noise using first order low pass filter as

$$\hat{N_k}(f) = |\tilde{N_k}(f)| = \lambda_n \cdot |\tilde{N}_{k-1}(f)| + (1-\lambda_n)|N_k(f)|$$

where $\tilde{N_k}(f)$ is the smoothed noise estimate in the i^{th} frame, λ_n is the filtering coefficient and $0.5 \leqslant \lambda_n \leqslant 0.9$.

4 Obtain the magnitude spectrum subtraction by $|\hat{S}(f)| = |X(f)| - \overline{|N(f)|}$, where $\overline{|N(f)|}$ is the time averaged magnitude spectrum of noise

5 Perform the de-reverberation on the de-noised signal by spectrum subtraction as

$$|\hat{Y}(f,\omega)| = max(|S(f,\omega)| - \alpha \cdot g(\omega)|S(f-1,\omega)|, \beta.|S(f,\omega)|)$$

where α is the noise over estimation factor, β is the spectra; floor parameter to avoid negative or underflow values and $g(\omega) = |1 - 0.9e^{j\omega}|$ $\alpha = 1$ *and* $\beta = 0.1$ are typical empirically estimated value

6 Perform source separation using fast ICA (for one unit) as explained below

rithm. This combination making the Blind separation of signals considered in a more effective way. The deconvolution process of the other three algorithms is not included in this algorithm. The SYMWHITE algorithm will act as a preprocessing step. The performance of this algorithm is better compared to SYMWHTE and in some cases it outperforms other new algorithms. The SYMWHITE and WASOBI algorithms are detailed in chapter 3. A general arrangement of the new-frameworks based on modified algorithms as the core is shown in the figure(4.12)

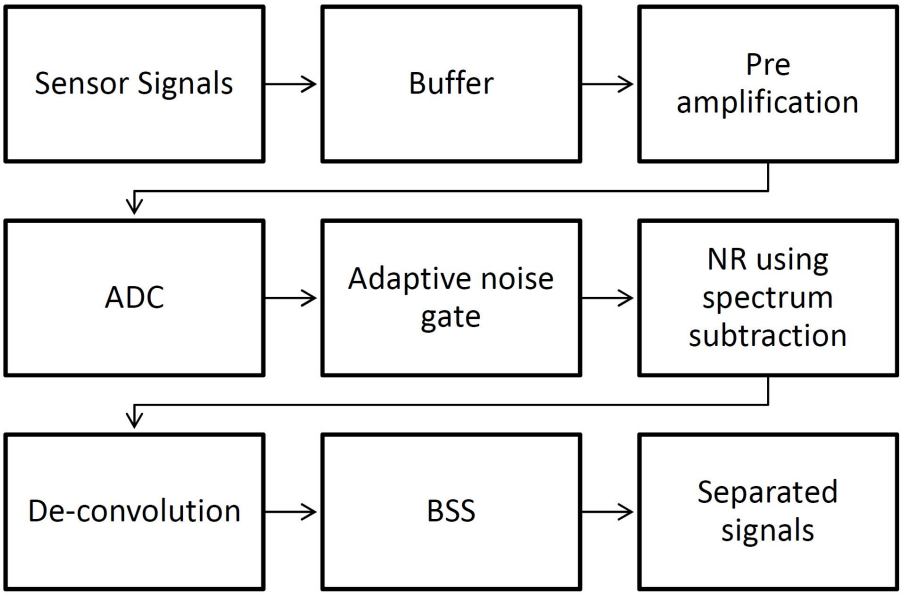

Figure 4.12: A general arrangement of the new frameworks using modified BSS

4.4 Summary

This chapter presented the niceties of the new frameworks for BSS of GBV. The modified BSS algorithms forms the heart of our frameworks were presented. We presented the justification and proof of extending BSS algorithms for GBV. For improving the effectiveness of the BSS, modifications for selected algorithms were presented and justified. The modified algorithms FastICA-DECONV, WASOBI-DECONV, SYMWHITE-DECONV and SYMWHITE-WASOBI were presented in the chapter. In this chapter we included the selection of algorithms for modification based on performance of various algorithms on real world signals. The semi- analytical model and convolution model were detailed in this chapter.The Noise reduction techniques and de-reverberation process based on spectral subtraction was also explained in this chapter.

Chapter 5

Blind Source Separation with the New Frameworks

5.1 Introduction

In the previous chapter we presented the new frameworks for GBVs. Different methods are employed in the evaluation of the performance of Blind Source Separation (BSS) algorithms. All methods are not good candidates for performance evolution of these particular cases. Artificial test cases can be used to examine the algorithm performance. Even if the ill conditioned cases are considered, the artificial cases fail to capture some elements of the real world cases. The complexity real world cases cannot be reproduced completely. For example the statistics of impulse response, the nature of convolution, presence and pattern of background noise etc. We studied the performance of the developed frameworks for benchmarked signals with synthetic mixing as well as for real world signals. It is observed that the performance of the algorithms varies with the nature of the input signals. The performance of various frameworks mostly depend on

the BSS algorithms,which form the kernel of the frameworks. This chapter gives various methods used for evaluating the algorithms and details of BSS performed by various frameworks. signal plots, tables and graphs are provided for visualizing the results. The test for assessing the performance of signal processing methods can be broadly classified as subjective and objective tests. In subjective testing, listening tests are conducted with many test persons, which implies a considerable effort. This is also achieved by comparing various waveforms and other visual presentations of results. To reduce the huge effort of subjective evaluations we used established objective measures to assess the performance of BSS algorithms. A discussion on performance measures was included in chapter 3.
BSS algorithms focus on the suppression of interfering point sources. Apart from this the limited capability of attenuating background noise of BSS models is considerably improved in our proposed frameworks employing modified algorithms. Though our experiments with real-world data was restricted to four channel with large samples due to technical limitations of the instruments,extension to more channel is straightforward at the expenses of computation time. The easiness of accommodating more channel was proved using benchmarked signals with 7,16 and 20 channels. The application development proposed in the thesis require only a few channels and small elevations in computational complexity do not affect the intended use.

5.2 Evaluation Criteria

Here we choose most popular methods of BSS evaluation techniques like Signal to Interference Ratio (some authors refer the concept as Interference to Signal Ratio (ISR)), Performance index of separability , scatter plot and signal plots to evaluate the performance of the algorithm. As already noted

the discussion on time complexity is mostly superficial. The first two methods are widely used for performance measures of BSS algorithms. Other statistical tests for independence can be performed for evaluation of the algorithm but not popular in literatures. The space-time complexity of the algorithms are not given much importance in the study. This is because the processing speed and space will not become a constraints while developing the critical application based on the frameworks. Here we mostly used the measures like signal to interference ratio and performance Index of separability for the comparisons.

5.2.1 Signal to Interference Ratio

The ratio of the useful signal power to the interference power that determines the performance of the separating system. This concept is also referred as Interface to Signal Ratio (ISR). This performance index could be used for full-rank or non-full rank analysis. The SIR is defined as for each pair of signals (y_i, s_j) [112] [113]. The coefficients a_{ij} are assumed different enough to make the matrix that they form invertible. Thus, there exists a matrix W with coefficients w_{ij}, such that we can separate s_i as

$$SIR\_S_{ij} = -10\ log10\left(\frac{||y_i - s_j||_2^2}{||s_j||_2^2}\right) \tag{5.1}$$

The one component estimation, we have

$$y_i = w_i^T X = (w_i^T A)S = g_i S = g_{ij} s_j \tag{5.2}$$

where y_i and s_j are the estimated component and the j^{th} source, respectively; w_i^T is a row vector of demixing matrix W, g_i is a normalized row vector [0 0 g_{ij} 0 0]. Because y_i is the estimation of s_j, the ideal normalized vector g_i is the unit vector $u_j = [0\ 0 \cdots 1 \cdots 0]$. Therefore, one analysis is successful if and only if its vector g_i similar to one unit vector u_j Actually,

vector g_i is one row of matrix G. So, the quality of each estimated component just depends on one row of matrix G. The more different each row of G is to each corresponding unit vector of $\mathbb{R}^{N\times N}$, the less quality of output we have. The expression which evaluates the succeed of one component separation is defined as

$$SIR\_g = -10\ log10\left(||g_i - u_j||_2^2\right) \tag{5.3}$$

For the problem of multi component estimation, the general procedure will be done as follows: *With each row vector* w_i^T *of matrix* W, *we find the corresponding value of SIR and the order of the most matchable component of the sources.*

5.2.2 Performance Index

The performance indices for separation resemble Amris index and work properly when the sources are normalized to unit variance. The Performance Index (PI), is defined by (5.4)[52][115] [129]

$$PI = \frac{1}{n(n-1)} \sum_{i=1}^{n} \left\{ \left(\sum_{k=1}^{n} \frac{|b_{tk}|}{max_j|b_{ij}|} - 1 \right) \left(\sum_{k=1}^{n} \frac{|b_{ki}|}{max_j|b_{ij}|} - 1 \right) \right\} \tag{5.4}$$

where b_{ij} is the $(i,j)^{th}$ element of the global system matrix B. Global system matrix is obtained by multiplying mixing matrix and demixing matrix. For real world signal it is taken as demixing matrix itself. The term $max_j|b_{ij}|$ is the maximum value along the i^{th} row of B and $max_j|b_{ji}|$ is the maximum value of the i^{th} column of B. When perfect separation is achieved, PI is zero. In practice this is too optimistic.

5.2.3 Scatter Plot

A scatter plot is a mathematical diagram using Cartesian coordinates to show values for typically two variables for a set of data. The data is displayed as a collection of points, having the values of variables determining the position on the axes. Scatter plots show how much one variable is related to another. The relationship between two variables is called their correlation. Scatter plot will illustrate only the degree of correlation between two variables. Scatter plots usually consist of a large body of data. The closer the data points come when plotted to making a straight line, the higher the correlation between the two variables, or the stronger the relationship. If the data points make a straight line going from the origin out to high x- and y-values, then the variables are said to have a positive correlation. If the line goes from a high-value on the y-axis down to a high-value on the x-axis, the variables have a negative correlation. A perfect positive correlation is given the value of 1. A perfect negative correlation is given the value of -1. If there is absolutely no correlation present the value given is 0. The closer the number is to 1 or -1, the stronger the correlation, or the stronger the relationship between the variables. The closer the number is to 0, the weaker the correlation. The scatter pot is good visual tool for evaluating the performance of the algorithm. The degree of correlation of the signal can be easily verified using scatter plot.

5.3 Benchmarked Signals

There are no benchmarked signals available for the performance evaluation of the type GBV signals under consideration. So we selected the signals with similar characteristic for the study. We selected the benchmarked signals[18] with similarity of the signal of the targeted application development. The work on these benchmarked signal can help in the targeted

Benchmarked Signal	No. Samples	Particulars
ABio7.mat	5000	This benchmarked signal contains 7 typical biological sources.This was proposed by Allan Barros
acspeech16.mat	3500	Contains 16 typical speech signals which have a temporal structure but are not precisely independent
Speech20.mat	3500	Benchmarks with 20 sounds (speech and music) sources

Table 5.1: Specification of benchmarked signals

application development. The three selected benchmarked signals and their specification are given in the table (5.1).

The signal plot of the benchmarked signals ABio7 is shown in the figure (5.1). The signal with added reverberation and noise is shown in the figure(5.2). These purposeful signal contamination was carried out to make the signals resembles like real world signal. The contaminated signals were mixed by artificial means using ill-conditioned random weights. The resultant signal plot is shown in the figure (5.3). The SNR of noisy source used is 20 dB. The tables (5.2), (5.3), (5.4), (5.5) show the performance of algorithms FastICA-DECONV, WASOBI-DECONV, SYMWHITE-DECONV and SYMWHITE-WASOBI and their comparisons with the base algorithms. The separation is performed for signals with and without reverberation and noise in the case of existing algorithms and separation is only performed for the contaminated signals in the case of proposed also algorithms. The plot of the signals, separated using WASOBI-DECONV is shown in figure (5.4)as an example. The scatter plot of the separated signals is also shown in figure(5.5). As explained earlier the correlation is more for the closer points making a straight line.

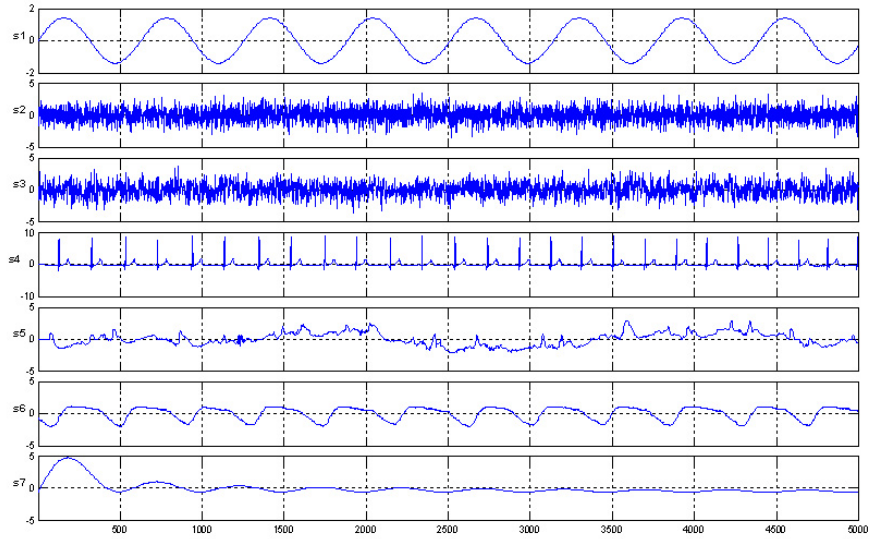

Figure 5.1: Plot of benchmark signal ABio7

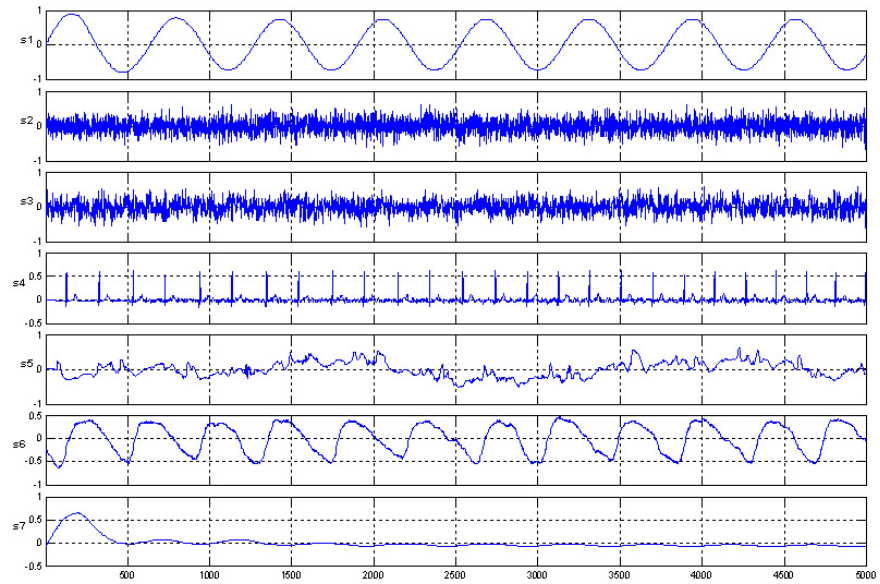

Figure 5.2: Plot of benchmark signal ABio7 with reverberation

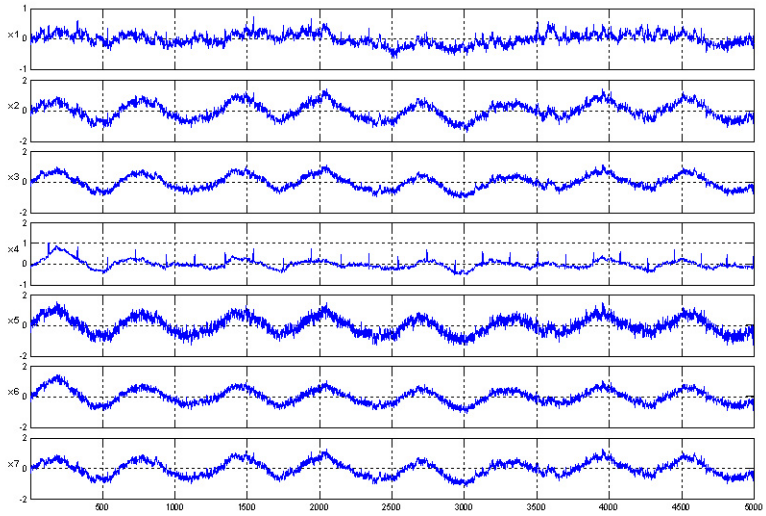

Figure 5.3: Plot of convoluted and mixed benchmark signal ABio7

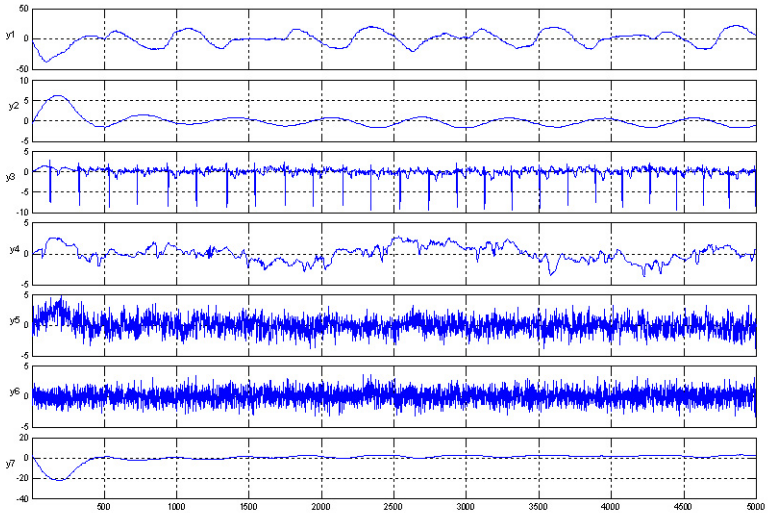

Figure 5.4: Plot of Blind source separated benchmark signal ABio7

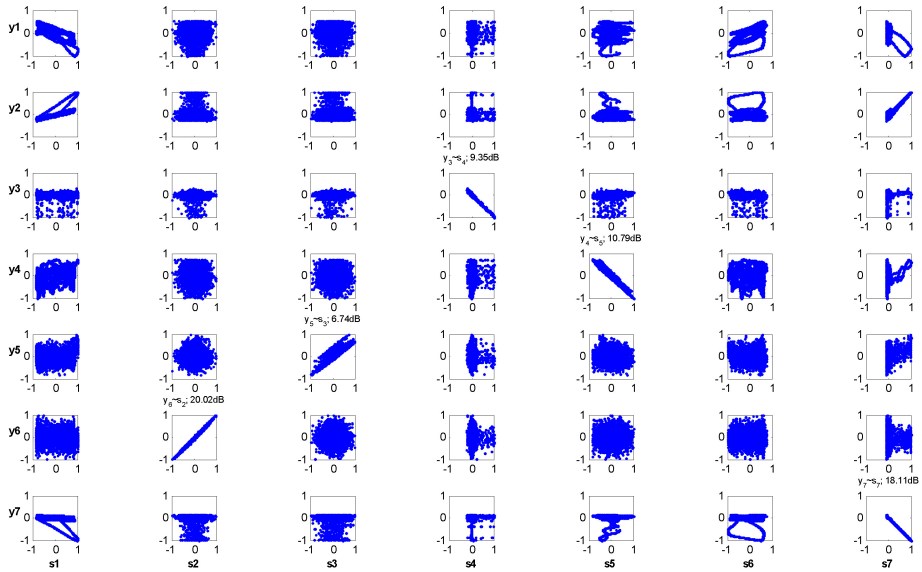

Figure 5.5: Scatter plot of separated benchmark signal ABio7

Algorithm	Signal Type	No of Channels	Benchmarked Signal	Time (s)	PI	SIR of Separated Signal (dB)		
						Mean Value	Highest Value	Lowest Value
WASOBI	No Contamination	7	ABio7	0.29	0.0957	12.1760	24	3
		16	acspeech16	2.91	0.0096	28.9296	58	10
		20	speech20	10.07	0.1248	4.3970	8.1	1.5
	With noise and Reverberation	7	ABio7	0.19	0.0715	10.8355	20	3
		16	acspeech16	3.55	0.1061	5.1732	8.5	1
		20	speech20	10.18	0.1203	4.2774	11	1.8
WASOBI -DECONV	With noise and Reverberation	7	ABio7	1.25	0.0393	22.6000	38	7
		16	acspeech16	4.68	0.0099	19.4416	21	17
		20	speech20	10.55	0.0842	6.4777	13.5	1.8

Table 5.2: Performance of WASOBI and WASOBI-DECONV for benchmarked signals

Algorithm	Signal Type	No of Channels	Benchmarked Signal	Time (s)	PI	SIR of Separated Signal (dB)		
						Mean Value	Highest Value	Lowest Value
SYMWHITE	No Contamination	7	ABio7	0.07	0.4277	2.5960	3.5	2
		16	acspeech16	0.01	0.3435	2.3352	3.2	1.6
		20	speech20	0.02	0.3891	1.2663	2.5	0.2
	With noise and Reverberation	7	ABio7	0.1	0.0166	28.3800	39	14
		16	acspeech16	0.01	0.3796	1.6714	2.4	0.8
		20	speech20	0.01	0.4031	1.2233	1.9	0.7
SYMWHITE -DECONV	With noise and Reverberation	7	ABio7	0.6	0.2631	3.0560	3.6	2.25
		16	acspeech16	0.07	0.0070	19.7154	21	19
		20	speech20	0.5	0.2987	1.9327	4	0.8

Table 5.3: Performance of SYMWHITE and SYMWHITE-DECONV for benchmarked signals

Algorithm	Signal Type	No of Channels	Benchmarked Signal	Time (s)	PI	SIR of Separated Signal (dB)		
						Mean Value	Highest Value	Lowest Value
FastICA	No Contamination	7	ABio7	9.53	0.1379	13.3501	27	2.5
		16	acspeech16	0.4	0.0725	9.8800	23	4
		20	speech20	6.85	0.1648	3.3950	7.5	0.8
	With noise and Reverberation	7	ABio7	14.17	0.2378	5.1515	13.5	1
		16	acspeech16	2.59	0.2002	3.1481	6.5	1.5
		20	speech20	1.96	0.2110	2.7279	5.2	1.5
FastICA -DECONV	With noise and Reverberation	7	ABio7	1.19	0.1629	7.7029	13.5	0.5
		16	acspeech16	1.37	0.0753	10.3326	17	4
		20	speech20	1.73	0.1387	4.1862	8.9	1.5

Table 5.4: Performance of FastICA and FastICA-DECONV for benchmarked signals

Algorithm	Signal Type	No of Channels	Benchmarked Signal	Time (s)	PI	SIR of Separated Signal (dB)		
						Mean Value	Highest Value	Lowest Value
SYMWHITE -WASOBI	With noise and Reverberation	7	ABio7	0.9	0.1077	12.0450	24	3
		16	acspeech16	2.93	0.3641	2.4740	4.2	1.6
		20	speech20	11.03	0.3728	1.9324	2.8	1.4

Table 5.5: Performance of SYMWHITE-WASOBI for benchmarked signals

The figure(5.6) shows the plot of mean SIR of various algorithms on separation of contaminated signals. The figure (5.7) given below shows the performance index of separability of the various algorithms on the contaminated signals.

Discussion on Performance

In general the performance of the frameworks with extended algorithms decrease with signal contaminations and number of channels. We conducted BSS with the modified algorithm namely FastICA-DECONV, WASOBI-DECONV, SYMWHITE-DECONV and SYMWHITE-WASOBI. The signal used was contaminated signal with noise and reverberations. The performance of the frameworks with modified algorithms showed significant improvements. SIR of the separated signals, mean value, the highest and lowest value of the separated components are shown. The quality of separation decreases with increased number of channels. The performance index of separability and time taken for execution is shown for comparison.

5.4 Field Data Collection

The experimental method developed as part of this work is based on the well established method of seismic refraction survey [131]. The fundamental difference is that our method is a multiple sources- multiple sensors method, instead of the signal source- multiple sensor method of seismic refraction survey. A brief introduction of seismic refraction survey is included in the following paragraph.

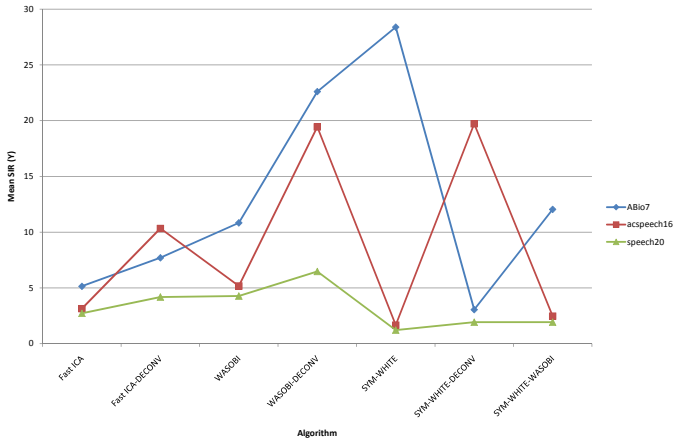

Figure 5.6: Plot of Mean SIR of separated benchmark signals

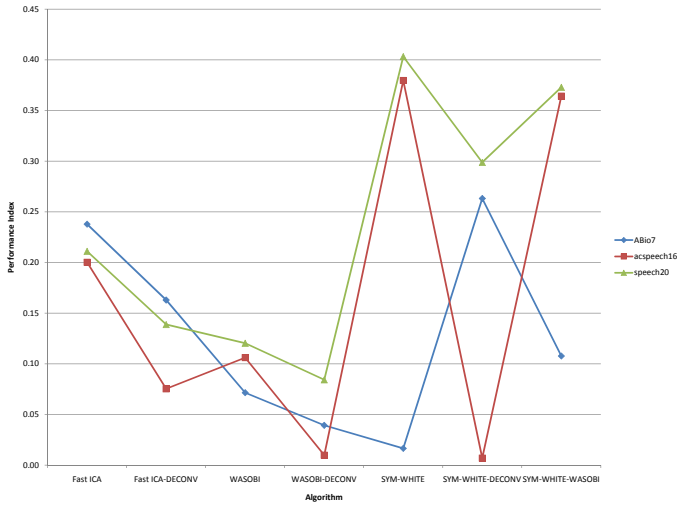

Figure 5.7: Plot of PI of separated benchmark signals

5.4.1 Seismic Refraction Method

The seismic refraction method of subsurface exploration is a non-invasive, geophysical technique primarily used to determine the depth of soil, partially weathered rock (PWR), and competent rock layers utilizing surface-sourced seismic waves. Impulses of low frequency seismic energy are created using a hammer-plate, weight drop or controlled explosion. The type of source is dependent on the ground conditions and required depth penetration. The seismic waves propagate downward through the ground until they are reflected or refracted off subsurface layers. Refracted waves are detected by arrays of 24 or 48 geophones spaced at regular intervals of 1 - 10 meters, depending on the desired depth penetration of the survey. Sources are positioned at each end of the geophones array to produce forward and reverse wave arrivals along the array. The basic components of a seismic trace are the direct wave, the reflected wave and the critically refracted wave. Wave refraction occurs at interfaces in the ground where the seismic velocity of the lower layer is greater than the velocity of the overlying layer. This condition normally applies in near surface site investigations where soil or fill overlies bedrock. At geophones positions close to the seismic source, the first seismic wave arrivals are direct waves. However, beyond a critical distance from the source, the first arrivals change to refracted waves due to the faster relative velocity of the refracted waves. Interpretation procedures involve the accurate measurement of first arrivals from the time traces recorded at each geophone position [131][132].

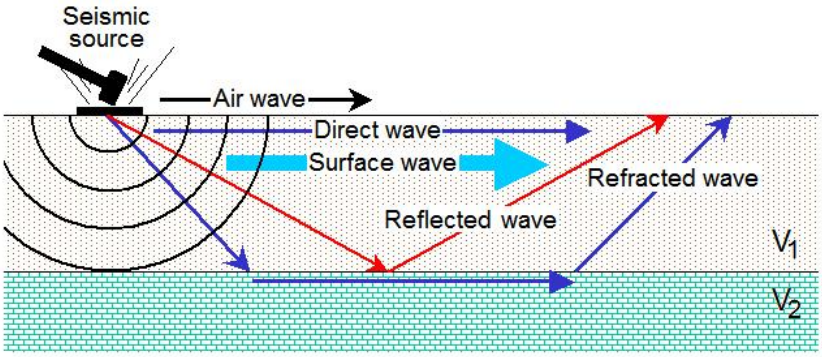

Figure 5.8: Layout of seismic refraction survey using hammer and plate for creating vibration

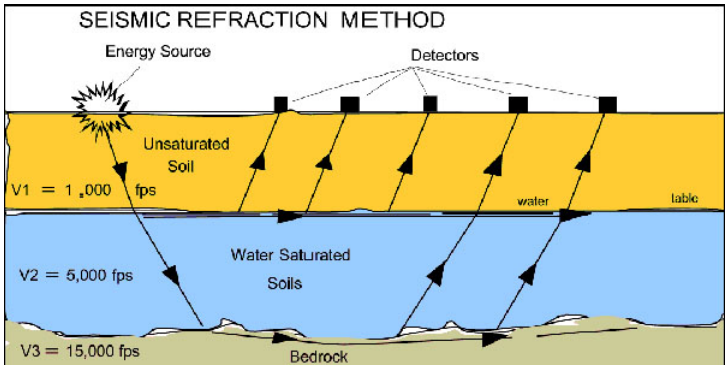

Figure 5.9: Layout of seismic refraction survey using explosion for creating vibration

[133]

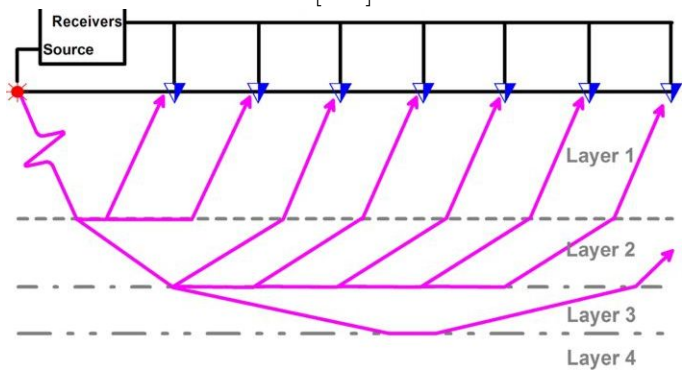

Figure 5.10: Seismic refraction survey: source-receiver arrangements

5.4.2 The Experimental Setup and Prototype

The Sensors

We used the factory calibrated accelerometer Minisense100 [134] as the sensor elements. This sensor element is properly mounted and housed for field measurements. This is a cantilever-type vibration sensor loaded by a mass to offer high sensitivity at low frequencies. The active sensor area is shielded for improved radio-frequency interference / Electromagnetic interference (RFI/EMI) rejection. Rugged, flexible Polyvinylidene fluoride, or polyvinylidene difluoride (PVDF) sensing element withstands high shock overload. Sensor has excellent linearity and dynamic range as shown in figure (5.11) [134], and may be used for detecting either continuous vibration or impacts. The mass may be modified to obtain alternative frequency. When the beam is mounted horizontally, acceleration in the vertical plane creates bending in the beam, due to the inertia of the mass at the tip of the beam. Strain in the beam creates a piezoelectric response, which may be detected as a charge or voltage output across the electrodes of the sensor. The sensor may be used to detect either continuous or impulsive vibration or impacts. The sensitivity at resonance is significantly higher. Impacts containing high-frequency components will excite the resonance frequency, as shown in the plot. It behaves electrically as an active capacitor: it may be modeled as a perfect voltage source (voltage proportional to applied acceleration) in series with the quoted device capacitance. The impedance of the sensor is approximately 650 M ohm at 1 Hz. Every care was taken to electrically shield the accelerometer and the circuits. Figure (5.11) shows the frequency response of the sensors.

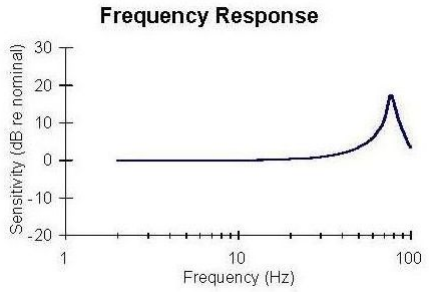

Figure 5.11: Frequency response of the sensors
[134]

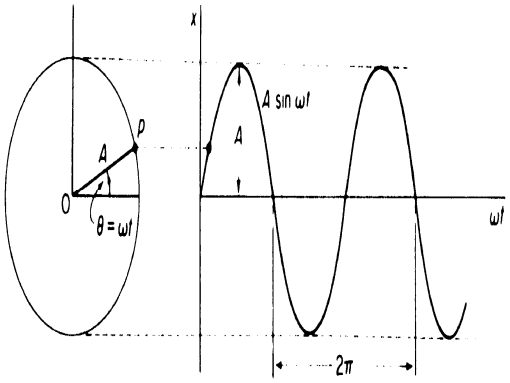

Figure 5.12: Model of eccentric rotating mass

Sources

The vibration sources are *four shakers V1, V2, V3 and V4*. See figure (5.21) (b). The Eccentric Rotating Mass vibration (ERM) motor is a system with a non-symmetric mass attached to the shaft of a motor [135]. These were used as the sources of vibration for the experiment. The mass movement is modeled as a sinusoidal wave as shown in the figure(5.12). The function $ASin\omega t$ is the excitation input, and the frequency of this sine

Source	Frequency peak (Hz) (Fundamental)
V1	118.4
V2	96.9
V3	96.9
V4	107.7

Table 5.6: Experimental source frequency

wave is the frequency at which it vibrates. The one degree of freedom vibration model can be shown as a mass, connected to a spring, with a damping factor. The equation of motion is built from the forces of these three components and the input force We can model the motion for the system mathematically as:

$$F_0 \sin(\omega t) = (M - m)\ \frac{d^2x}{dt^2} + C\frac{dx}{dt} + kx \tag{5.5}$$

where m the mass of the eccentric is mass, and r is the distance from the motor shaft to the center of the eccentric mass,ω is the angular velocity of the motor k stiffness of spring in the model and F_0 is the centripetal force of the eccentric mass.

In the model the first term refers mass of the source except eccentric mass, second term refers damping force and the third term refers to the displacement of the eccentric mass. Theoretically it produces a vibration of sinusoidal pattern. The following table shows the frequency peak in hertz of the vibration sources used for the experiment. Here all the sources are low frequency and two sources are of same frequency.

The Amplifier

We used non-inverting type of charge amplifier [136] for amplification of signals from the sensors. The gain of the amplifier is set using resistors and

Sub units	Specifications
Analog input	Channel: 4 channel input Level:-10 dBV unbalanced impedance: 10 k ohm
Analog output	Channel: 4 channel output level:-10 dBV unbalanced impedance: 100 ohm sampling rate: 44.1 kHz,48 kHz Bits resolution: 16 bits
Analog to digital converter	Dynamic range: 85 dB A-Weighted (typical) Frequency response: 20 ∼20 kHz@fs=48kHz Bits resolution: 18 bits
Digital to analog converter	Dynamic range: 87dB A-Weighted (typical) Frequency response: 20 ∼20 kHz@fs=48kHz Bits resolution: 20 bits

Table 5.7: Specifications of the interface card
[137]

gain here set to 100. The circuit schematic and various characteristics like distortion and noise versus frequency and open loop gain is included for reference in the figures(5.13) (5.14) (5.11) (5.16)

Analog to Digital Converter

We used higher end USB interfaced card supporting low latency driver for converting the output of charge amplifier for our simulation experiments. The specification of the interface card used for experiments is given in table (5.7) and the block schematic is given in the figure (5.17)

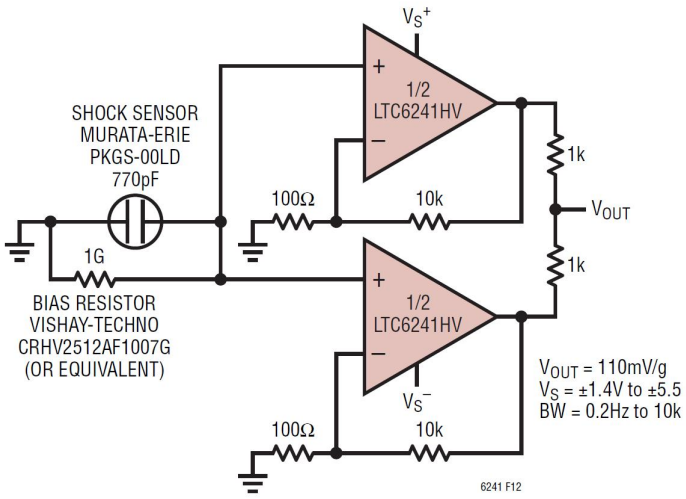

Figure 5.13: Schematic of charge amplifier for sensors [136]

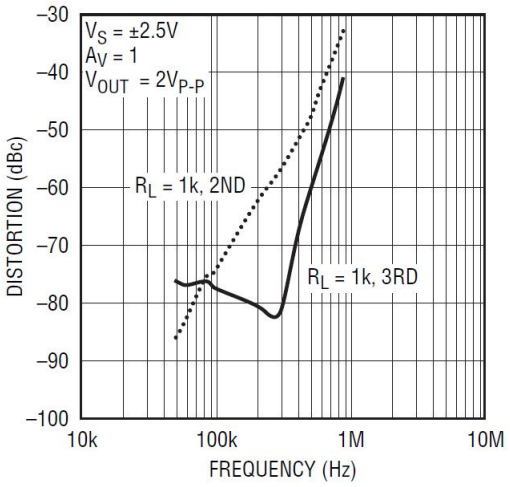

Figure 5.14: Distortion Vs Frequency characteristics of the amplifier [136]

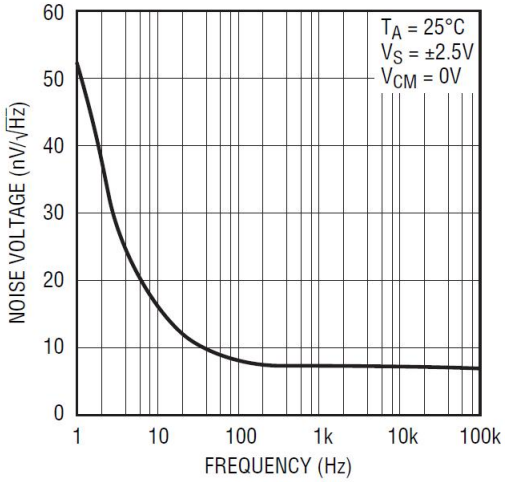

Figure 5.15: Noise Vs Frequency characteristics of the amplifier [136]

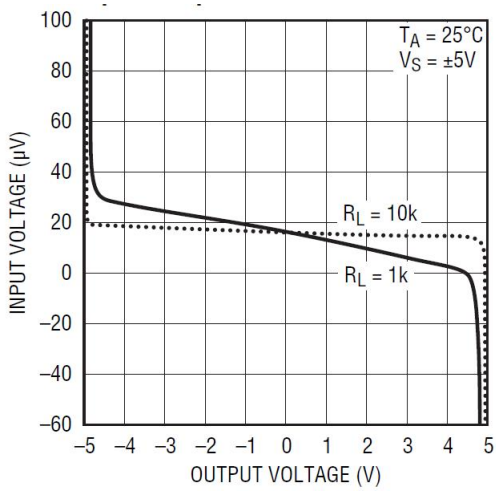

Figure 5.16: Gain characteristics of the amplifier [136]

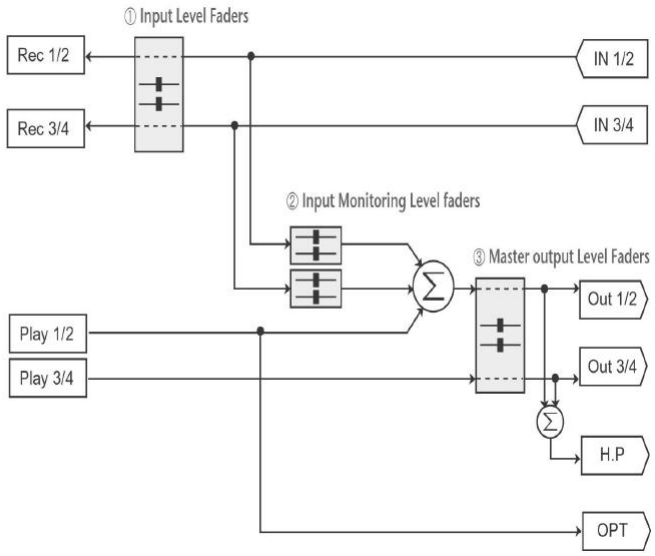

Figure 5.17: Block schematic of the interface card [137]

5.4.3 Experiment on Influence of Earth as a Medium

An independent experiment was conducted to study the influence of the propagation medium on signals. The experiment was conducted at the same geographical area of the main experiments. The influence of earth as a medium on vibration amplitude and signal strength was measured using four sensors at varying source-sensor distance. The sensors were placed at various locations and measurements were taken for vibration source and the graphs were plotted. Here we used a single source with fundamental frequency 107.7 Hz for this experiment. The figure (5.18) shows the Signal to Noise Ratio (SNR) decreases almost linearly with source sensor distance. The effect of non homogeneity of the soil or geography influences the signal strength. The plot of amplitude against source- sensor distance in figure (5.19) also show a similar behavior for the samples.

5.4.4 BSS of GBV-Experimental Procedure

The experiment was conducted using four shakers as the vibration sources capable of producing low level stable vibrations. These sources can be modeled as point sources. The sensors are sensitive vibration sensors with 5 V/g at resonance. The signals are amplified using a low noise amplifier and converted to digital signals using a 18 bit ADC. The setup for field data collection is shown in figure (5.20) and the developed prototype and the subsystems used for field data collection is shown in the figure (5.21)

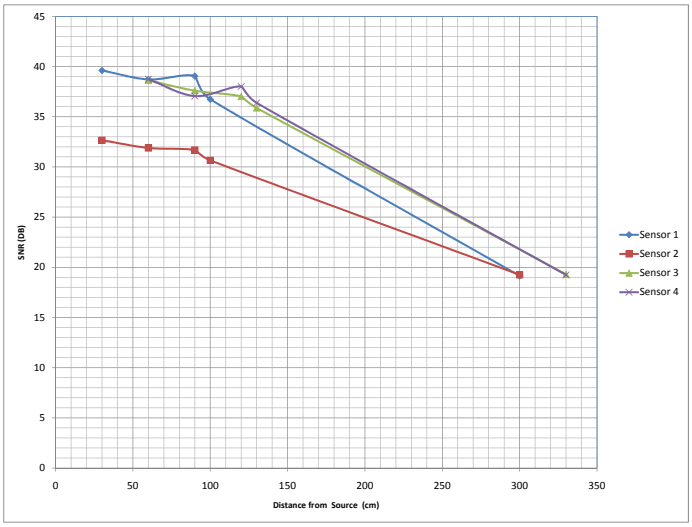

Figure 5.18: Plot showing the variation of SNR with source-sensor distance

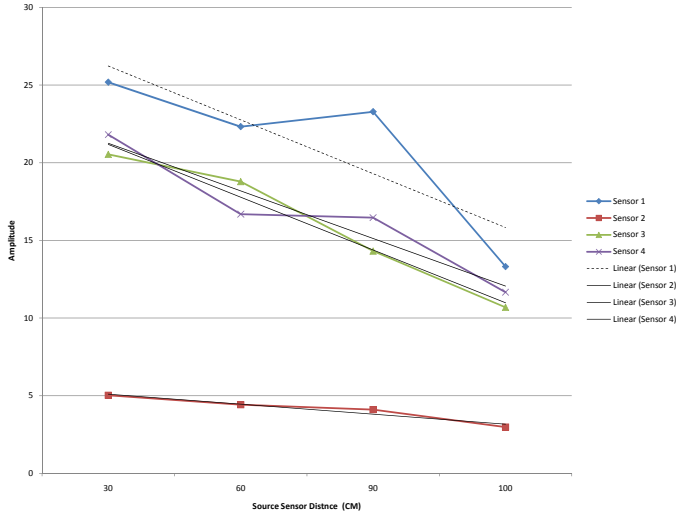

Figure 5.19: Plot showing the variation of signal amplitude with source-sensor distance

(a)

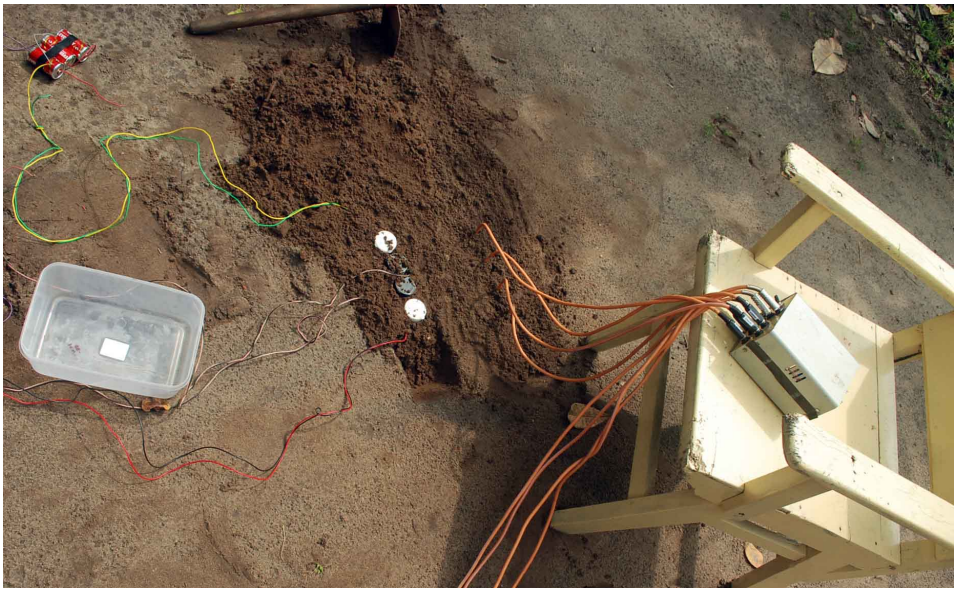

(b)

Figure 5.20: Field data collection using instrument prototype

We considered 3 seconds duration clips. Since the outdoor field measurements are susceptible to weather condition the acquisition of the low level ground vibration is a challenging problem and hence rugged instruments were used.

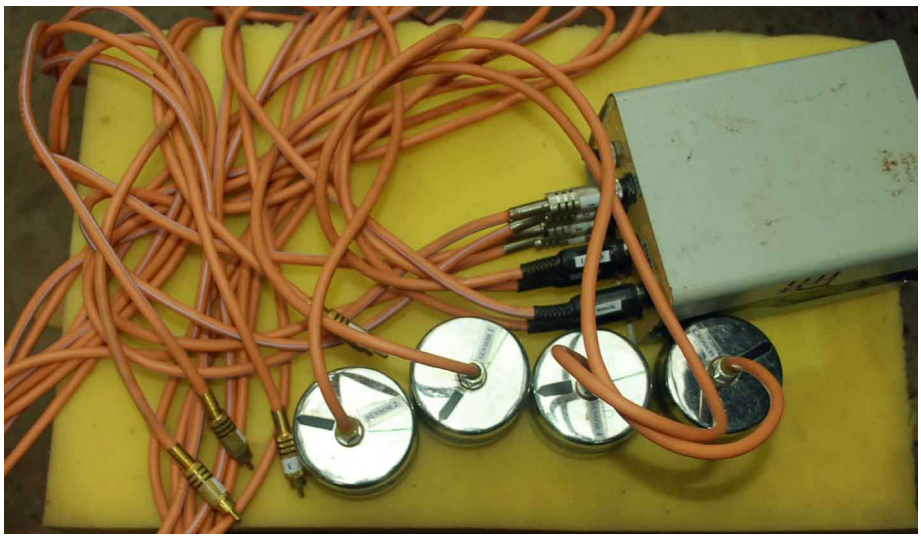

(a) Amplifier

(b) Shakers

(b) Sensor assembly

Figure 5.21: Subsystem for field data collection

The vibration signals from the sources, *four shakers V1, V2, V3 and V4* were recorded in the ground at various perpendicular distances from the line joining the sensors. Both the sensors and sources were buried in ground at a depth not greater than $5\ cm$ and the airborne noise was considered negligible. The signal processing and simulation[138] was performed using MATLAB 7.3 environment. We used 15 sets with 20000 samples for the experiments in each source-sensor distance A general arrangement and data collection procedure for data acquisition is shown in the figure (5.22) (5.23)

5.5 Performance Evaluation and Discussion

The discussion on performance evaluation and visualization of the results are restricted to selected cases of the frameworks due to space constraints.

5.5.1 WASOBI and WASOBI-DECONV

The table (5.8) (5.9) shows the values of Performance Index of algorithm WASOBI and WASOBI-DECONV for different source sensor distance for 15 sets of signals each with 4000 samples. The performance Index of separability for 15 samples for a source sensor distance of 160 cm is given in the figure (5.24). The PI of WASOBI varies between 0.09 and 0.29 and that of WASOBI-DECONV varies between .12 and .39. The figure (5.24) shows WASOBI DECONV out performs the WASOBI algorithm for the set of data. It should be note that the lesser the value of PI better the separation.

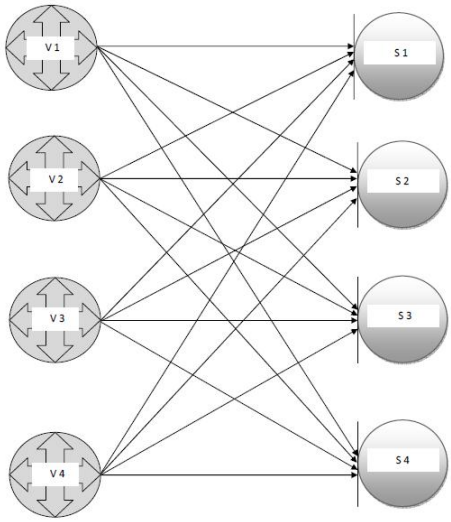

Figure 5.22: The source-sensor arrangement

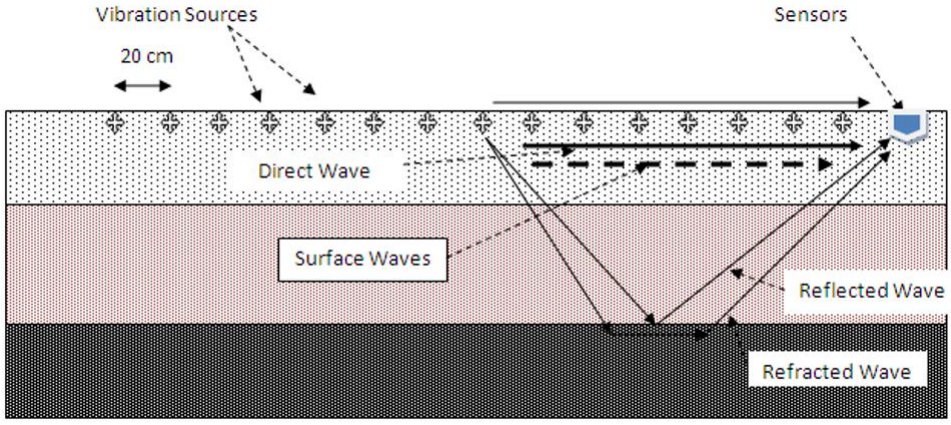

Figure 5.23: Layout of field data collection

Readings	Source-Sensor Distance in cm										
	20	40	60	80	100	120	140	160	180	200	220
Set 1	0.0593	0.1287	0.1895	0.1710	0.1943	0.2166	0.2269	0.2377	0.2748	0.2009	0.2434
Set 2	0.1070	0.1741	0.2109	0.1695	0.1731	0.2293	0.2673	0.2136	0.2807	0.2262	0.2342
Set 3	0.0765	0.1260	0.2463	0.1682	0.1860	0.1772	0.2653	0.2464	0.3131	0.2422	0.3312
Set 4	0.0578	0.1574	0.2643	0.1934	0.1925	0.1521	0.2859	0.2067	0.3268	0.2937	0.2537
Set 5	0.0620	0.1599	0.2266	0.1668	0.2264	0.1835	0.2765	0.2261	0.2624	0.2910	0.2289
Set 6	0.0645	0.1964	0.2285	0.1590	0.2159	0.1798	0.2998	0.2249	0.0645	0.2533	0.2664
Set 7	0.0647	0.1883	0.2515	0.1903	0.2054	0.1725	0.2924	0.2221	0.2721	0.2848	0.2361
Set 8	0.0727	0.1493	0.2401	0.1816	0.1988	0.1670	0.2449	0.2098	0.2767	0.3278	0.2477
Set 9	0.2888	0.1429	0.2186	0.1880	0.1863	0.1709	0.2323	0.2221	0.2720	0.3176	0.2216
Set 10	0.1911	0.1706	0.2342	0.1512	0.2054	0.1899	0.3076	0.2123	0.2511	0.3164	0.3307
Set 11	0.0625	0.1795	0.2458	0.1895	0.2110	0.1872	0.3236	0.2166	0.2721	0.3225	0.2224
Set 12	0.0571	0.1739	0.2430	0.1765	0.1776	0.1755	0.3355	0.1962	0.2580	0.3459	0.2589
Set 13	0.0716	0.1986	0.2363	0.1702	0.1752	0.1990	0.3135	0.2108	0.2605	0.3541	0.2468
Set 14	0.1296	0.1934	0.2353	0.1793	0.1951	0.1600	0.2133	0.2332	0.3116	0.2888	0.2051
Set 15	0.0989	0.1879	0.2516	0.1700	0.1996	0.1752	0.3366	0.2184	0.2955	0.2925	0.2525

Table 5.8: PI of WASOBI for various source sensor distances

Readings	Source-Sensor Distance in cm										
	20	40	60	80	100	120	140	160	180	200	220
Set 1	0.0576	0.0900	0.0550	0.1611	0.1715	0.1897	0.1054	0.2165	0.1866	0.1921	0.3727
Set 2	0.0434	0.1184	0.1063	0.1274	0.1580	0.1426	0.1947	0.1791	0.1873	0.2084	0.2335
Set 3	0.1532	0.0658	0.0733	0.1503	0.1223	0.1725	0.1231	0.1979	0.2058	0.2276	0.3411
Set 4	0.1587	0.0533	0.9335	0.1766	0.1476	0.1427	0.2091	0.1607	0.2019	0.2837	0.2588
Set 5	0.2088	0.0279	0.0675	0.1302	0.1512	0.1578	0.1516	0.1620	0.2053	0.2957	0.2341
Set 6	0.0254	0.0998	0.0798	0.1304	0.1697	0.1371	0.1740	0.1789	0.2201	0.2415	0.2640
Set 7	0.0306	0.1490	0.0817	0.1468	0.1697	0.1502	0.2706	0.1577	0.2279	0.2914	0.2443
Set 8	0.0478	0.0790	0.8694	0.1952	0.1541	0.1302	0.1971	0.1857	0.2386	0.3281	0.2592
Set 9	0.1626	0.0811	0.0869	0.1494	0.1501	0.1591	0.1834	0.1727	0.2473	0.3158	0.2244
Set 10	0.2254	0.1328	0.0624	0.1429	0.0126	0.1443	0.2080	0.1531	0.2269	0.3159	0.3428
Set 11	0.2689	0.4016	0.0580	0.1391	0.3176	0.1559	0.2807	0.1732	0.2201	0.3224	0.2275
Set 12	0.0681	0.1334	0.0799	0.1352	0.0206	0.1472	0.1836	0.1265	0.2233	0.3460	0.2565
Set 13	0.2385	0.1624	0.8412	0.1454	0.1340	0.1392	0.2058	0.1409	0.2237	0.3556	0.2553
Set 14	0.1294	0.1527	0.5943	0.1464	0.0154	0.1266	0.1696	0.1698	0.2302	0.2902	0.2165
Set 15	0.1236	0.1527	0.6754	0.1481	0.1516	0.1333	0.2066	0.1852	0.2348	0.2811	0.2584

Table 5.9: PI of WASOBI-DECONV for various source sensor distances

Source-Sensor Distance (cm)	Time to converge (s)	Avg.PI	Avg.SIR (W) (dB)
20	0.1833	0.0976	16.6013
40	0.1887	0.1684	12.4446
60	0.1760	0.2348	6.6789
80	0.1156	0.1961	12.9307
100	0.1613	0.1962	14.0566
120	0.1343	0.2014	12.0189
140	0.1627	0.2814	8.5453
160	0.1600	0.1701	10.1780
180	0.1587	0.2661	8.6413
200	0.1613	0.2905	6.3227
220	0.1540	0.2520	6.1315

Table 5.10: Performance of WASOBI

The table (5.10) (5.11) shows the average PI and average SIR of the demixing matrix W and the time to separate the components in our experimental computing environment. The performance index of WASOBI and WASOBI-DECONV with various source-sensor distances in figure (5.25) shows a linear degradation of the performance with distance. This degradation is more for WASOBI and the performance of WASOBI-DECONV is better for all source-sensor distance

Figure (5.26) shows the signal to Interference Ratio (SIR) of different signals on separation with WASOBI-DECONV. The graph shows that some components have higher value of SIR. This shows that the component is separated more effectively. The separation decreases slightly with increase in source- sensor distance. In the case of SIR, higher the value the better the separation is.

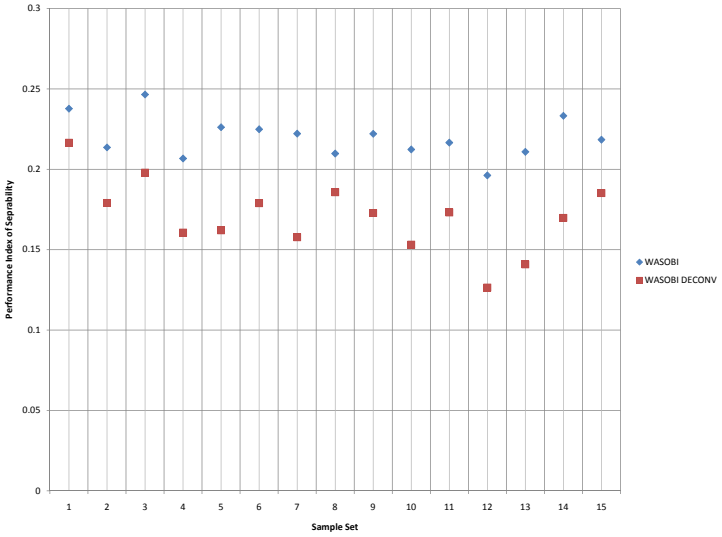

Figure 5.24: Performance of WASOBI and WASOBI-DECONV algorithm for source-sensor distance equal to 160 cm

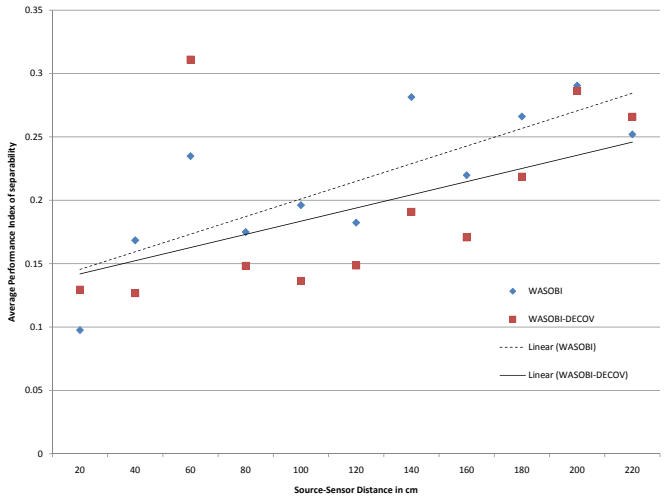

Figure 5.25: Performance index of WASOBI and WASOBI-DECONV with various source-sensor distances

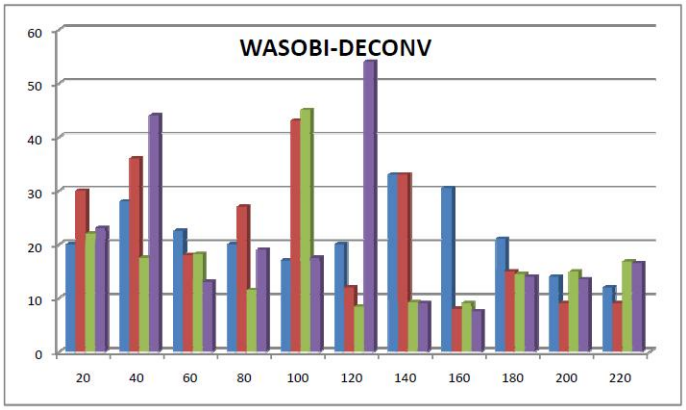

Figure 5.26: SIR of separated components with WASOBI-DECONV algorithm for various source-sensor distances

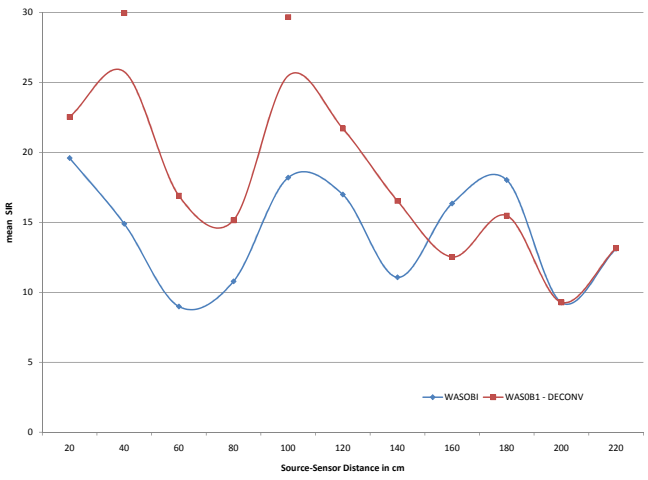

Figure 5.27: Mean SIR of separated components with WASOBI and WASOBI-DECONV algorithm for various source-sensor distances

Source-Sensor Distance (cm)	Time to converge (s)	Avg.PI	Avg.SIR (W) (dB)
20	0.1607	0.1295	13.5770
40	0.1750	0.1248	25.2291
60	0.1713	0.3110	20.7721
80	0.1701	0.1483	19.3860
100	0.1700	0.1364	28.9728
120	0.1660	0.1486	25.6249
140	0.1693	0.1909	11.3312
160	0.1720	0.1707	11.3827
180	0.1653	0.2186	10.0538
200	0.1633	0.2864	6.6486
220	0.1653	0.2659	6.0160

Table 5.11: Performance of WASOBI-DECONV

The plot(5.27) of the SIR of separated components with WASOBI and WASOBI-DECONV algorithm for various source-sensor distances shows a good separation for a sourcesensor distance upto 140cm. The performance of algorithm decreses beyond 180 cm. The performance of WASOBI-DECONV shows degradation with distance and coincides with WASOBI algorithm.

5.5.2 SYMWHITE and SYMWHITE DECONV

The performance Index of separability for 15 samples for a source sensor distance of 80 cm is plotted in the figure(5.28). The PI of SYMWHITE varies between 0.26 and 0.31 and that of SYMWHITE-DECONV varies between 0 .15 and 0.20. The figure shows SYMWHITE-DECONV out performs the SYMWHITE algorithm for the set of data. It should be note that the lesser the value of PI better the separation. The performance

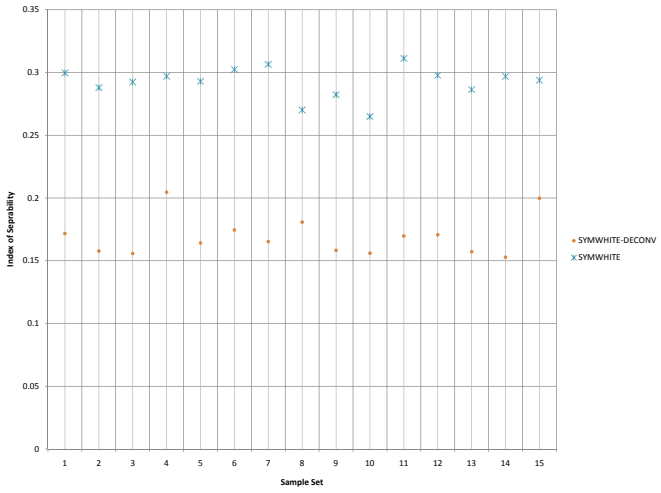

Figure 5.28: Performance of SYMWHITE and SYMWHITE DECONV algorithm for source-sensor distance equal to 80 cm

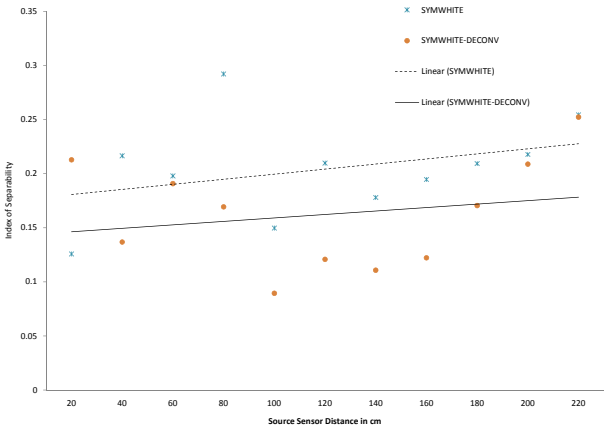

Figure 5.29: Performance index of SYMWHITE and SYMWHITE-DECONV with various source-sensor distances

index of SYMWHITE and SYMWHITE-DECONV with various source-sensor distances in figure(5.29) shows a linear degradation of the performance with distance. This degradation is more for SYMWHITE and the performance of SYMWHITE-DECONV is better for all source-sensor distance. Figure(5.30) shows the signal to Interference Ratio (SIR) of different signals on separation with SYMWHITE-DECONV. The graph shows that some components have higher value of SIR. This shows that the component is separated more effectively. The separation performance very slight decreases only with increase in source- sensor distance. In the case of SIR, higher the value the better the separation.

The plot of the SIR of separated components with SYMWHITE-DECONV and SYMWHITE algorithms for various source-sensor distances in figure (5.31) shows a fair separation up to a source sensor distance up to 200 cm. The performance of algorithm decreases beyond 200 cm. The performance of SYMWHITE-DECONV shows degradation with distance and coincides with SYMWHITE algorithm. The table (5.12) (5.13) shows the performance index of separability of SYMWHITE and SYMWHITE-DECONV for various source-sensor distances and for different set of data. The table (5.14) (5.15) shows the average PI and average SIR of the demixing matrix W and the time to separate the components in our experimental computing environment.

Readings	Source-Sensor Distance in cm										
	20	40	60	80	100	120	140	160	180	200	220
Set 1	0.1291	0.2343	0.1934	0.2997	0.1471	0.3201	0.1938	0.2129	0.1928	0.1440	0.3103
Set 2	0.1266	0.2362	0.2023	0.2879	0.1339	0.2870	0.2046	0.2114	0.1809	0.1627	0.3725
Set 3	0.1313	0.2282	0.2060	0.2924	0.1438	0.1899	0.1883	0.2120	0.1794	0.1795	0.3303
Set 4	0.1240	0.2014	0.2106	0.2970	0.1422	0.1965	0.2209	0.1900	0.1869	0.1997	0.2217
Set 5	0.1253	0.2127	0.1924	0.2930	0.1437	0.2152	0.1886	0.1899	0.1861	0.2092	0.2261
Set 6	0.1122	0.2284	0.1913	0.3025	0.1586	0.1888	0.1884	0.2009	0.2201	0.1829	0.2236
Set 7	0.1231	0.2304	0.2083	0.3065	0.1819	0.2102	0.1473	0.1965	0.2477	0.2081	0.2311
Set 8	0.1251	0.1139	0.2112	0.2701	0.1768	0.1830	0.1491	0.1849	0.2640	0.2347	0.2385
Set 9	0.1282	0.2148	0.1755	0.2823	0.1513	0.2004	0.1598	0.1881	0.2538	0.2300	0.2424
Set 10	0.1252	0.2145	0.1863	0.2650	0.1578	0.1969	0.1719	0.1935	0.2253	0.2445	0.2760
Set 11	0.1248	0.2237	0.2031	0.3113	0.1337	0.2101	0.1294	0.1858	0.1980	0.2481	0.2126
Set 12	0.1275	0.2234	0.1972	0.2978	0.1124	0.1916	0.1737	0.1871	0.1954	0.2482	0.2310
Set 13	0.1283	0.2371	0.1963	0.2863	0.1461	0.1987	0.1874	0.1758	0.1988	0.2619	0.2277
Set 14	0.1275	0.2242	0.1968	0.2969	0.1789	0.1612	0.1739	0.1941	0.2009	0.2976	0.2366
Set 15	0.1271	0.2244	0.1979	0.2938	0.1364	0.1956	0.1920	0.1954	0.2095	0.2147	0.2355

Table 5.12: PI of SYMWHITE for various source sensor distances

Readings	Source-Sensor Distance in cm										
	20	40	60	80	100	120	140	160	180	200	220
Set 1	0.1055	0.1579	0.8689	0.1716	0.0982	0.1948	0.1017	0.1460	0.1391	0.1119	0.3051
Set 2	0.0993	0.1250	0.1342	0.1578	0.0827	0.1634	0.1179	0.1560	0.1390	0.1362	0.3465
Set 3	0.1026	0.1281	0.1117	0.1558	0.0727	0.1398	0.1012	0.1475	0.1458	0.1602	0.3303
Set 4	0.1078	0.1222	0.2087	0.2046	0.0789	0.0920	0.1455	0.1123	0.1494	0.1900	0.2217
Set 5	0.1086	0.1244	0.2223	0.1642	0.1527	0.1288	0.1096	0.1296	0.1487	0.2091	0.2261
Set 6	0.0957	0.1105	0.1860	0.1745	0.1437	0.1140	0.1043	0.1049	0.1671	0.1650	0.2236
Set 7	0.0904	0.1409	0.1690	0.1654	0.1208	0.1292	0.0689	0.1139	0.1984	0.2033	0.2311
Set 8	0.1008	0.1512	0.1654	0.1808	0.1070	0.1065	0.0907	0.1268	0.2182	0.2321	0.2385
Set 9	0.8858	0.1380	0.2620	0.1583	0.1027	0.0878	0.1148	0.1218	0.2167	0.2253	0.2424
Set 10	0.1057	0.1332	0.0805	0.1560	0.0472	0.1009	0.1096	0.1151	0.1966	0.2420	0.2760
Set 11	0.1017	0.1415	0.0909	0.1697	0.0604	0.1293	0.1167	0.1272	0.1722	0.2479	0.2126
Set 12	0.0980	0.1357	0.0817	0.1707	0.0685	0.1237	0.0992	0.1014	0.1646	0.2452	0.2310
Set 13	0.1087	0.1559	0.0979	0.1572	0.0744	0.1164	0.1277	0.0921	0.1705	0.2608	0.2277
Set 14	0.9739	0.1451	0.0822	0.1528	0.0459	0.0739	0.1345	0.1313	0.1678	0.2972	0.2366
Set 15	0.1073	0.1415	0.1005	0.1998	0.0845	0.1109	0.1180	0.1063	0.1633	0.2059	0.2355

Table 5.13: PI of SYMWHITE-DECONV for various source sensor distances

Source-Sensor Distance (cm)	Time to converge (s)	Avg.PI	Avg.SIR (W) (dB)
20	0.0133	0.1257	15.2971
40	0.0187	0.2165	10.1047
60	0.0167	0.1979	8.2733
80	0.0180	0.2922	9.5625
100	0.0167	0.1497	15.8600
120	0.0167	0.2097	11.8528
140	0.0180	0.1779	12.7070
160	0.0160	0.1946	12.1663
180	0.0187	0.2093	11.3686
200	0.0187	0.2177	9.2704
220	0.0127	0.2544	9.1963

Table 5.14: Performance of SYMWHITE

5.5.3 SYMWHITE and SYMWHITE-WASOBI

The performance Index of separability for 15 samples for a source sensor distance of 80 cm is plotted in figure (5.32). The PI of SYMWHITE varies between 0.26 and 0.31, SYMWHITE-WASOBI varies between 0 .16 and 0.18 and that of WASOBI varies between 0.15 and 0.19. The figure shows SYMWHITE-WASOBI performance is slightly inferior to WASOBI and better than SYMWHITE for the particular distance. It should be note that the lesser the value of PI better the separation.

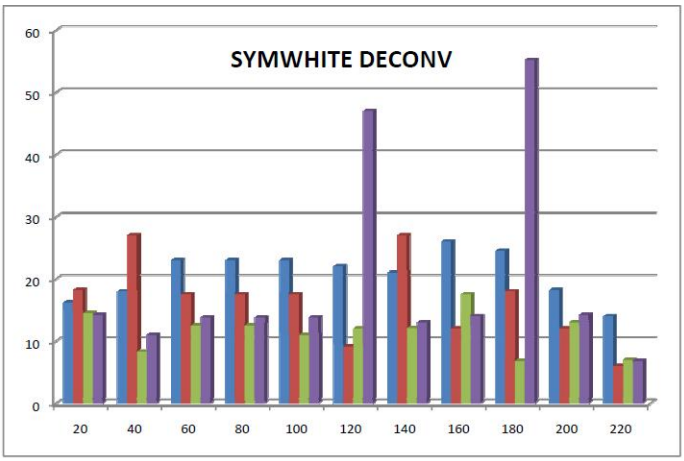

Figure 5.30: SIR of separated components with SYMWHITE-DECONV algorithm for various source-sensor distances

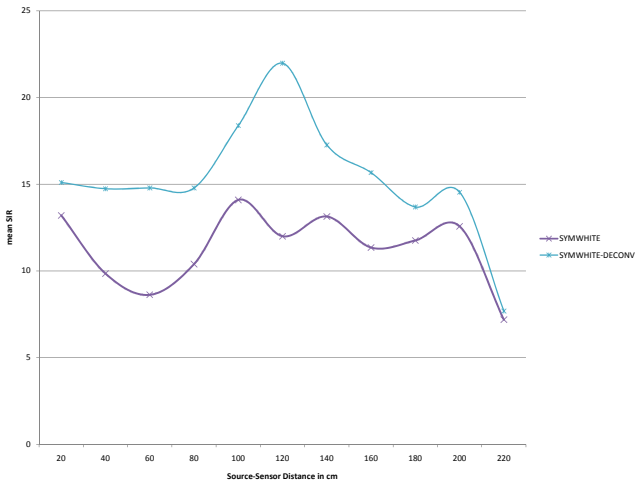

Figure 5.31: Mean SIR of separated components with SYMWHITE-DECONV and SYMWHITE algorithm for various source-sensor distances

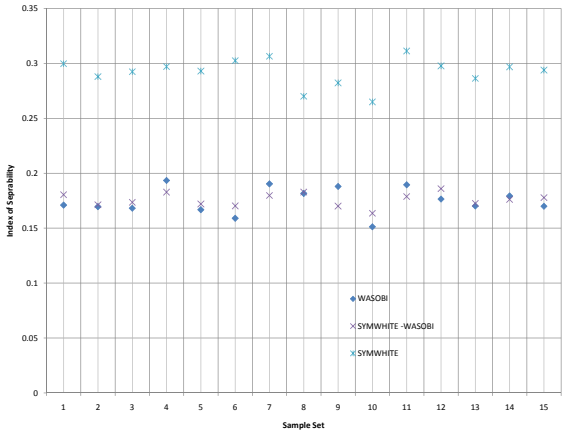

Figure 5.32: Performance of WASOBI, SYMWHITE and SYMWHITE-WAOBI algorithm for source-sensor distances equal to 80 cm

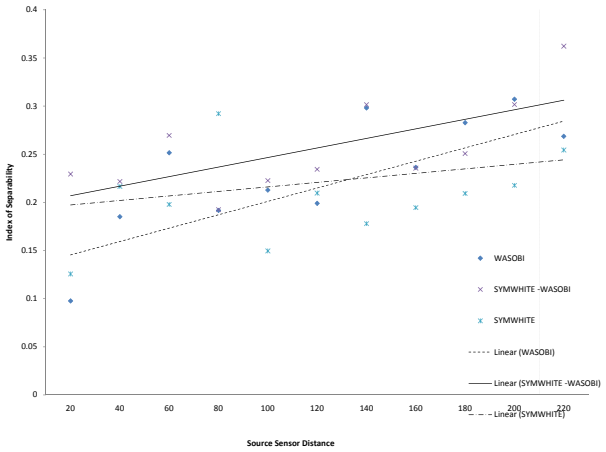

Figure 5.33: Performance index of SYMWHITE, WASOBI and SYMWHITE -WASOBI with various source-sensor distances

Source-Sensor Distance (cm)	Time to converge (s)	Avg.PI	Avg.SIR (W) (dB)
20	0.0173	0.2128	17.9100
40	0.0167	0.1367	18.1400
60	0.0167	0.1908	17.1286
80	0.0167	0.1693	18.2171
100	0.0180	0.0894	28.5653
120	0.0160	0.1208	22.6951
140	0.0173	0.1107	16.4709
160	0.0367	0.1221	15.8557
180	0.0367	0.1705	13.0159
200	0.0387	0.2088	9.8036
220	0.0387	0.2523	9.2713

Table 5.15: Performance of SYMWHITE-DECONV

Readings	Source-Sensor Distance in cm										
	20	40	60	80	100	120	140	160	180	200	220
Set 1	0.1055	0.1851	0.2045	0.1804	0.2140	0.3677	0.2654	0.2358	0.2175	0.2007	0.4991
Set 2	0.0993	0.1960	0.2098	0.1712	0.2237	0.2971	0.2438	0.2209	0.2215	0.2198	0.4653
Set 3	0.1026	0.1509	0.2476	0.1736	0.1984	0.2251	0.2313	0.2470	0.2545	0.2335	0.3312
Set 4	0.1078	0.1847	0.2718	0.1828	0.2200	0.2082	0.2586	0.2052	0.2682	0.2843	0.3342
Set 5	0.1086	0.1935	0.2650	0.1720	0.2438	0.2017	0.3409	0.2278	0.2266	0.2852	0.2984
Set 6	0.0957	0.2334	0.2652	0.1703	0.2185	0.1880	0.2949	0.2262	0.2425	0.2477	0.3972
Set 7	0.0904	0.2213	0.2596	0.1797	0.1935	0.2050	0.3117	0.2166	0.2306	0.2770	0.2864
Set 8	0.1008	0.1916	0.2320	0.1828	0.1846	0.1927	0.2522	0.2044	0.2374	0.3198	0.2952
Set 9	0.8858	0.1718	0.2610	0.1700	0.1915	0.2032	0.2455	0.2187	0.2431	0.3135	0.3021
Set 10	0.1057	0.2229	0.2639	0.1636	0.2070	0.2071	0.3059	0.2113	0.2301	0.3105	0.3544
Set 11	0.1017	0.1779	0.2596	0.1788	0.2194	0.2043	0.3451	0.2124	0.2187	0.3193	0.3208
Set 12	0.0980	0.2477	0.2479	0.1859	0.2012	0.1822	0.3323	0.1904	0.2193	0.3442	0.3191
Set 13	0.1087	0.2412	0.2751	0.1726	0.2158	0.1951	0.3068	0.2119	0.2125	0.3478	0.2825
Set 14	0.9739	0.2246	0.2749	0.1761	0.1682	0.1963	0.2160	0.2369	0.2456	0.2848	0.4144
Set 15	0.1073	0.2345	0.2569	0.1778	0.1917	0.1929	0.3232	0.2182	0.2433	0.2879	0.2842

Table 5.16: PI of SYMWHITE-WASOBI for various source sensor distances

Source-Sensor Distance (cm)	Time to converge (s)	Avg.PI	Avg.SIR (W) (dB)
20	0.0173	0.2128	17.9100
40	0.1660	0.2051	8.5746
60	0.0173	0.1664	17.0819
80	0.0917	0.1694	16.4275
100	0.1600	0.2061	9.2624
120	0.0731	0.1683	16.2321
140	0.0731	0.1683	16.2321
160	0.0876	0.1694	15.4743
180	0.0855	0.1755	14.5256
200	0.1740	0.2851	6.3097
220	0.1600	0.3456	5.5158

Table 5.17: Performance of SYMWHITE-WASOBI

The performance index of SYMWHITE, WASOBI and SYMWHITE-WASOBI with various source-sensor distances in figure (5.33)shows a linear degradation of the performance with distance. This degradation is more for WASOBI and the performance of SYMWHITEWASOBI and WASOBI coincides at a distance of 220 cm.

The plot (5.34) of the SIR of separated components with WASOBI, SYMWHITE and SYMWHITE-WASOBI algorithms for various source-sensor distances shows a fair separation. The performance of SYMWHITE algorithm decreases beyond 200 cm. The performance of SYMWHITE-WASOBI is not showing much variation with distance. The table (5.16) shows the performance index of separability of SYMWHITE-WASOBI for various source-sensor distances and for different set of data. The table (5.17) shows the average PI and average SIR of the demixing matrix W and the time to separate the components in our experimental computing environment.

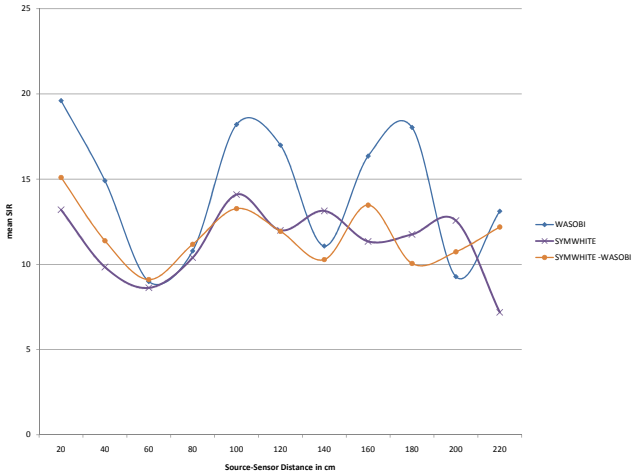

Figure 5.34: Mean SIR of separated components with WASOBI, SYMWHITE and SYMWHITE-WASOBI algorithm for various source-sensor distances

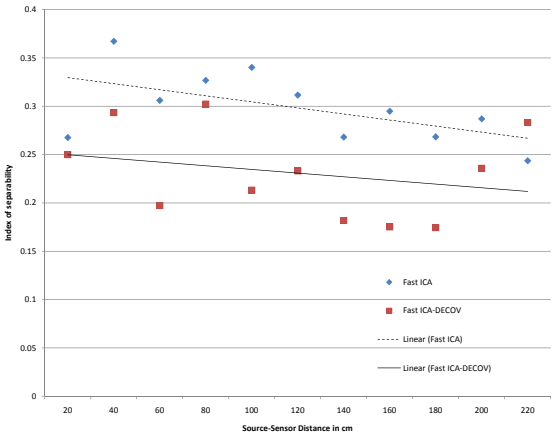

Figure 5.35: Performance index of FastICA and FastICA-DECONV with various source-sensor distances

Source-Sensor Distance (cm)	Time to converge (s)	Avg.PI	Avg.SIR (W) (dB)
20	0.5200	0.2677	9.3965
40	0.5750	0.3672	7.0763
60	0.4750	0.3061	7.4887
80	0.7050	0.3268	9.0803
100	0.5350	0.3402	7.4351
120	0.6600	0.3116	9.4648
140	0.6300	0.2681	7.7455
160	0.7150	0.2949	7.5430
180	0.4950	0.2683	11.3697
200	0.4550	0.2870	9.5913
220	0.6950	0.2437	9.4569

Table 5.18: Performance of FastICA

5.5.4 FastICA and FastICA-DECONV

The performance index of FastICA and FastICA-DECONV with various source-sensor distances in figure (5.35) shows a slight improvement in the performance with distance. This behavior is very different from the other algorithms considered. This is because of the parameters of the captured signals varies with distance. The plot (5.36) of the SIR of separated components with FastICA-DECONV algorithm for various source-sensor distances shows a fair separation . The performance of FastICA-DECONV algorithm shows an exponential decreases beyond 180 cm. The performance of FastICA shows a slight improvement with increase in distance. The table (5.18) (5.19) shows the average PI and average SIR of the demixing matrix W and the time to separate the components in our experimental computing environment.

Source-Sensor Distance (cm)	Time to converge (s)	Avg.PI	Avg.SIR (W) (dB)
20	0.6350	0.2499	20.3031
40	0.4150	0.2934	22.9334
60	0.4350	0.1972	19.1646
80	0.6500	0.3023	13.3294
100	0.5700	0.2132	14.4268
120	0.6150	0.2332	16.7149
140	0.4400	0.1818	22.0261
160	0.5250	0.1752	16.1132
180	0.5550	0.1744	22.1980
200	0.5300	0.2359	16.2800
220	0.7550	0.2832	6.8752

Table 5.19: Performance of FastICA-DECONV

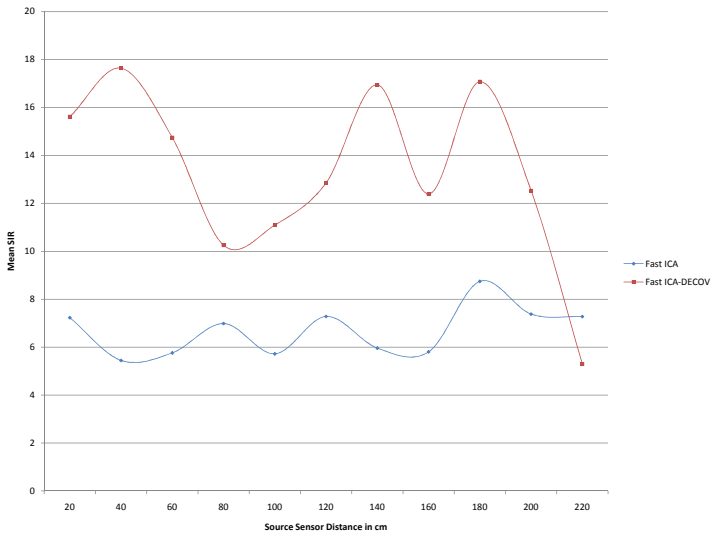

Figure 5.36: Mean SIR of separated components with FastICA and FastICA-DECONV algorithm for various source-sensor distances

5.6 Summary

The BSS were preformed using new frameworks with existing algorithms and with modified algorithms. We used three sets of benchmarked signals with different statistical properties and behaviors closely related to our target real world signals. The real world signals from actual field experiments with various source-sensor distances were source separated using existing as well as proposed algorithms. The discussion on the performance of various algorithms was included in the chapter. The study of the behavior of the propagation medium on amplitude and SNR was conducted and graph for various source sensor were plotted. The field data collection method, and the standard procedure for seismic refraction survey were narrated in the chapter. The details of various sub-units and the instrument prototype developed used for data collection and the performance characteristics were included in this chapter.

Chapter 6

Comparative Analysis and Discussion

6.1 Introduction

This chapter includes the performance evaluation of the new frameworks with modified algorithms. The performance evaluation of SYMWHITE-WASOBI is also included. The performance was evaluated for the benchmarked signals with synthetic mixing as well as for real world signals. The performance of the frameworks with base algorithms and modified algorithms were compared in the previous chapter. A detailed performance comparisons of the new frameworks with modified algorithms as the core were conducted. The results of the study and comparison is included in this chapter. The signal to interference ratio (SIR) and performance index of separability or index of separability of each algorithm is plotted for benchmarked as well as captured real world signals. The plots of selected source signals and processed signals are also included. The scatter plots (with normalized values) of source signals against separated components are plotted

for comparison of performance. *In the various signal plots X-axis shows signal samples and Y-axis shows normalised amplitudes.*

6.2 Comparison of New Frameworks with Modified Algorithms for Benchmarked Signals

Figure (6.1) shows the mean SIR of the four algorithms for benchmarked signals namely *ABio7, acspeech16 and Speech20.* The graph shows that maximum separation is achieved by WASOBI-DECONV. The separation by FastICA-DECONV and SYMWHITE-DECONV shows a good separation for the signal acspeech16. All the three algorithms show lowest separation performance for speech20.

Figure (6.2) shows the trend of the new algorithm for the three benchmarked signals ABio7, acspeech16 and Speech20 with number of channels 7, 16 and 20 and having different statistical properties. SIR of separated signals for the four algorithms shows negative slopes characteristics. WASOBI-DECONV shows the highest deterioration in performance and FastICA-DECONV shows the lowest. It should be noted that the performance of WASOBI-DECONV is the best and SYMWHITE-DECONV is the lowest. The figure (6.3) shows SIR of highest separated components. SYMWHITE-WASOBI gives the highest SIR value. In the figure(6.4) SYMWHITE-WASOBI shows different behavior compare to other algorithms. It shows the highest separation for the signal acspeech16. We can infer that all the algorithms could separate at least one component clearly from the signals. The table (6.1) shows the performance of the modified algorithm on bench marked signals. The table shows performance of separability and mean SIR of the separated components. The time for computation of the modified algorithm is also shown.

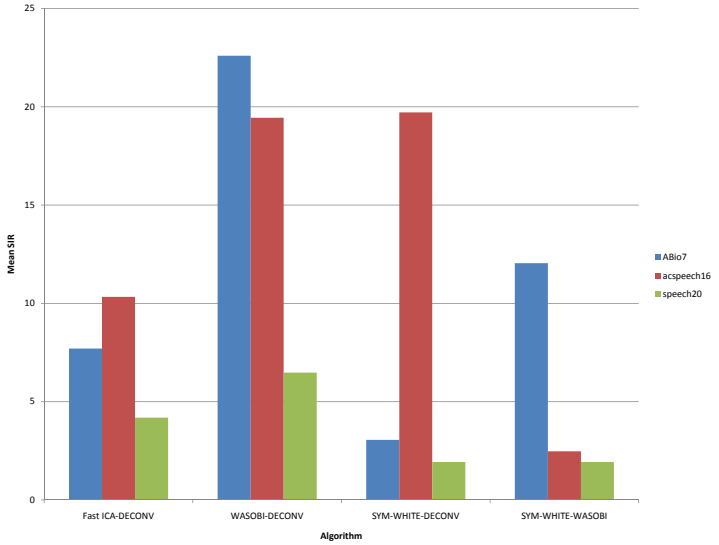

Figure 6.1: Mean SIR of algorithms for benchmarked signals

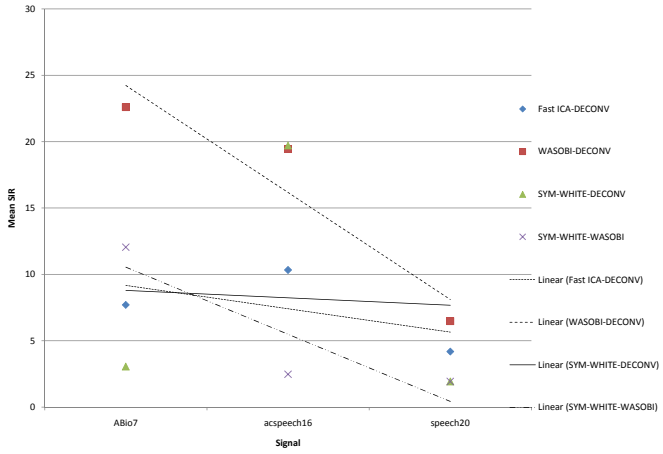

Figure 6.2: Performance comparison of algorithms based on SIR

Algorithm	No of Channels	Signal	Time (s)	PI	Mean SIR (dB)
WASOBI-DECONV	7	ABio7	1.25	0.0393	22.6
	16	acspeech16	4.68	0.0098	19.44
	20	speech20	10.55	0.0842	6.48
SYMWHITE-DECONV	7	ABio7	0.6	0.2631	3.06
	16	acspeech16	0.07	0.0070	19.72
	20	speech20	0.5	0.2987	1.93
FastICA-DECONV	7	ABio7	1.19	0.1629	7.70
	16	acspeech16	1.37	0.0753	10.33
	20	speech20	1.73	0.1387	4.19
SYMWHITE-WASOBI	7	ABio7	0.9	0.1077	12.05
	16	acspeech16	2.93	0.36410	2.474
	20	speech20	11.03	0.372848	1.9324

Table 6.1: Performance of new frameworks with modified algorithms on benchmarked signals

Source-Sensor Dist.(cm)	WASOBI-DECONV		SYMWHITE-DECONV		FastICA-DECONV		SYMWHITE-WASOBI	
	PI	SIR(W) (dB)	PI	SIR(W) (dB)	PI	SIR(W) (dB)	PI	SIR(W) (dB)
20	0.1295	13.58	0.2128	17.91	0.2499	20.30	0.2128	17.91
40	0.1248	25.23	0.1367	18.14	0.2934	22.93	0.2051	8.57
60	0.3110	20.77	0.1908	17.13	0.1972	19.16	0.2128	17.91
80	0.1483	19.39	0.1693	18.22	0.3023	13.33	0.2090	13.24
100	0.1364	28.97	0.0894	28.57	0.2132	14.43	0.2061	9.26
120	0.1486	25.62	0.1208	22.70	0.2332	16.71	0.2099	14.41
140	0.1909	11.33	0.1107	16.47	0.1818	22.03	0.2099	14.41
160	0.1707	11.38	0.1221	15.86	0.1752	16.11	0.2093	13.55
180	0.2186	10.05	0.1705	13.02	0.1744	22.03	0.2094	13.67
200	0.2864	6.65	0.2088	9.80	0.2359	16.28	0.2851	6.31
220	0.2659	6.02	0.2523	9.27	0.2832	6.88	0.3456	5.52

Table 6.2: Performance of new frameworks with modified algorithms on real-world signals

SOURCE-SENSOR Distance (cm)	WASOBI-DECONV	SYMWHITE-DECONV	FastICA-DECONV	SYMWHITE-WASOBI
	Time (s)	Time(s)	Time(s)	Time(s)
20	0.16067	0.01733	0.63500	0.01733
40	0.17500	0.01667	0.41500	0.16600
60	0.17133	0.01667	0.43500	0.01733
80	0.17011	0.01667	0.65000	0.09167
100	0.17000	0.01800	0.57000	0.16000
120	0.16600	0.01600	0.61500	0.07308
140	0.16933	0.01733	0.44000	0.07308
160	0.17200	0.03667	0.52500	0.08757
180	0.16533	0.03667	0.55500	0.08550
200	0.16333	0.03867	0.53000	0.17400
220	0.16533	0.03867	0.75500	0.16000

Table 6.3: Convergence time of modified algorithms

The plot(6.5) of index of separability of the four algorithms shows WASOBI-DECONV shows the highest performance and lowest performance is by SYMWHITE-WASOBI. This graph shows the performance algorithms is highly depend on the characteristics of input signals. This once again justifies the new frameworks for GBV signals. The performance of WASOBI-DECONV is superior for all signals. The performance of SYMWHITE-WASOBI is shows degradation for the signal acspeech16 and speech20. FastICA-DECONV shows a constant fair performance for all the three signals.

6.3 Comparison of New Frameworks with Modified Algorithms for Real world Signals

The table (6.2) shows the performance index and SIR of demixing matrix for modified algorithms on various source-sensor distances. The figure (6.6) (6.7) shows the variation of mean SIR with distance for various algorithms. All the algorithms show a negative slope with increase in distance. This is due to the reduced SNR of signals with distance , convolution and signal contaminations. The weight of the mixing matrix varies depend on the source-sensor distance. The WASOBI-DECONV shows the highest performance.

The graph(6.8) shows another representation of mean SIR with distance. The intersection in the contour shows the variation in performance of different algorithms with distance is not uniform. The other factors

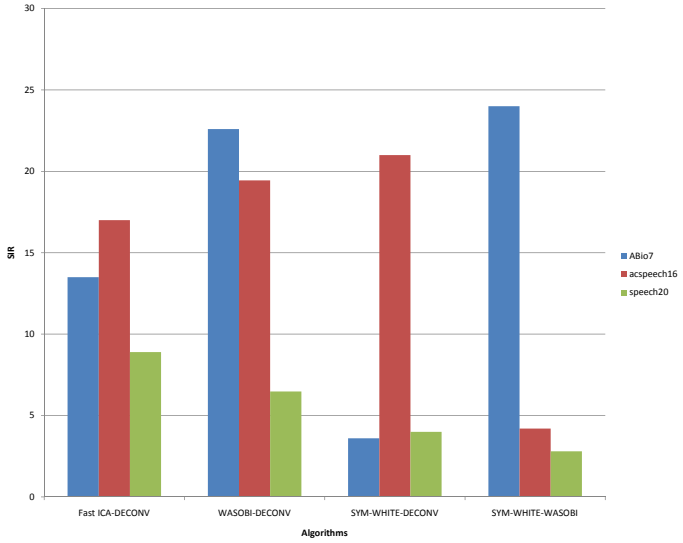

Figure 6.3: Separated components with highest SIR

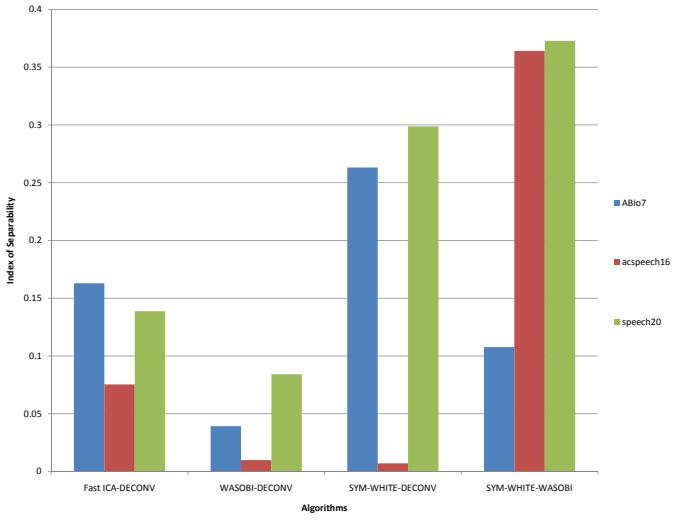

Figure 6.4: PI of separability of algorithms for benchmarked signals

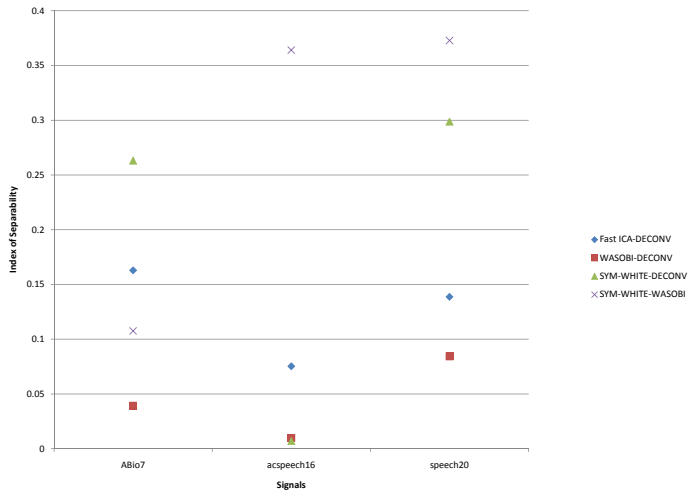

Figure 6.5: Performance comparison of algorithms based on index of separability

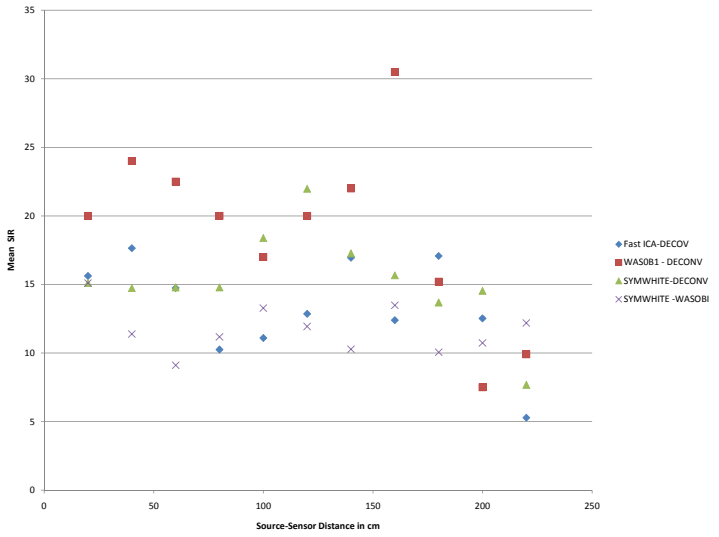

Figure 6.6: Performance comparison of algorithms based on SIR

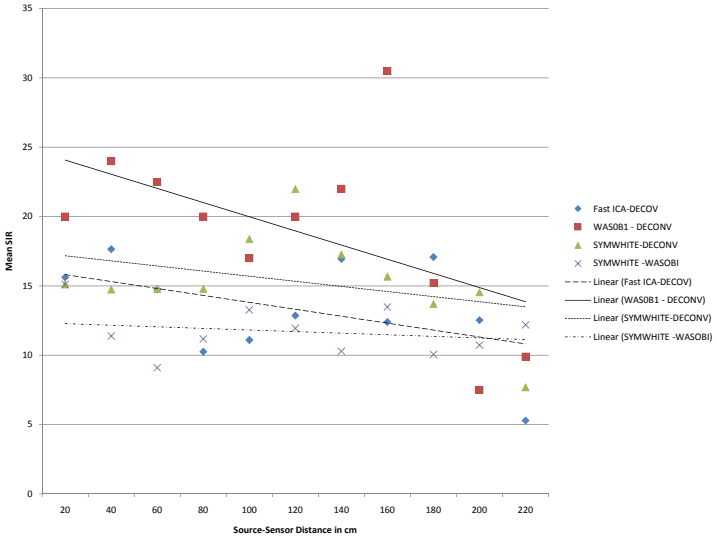

Figure 6.7: Performance comparison of algorithms based on SIR with trending

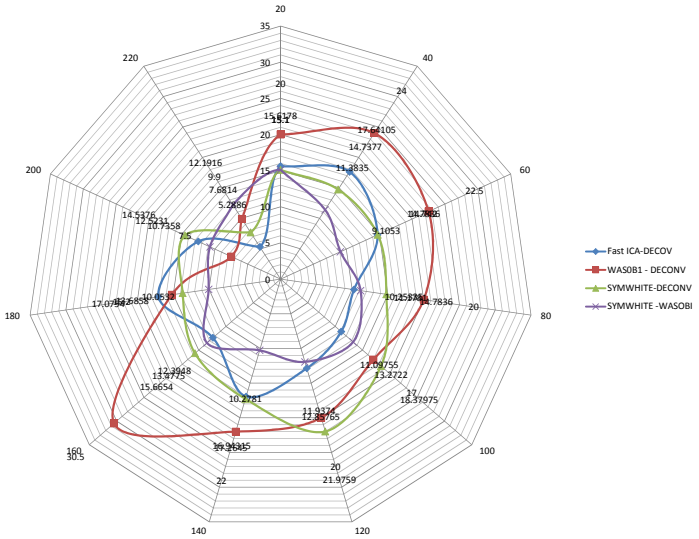

Figure 6.8: SIR for various source-sensor distance

like non-uniformity of propagation medium and environment where reflection, diffraction and/or refraction occurs, geographical surprises etc. can affect the BSS of GBV. Interestingly these factors have a direct relation wit source-sensor distance. From the previous results, the probability that these factors appear or influence increases with distance.

The plot (6.9) shows mean SIR of algorithm for various source sensor distances. The performance of WASOBI-DECONV is better in most case. Figure (6.10) shows index of separability of each algorithm for various source sensor distance. SYMWHITE-DECONV shows minimum value for source-sensor distance=100 cm, which is the best value achieved.

The figure (6.11) shows the variation of index of separability with distance for various algorithms. All the algorithms show a positive slope with increase in distance except FastICA-DECONV. This positive slope characteristics is due to the reduced SNR of signals with distance and convolution. The mixing matrix varies depend on the source-sensor distance. The WASOBI-DECONV shows the highest performance. The slight negative characteristics of FastICA-DECONV can be due to the effect of preprocessing steps employed in the algorithm on signals.

6.4 Source Signals for Varying Source-Sensor Distance

The figures (6.12) to (6.14) shows selected plots of various source signals (sensor signals). The signals acquired using four sensors P_1, P_2, P_3, P_4 are

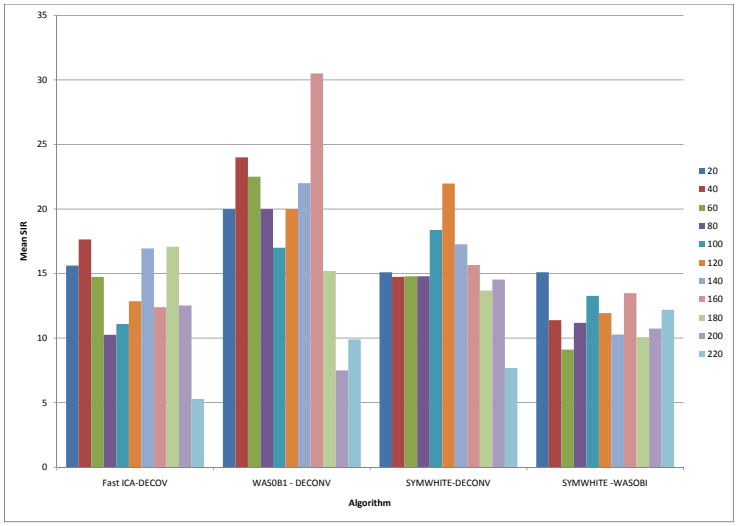

Figure 6.9: Mean SIR of separated components for various source-sensor distances

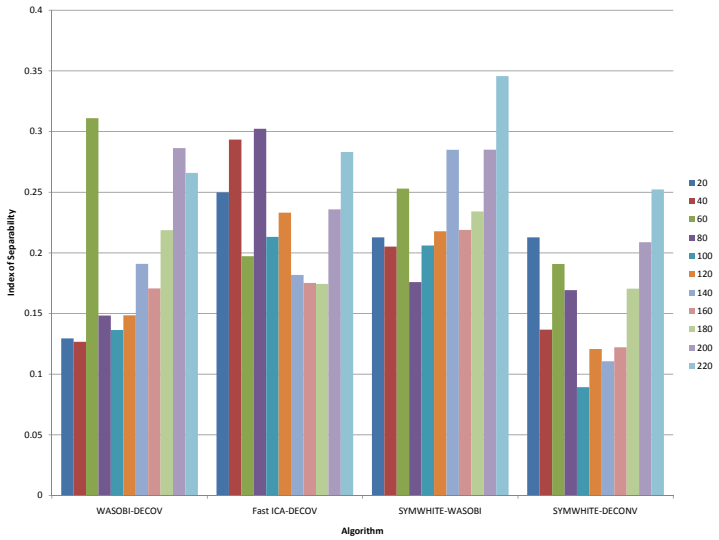

Figure 6.10: PI of separability of algorithms for various source-sensor distances

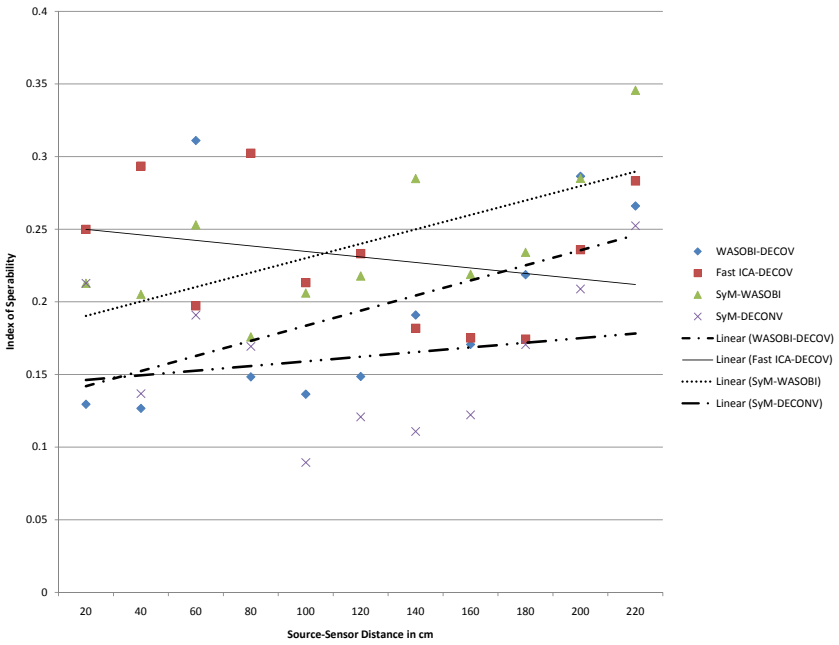

Figure 6.11: Performance comparison of algorithms based on SIR of separated components with trending

shown as s_1, s_2, s_3, s_4 respectively. The variations in the signal with distance and noise contaminations can be seen from the plots. The similar pattern in all channels shows the dependence between the signals.

6.5 Signals after Noise Reduction and Dereverberation

The figures (6.15) to (6.17) shows the signal after noise reduction and deconvolution. As explained in the previous chapters, the noise reduction

Figure 6.12: Source signals for a source-sensor distance of 20 cm

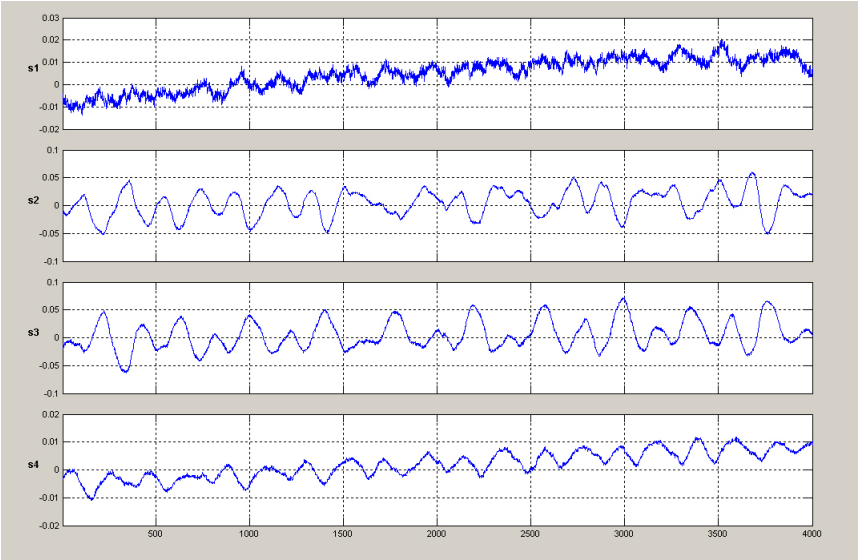

Figure 6.13: Source signals for a source-sensor distance of 120 cm

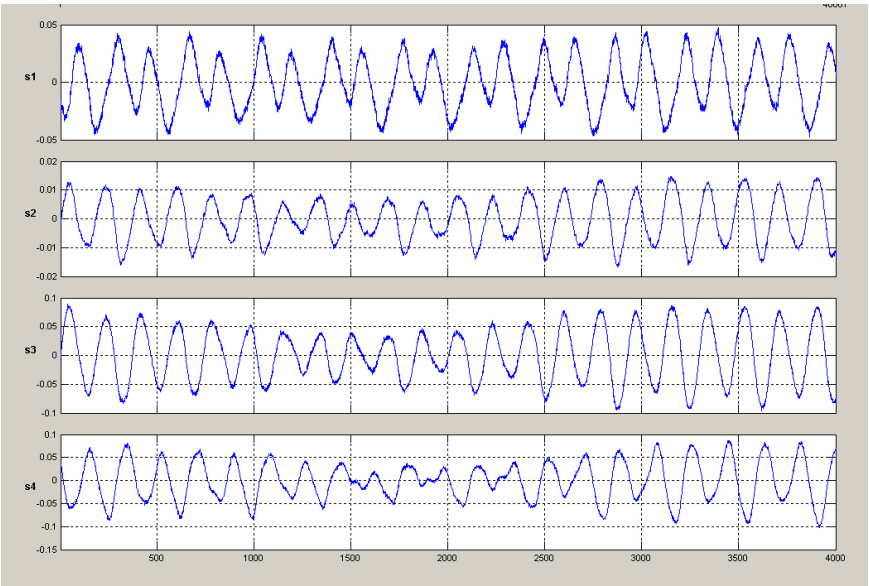

Figure 6.14: Source signals for a source-sensor distance of 220 cm

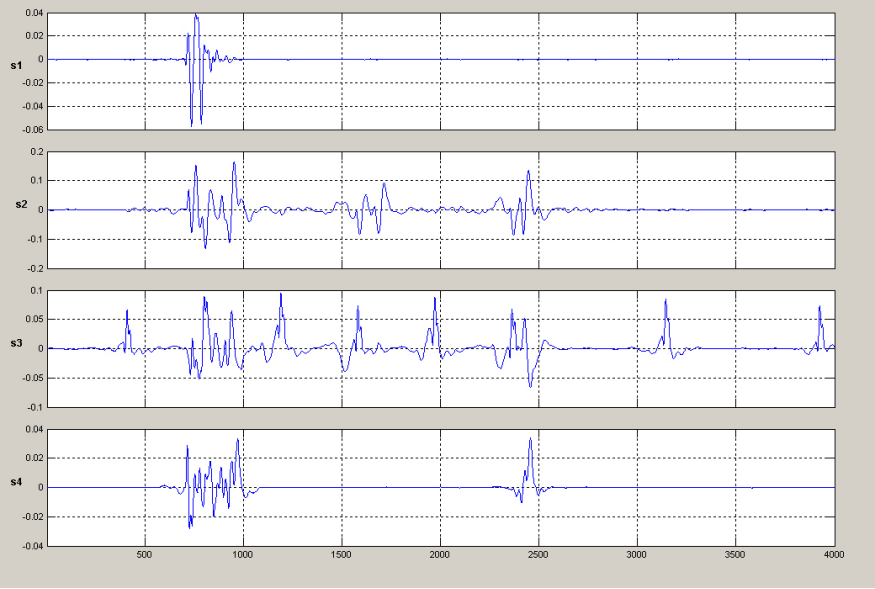

Figure 6.15: Signals for a source-sensor distance of 20 cm after Noise reduction and De reverberation process

and deconvolution were performed adaptively to reduce the information loss from the signals.

6.6 WASOBI-DECONV: Separated Components

The figures (6.18) to (6.23) shows the separated component signals and scatter plots of sensor signals and separated signals for source-sensor distance = 20 cm , 120 cm and 220 cm using WASOBI-DECONV.

6.7 SYMWHITE-DECONV: Separated Components

The figures (6.24) to (6.29) shows the separated component signals and scatter plots of sensor signals and separated signals for source-sensor distance = 20 cm , 120 cm and 220 cm using SYMWHITE-DECONV.

6.8 SYMWHITE-WASOBI:Separated Components

The figures (6.30) to (6.35) shows the separated component signals and scatter plots of sensor signals and separated signals for source-sensor distance = 20 cm , 120 cm and 220 cm using SYMWHITE-WASOBI.

6.9 FastICA-DECONV: Separated Components

The figures (6.36) to (6.41) shows the separated component signals and scatter plots of sensor signals and separated signals for source-sensor distance = 20 cm , 120 cm and 220 cm using FastICA-DECONV.

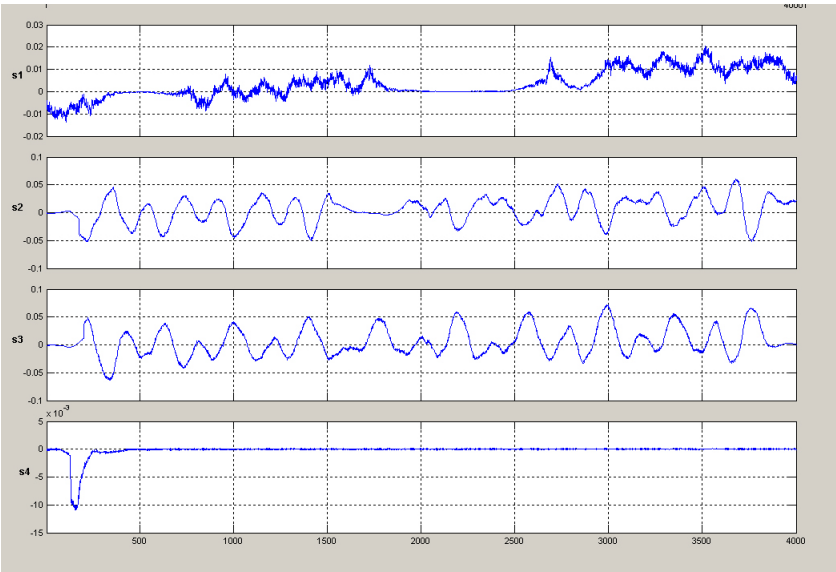

Figure 6.16: Signals for a source-sensor distance of 120 cm after Noise reduction and De reverberation process

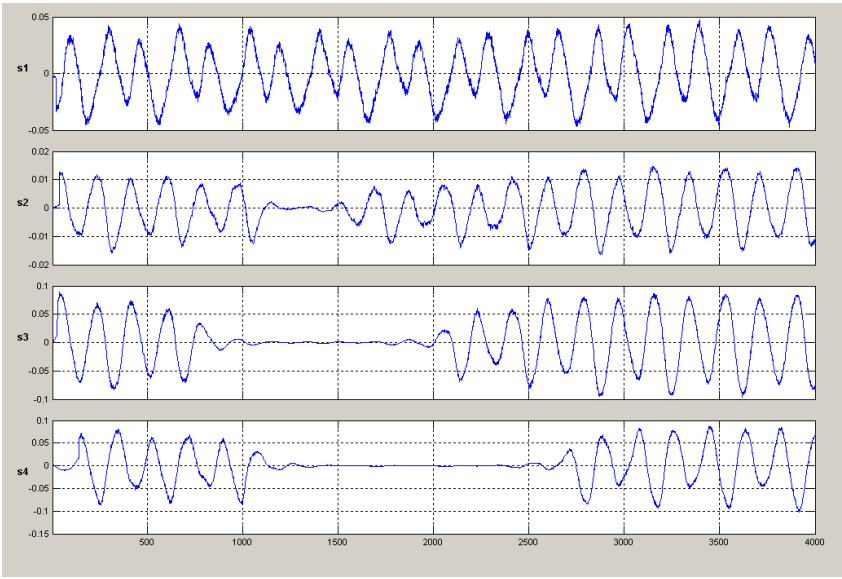

Figure 6.17: Signals for a source-sensor distance of 220 cm after Noise reduction and De reverberation process

6.10 Summary

The performances of the modified algorithms were compared and various performance measures were plotted. We can see that the performance of WASOBI-DECONV algorithm shows a better performance compared to other algorithms in most case. The various signal plot was also given for comparison of the various wave forms. The algorithms succeeded to recover at least one source even at a source-sensor distance of 220 cm.This is a very promising result in the case of GBV and the low level source signals used for experiment.

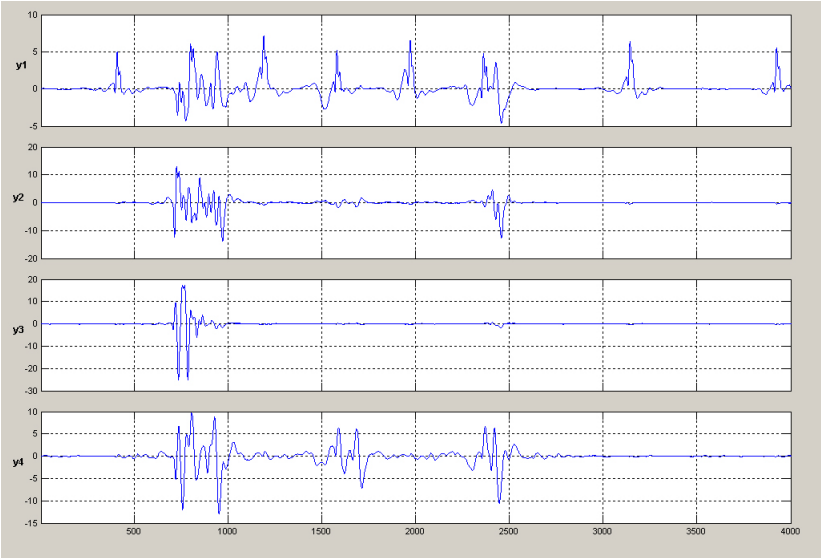

Figure 6.18: Separated component signals for a source-sensor distance of 20 cm using algorithm WASOBI-DECONV

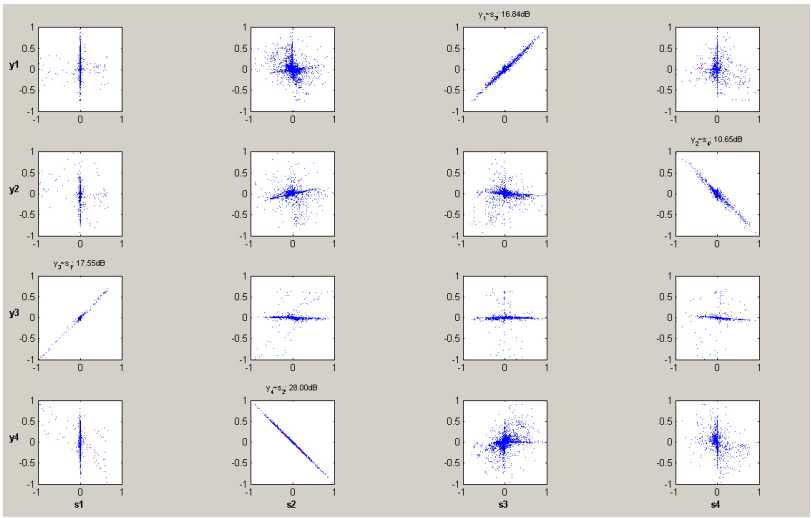

Figure 6.19: The scatter plot of sensor signals and separated signals, for a source-sensor distance of 20 cm using algorithm WASOBI-DECONV

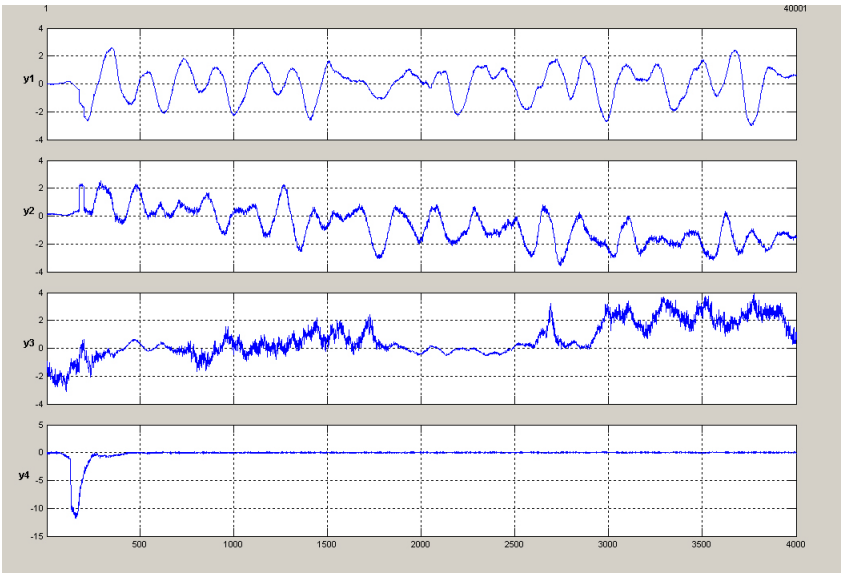

Figure 6.20: Separated component signals for a source-sensor distance of 120 cm using algorithm WASOBI-DECONV

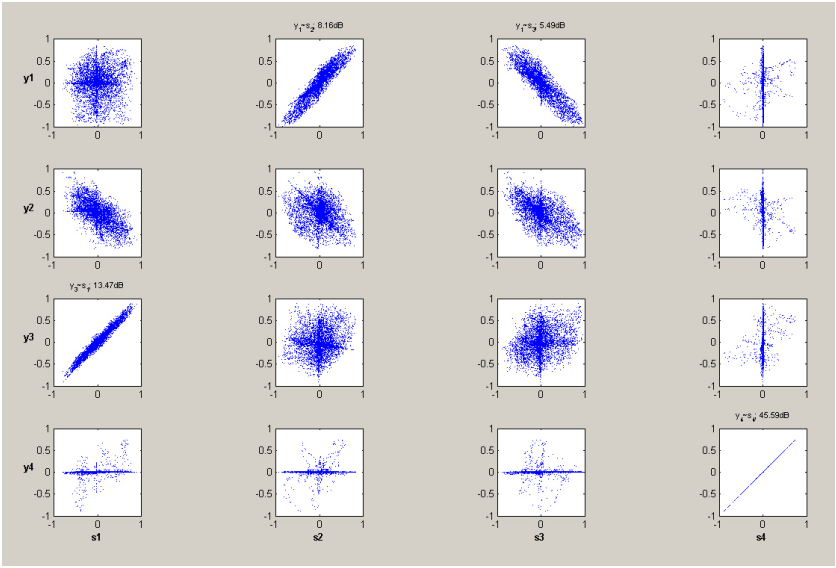

Figure 6.21: The scatter plot of sensor signals and separated signals, for a source-sensor distance of 120 cm using algorithm WASOBI-DECONV

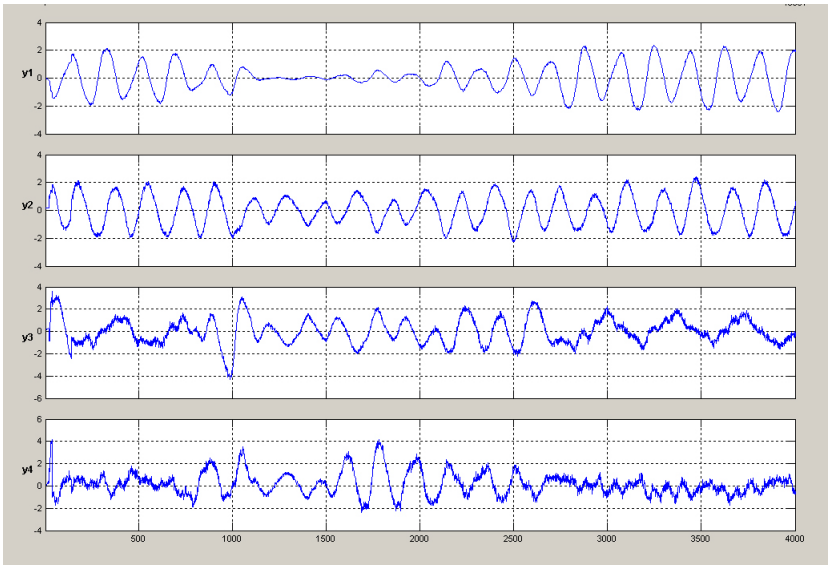

Figure 6.22: Separated component signals for a source-sensor distance of 220 cm using algorithm WASOBI-DECONV

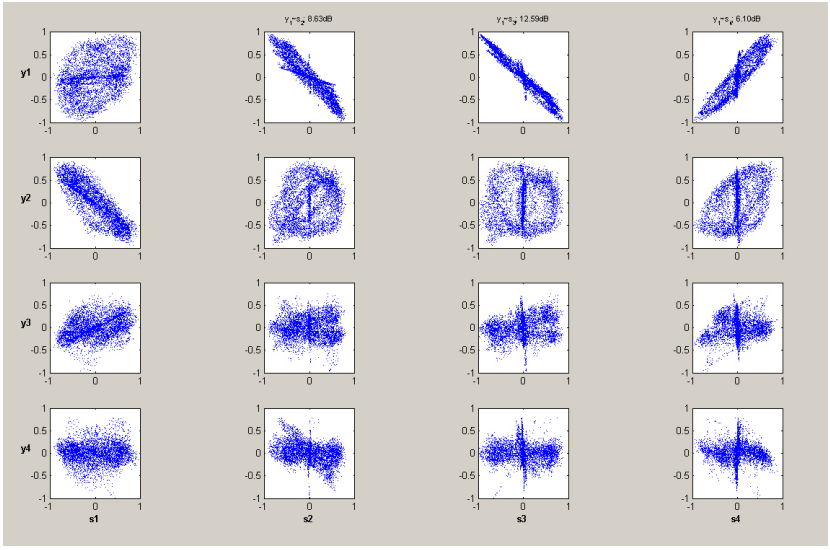

Figure 6.23: The scatter plot of sensor signals and separated signals, for a source-sensor distance of 220 cm using algorithm WASOBI-DECONV

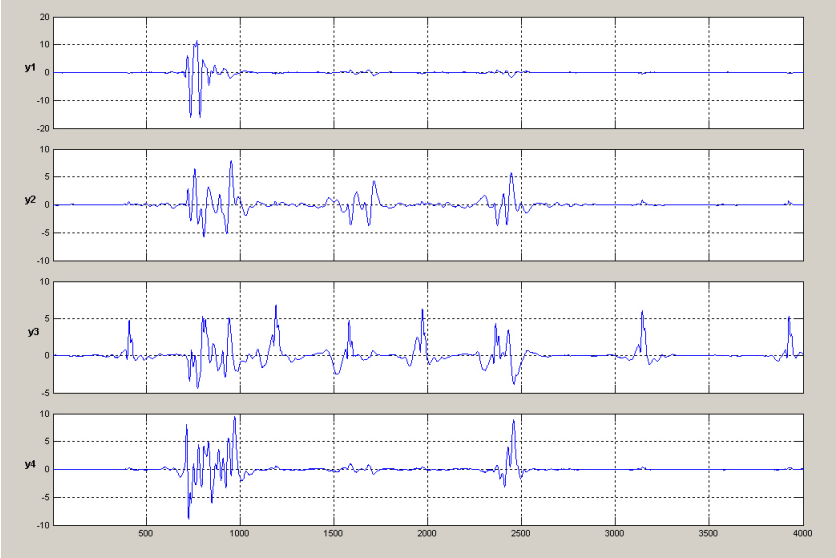

Figure 6.24: Separated component signals for a source-sensor distance of 20 cm using algorithm SYMWHITE-DECONV

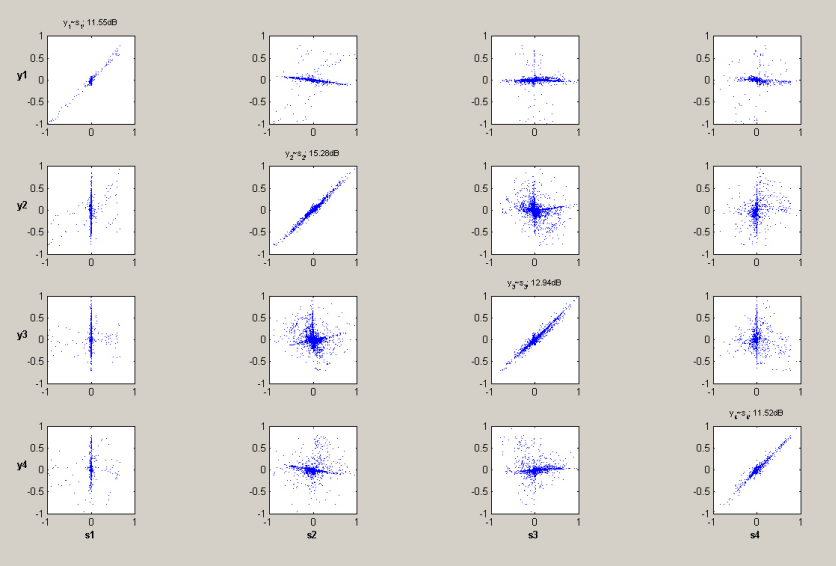

Figure 6.25: The scatter plot of sensor signals and separated signals, for a source-sensor distance of 20 cm using algorithm SYMWHITE-DECONV

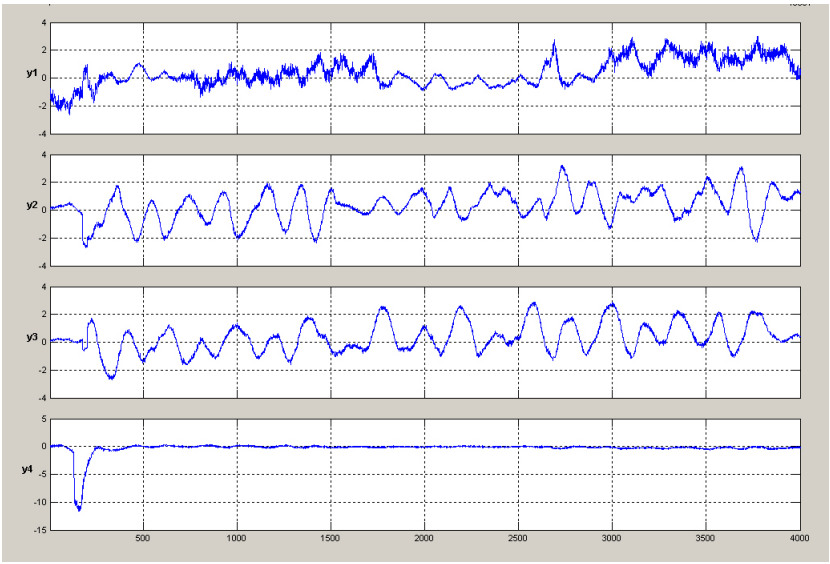

Figure 6.26: Separated component signals for a source-sensor distance of 120 cm using algorithm SYMWHITE-DECONV

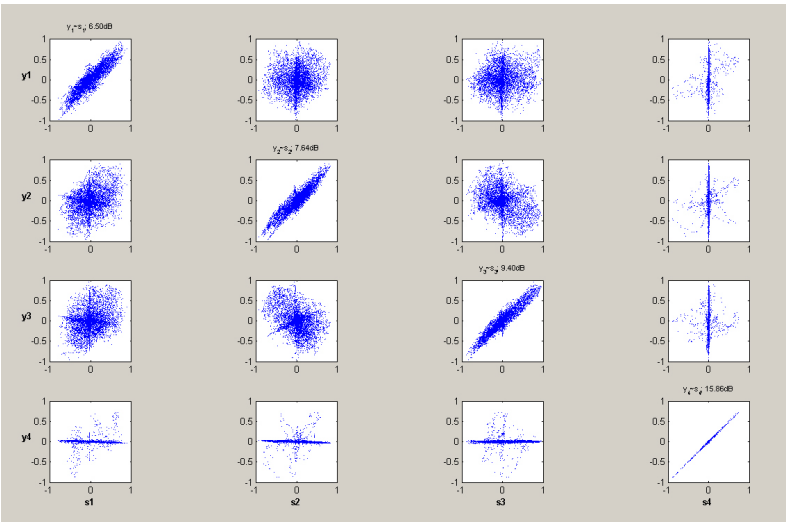

Figure 6.27: The scatter plot of sensor signals and separated signals, for a source-sensor distance of 120 cm using algorithm SYMWHITE-DECONV

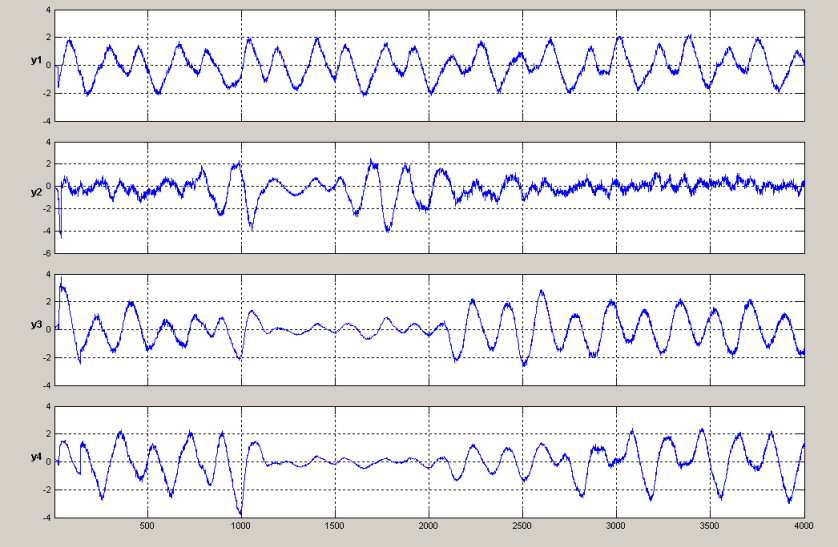

Figure 6.28: Separated component signals for a source-sensor distance of 220 cm using algorithm SYMWHITE-DECONV

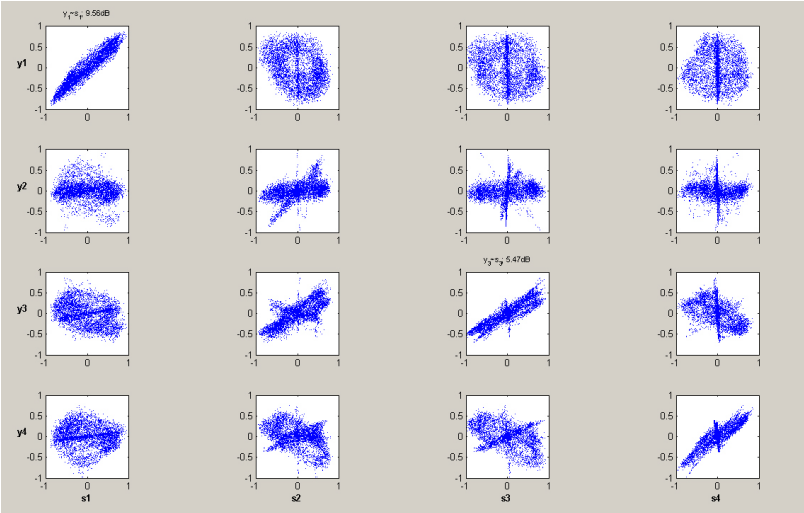

Figure 6.29: The scatter plot of sensor signals and separated signals, for a source-sensor distance of 220 cm using algorithm SYMWHITE-DECONV

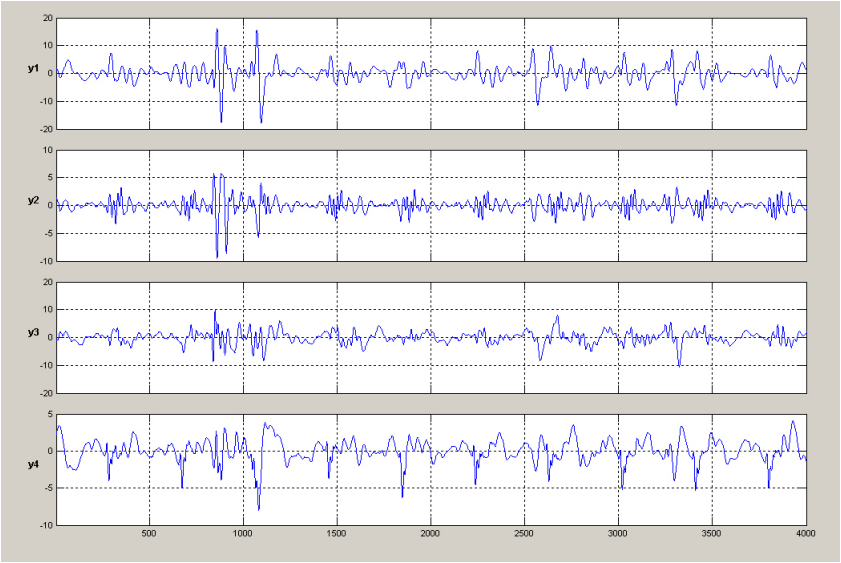

Figure 6.30: Separated component signals for a source-sensor distance of 20 cm using algorithm SYMWHITE-WASOBI

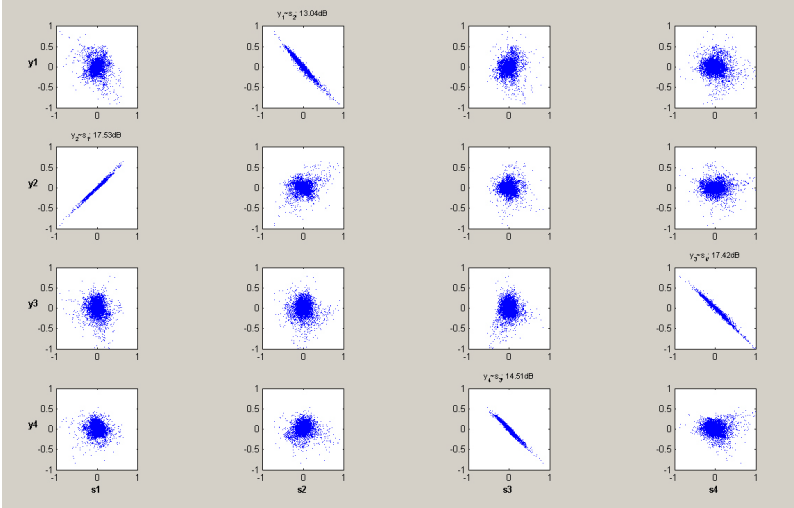

Figure 6.31: The scatter plot of sensor signals and separated signals, for a source-sensor distance of 20 cm using algorithm SYMWHITE-WASOBI

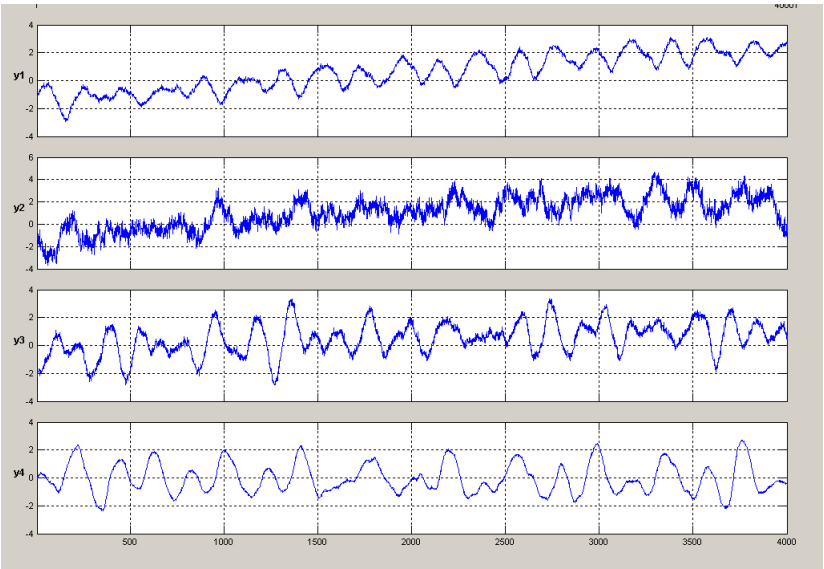

Figure 6.32: Separated component signals for a source-sensor distance of 120 cm using algorithm SYMWHITE-WASOBI

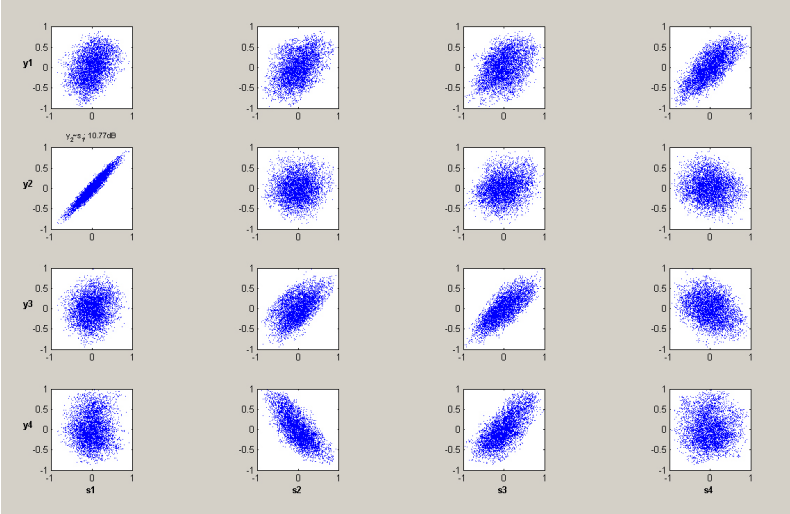

Figure 6.33: The scatter plot of sensor signals and separated signals, for source-sensor distance of 120 cm using algorithm SYMWHITE-WASOBIV

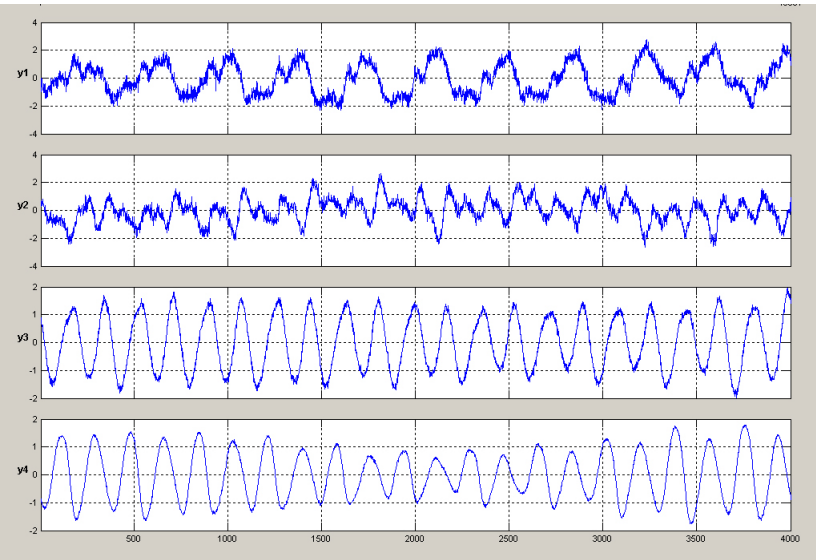

Figure 6.34: Separated component signals for a source-sensor distance of 220 cm using algorithm SYMWHITE-WASOBI

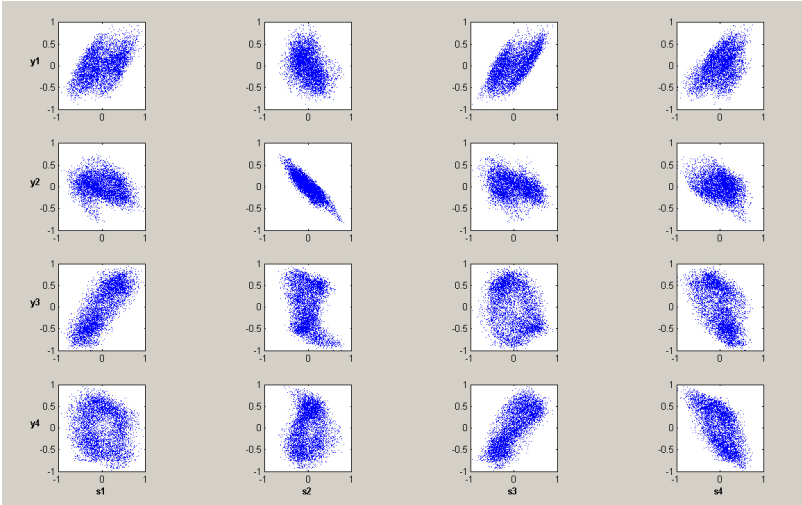

Figure 6.35: The scatter plot of sensor signals and separated signals, for a source-sensor distance of 220 cm using algorithm SYMWHITE-WASOBI

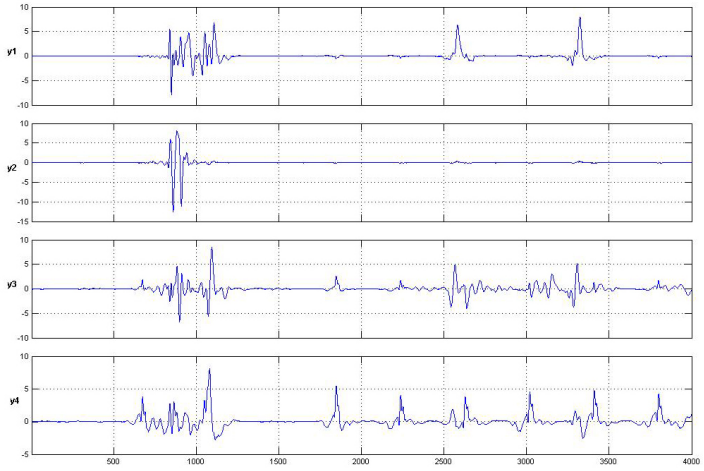

Figure 6.36: Separated component signals for a source-sensor distance of 20 cm using algorithm FastICA-DECONV

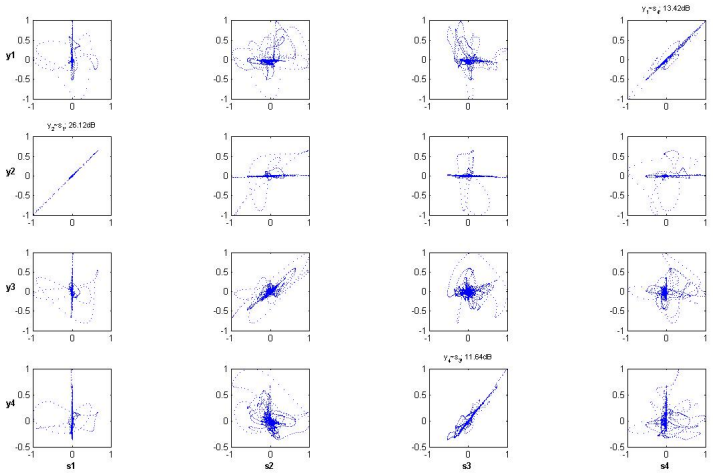

Figure 6.37: The scatter plot of sensor signals and separated signals, for source-sensor distance of 20 cm using algorithm FastICA-DECONV

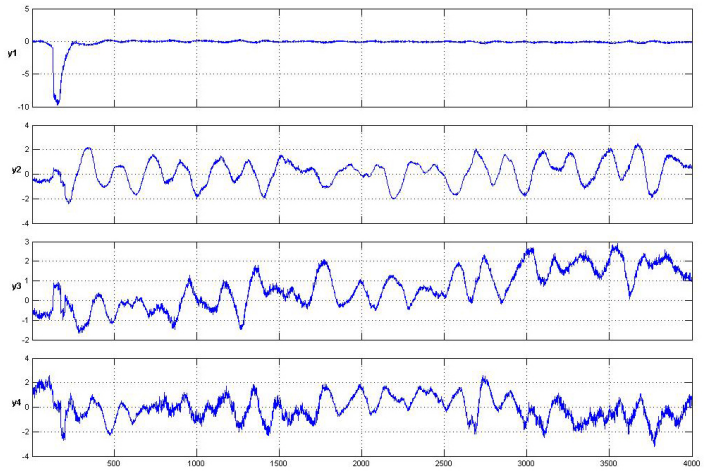

Figure 6.38: Separated component signals for a source-sensor distance of 120 cm using algorithm FastICA-DECONV

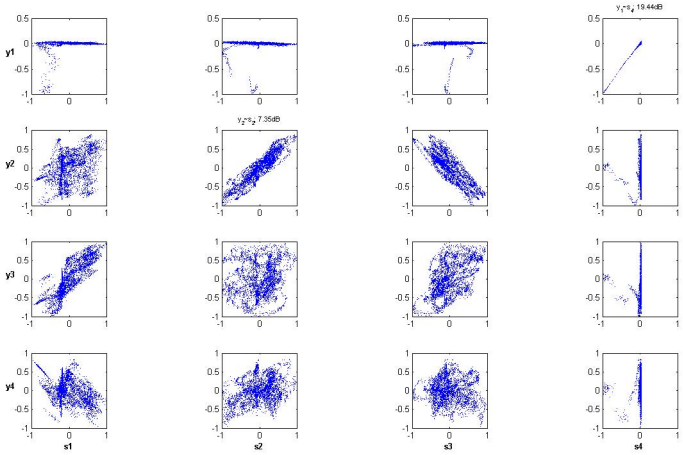

Figure 6.39: The scatter plot of sensor signals and separated signals, for a source-sensor distance of 120 cm using algorithm FastICA-DECONV

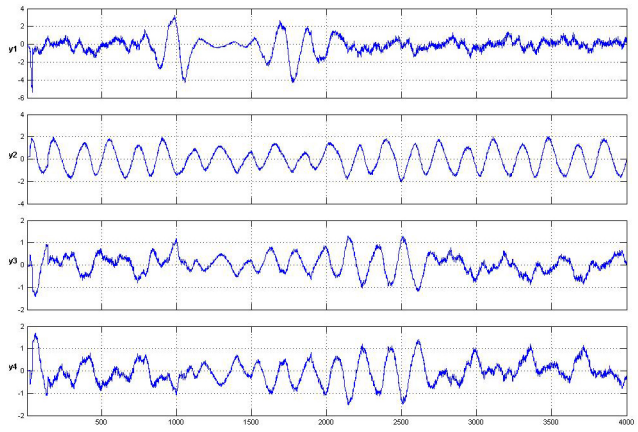

Figure 6.40: Separated component signals for a source-sensor distance of 220 cm and using algorithm FastICA-DECONV

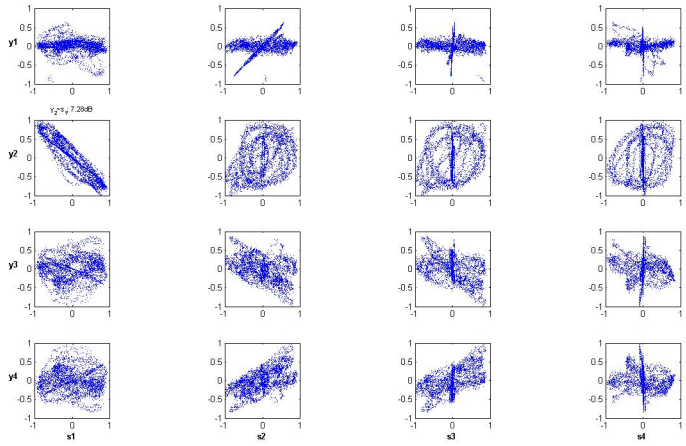

Figure 6.41: The scatter plot of sensor signals and separated signals, for source-sensor distance of 220 cm using algorithm FastICA-DECONV

Chapter 7

Applications of the New Frameworks

7.1 Introduction

The BSS of GBV being a statistical signal processing technique finds application in many emerging new application areas such as seismic survey, vibration analysis of rail and road transportation system, detecting the presence of moving train, fault detection of machinery, detecting the presence of life buried in the ground etc. The application of BSS can also extend to other areas like heartbeats separation, biomedical signal processing and telecommunications. In the next sections we discuss three application developments targeted using the new frameworks.

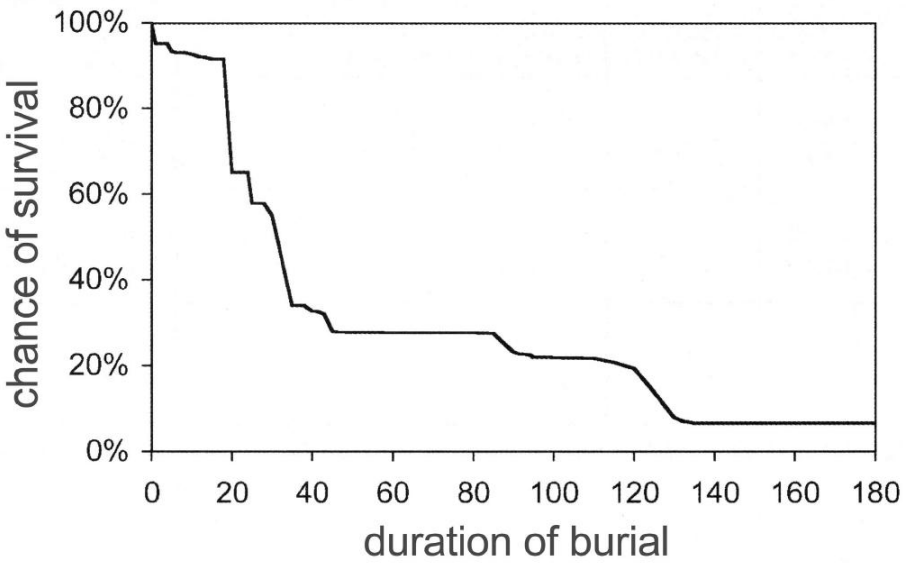

Figure 7.1: Survival chance of person buried completely due to landslide [88]

7.2 A Life Saving Device

7.2.1 Background

Landslides cause enormous casualties and relentless losses worldwide. For last 40 years almost 30000 people have been killed in landslides and avalanches worldwide. That is a rate of 1 person per 10 million dying due to landslides. The most deaths occurred in the land slide prone area like India, China, Colombia and the Philippines. The Indian subcontinent has a highly diversified range of natural features. The population density of this area is high compare to other areas in the world further adds to the damage caused by the natural disasters. The survival chances for persons caught in landslides are dependent on several factors. Survival chances depends on whether the victim is able to breath, and in case of a critical burial (head and the upper part of the body in the earth), and how fast

the victim is dug out. If the airway of the buried person is not clear and if there is no air pocket round the victim, after 35 minutes the victims fate is unpredictable and any help will be too late. However, with a clear air way and an air pocket, it is possible to survive longer. Survival of totally buried persons is also influenced by hypothermia and other unknown co-factors. Data show approximately 75% of landslide fatalities are due to asphyxia, 15 to 20% due to deadly trauma and 5 to 10% due to hypothermia and other factors. Chance of survival over time in a complete landslide burial is not linear. See figure (7.1) In a complete burial situation, there are phases where the survival rate drops very rapidly - a high risk to die in the first 18 to 35 minutes of burial (asphyxia phase) - and phases with an almost stable survival rate a greatly reduced risk to die between 35 and 90 minutes of burial (the latency phase) [88]

In principle, by reducing the burial time, mortality can be reduced. The effectiveness of this strategy depends on which phase of the survival curve is affected. Safety equipment is especially effective when the steep parts of the survival curve are affected. This shows the importance of availability of life-detecting systems immediately in the spot after the disaster. Transporting the life detecting systems from far places is not an effective solution. So a better solution is many units of these instruments deployed in the prone area. The major limiting factor in procuring the high technology instrument like radars using ultra wide-band (UWB) technology is the capital involved and the skilled technicians. The proposed safety equipment is a low cost instrument and reduces burial time by detecting the life buried and helps us to detect the required area to be dug.

7.2.2 The Methodology

The basic idea behind this low cost instrument is recording or examining the GBV signals picked up from earths surface or pits by very high sensitive

sensors We can examine for motion as slight as shallow breathing, heartbeat, small voice made by the victim, sounds of the movements of limbs etc. we can detect through wood, brick, concrete; virtually any material. The captured signals can be cleaned and source separated to get rid of various noises including the noise created by humans and machinery during the rescue operations. The output can be analyses to predict human lives buried in the affected area[12][139][140]

Various advantages of the proposed systems include; low cost, simple technology, the detection of vibration caused movement of limbs or shallow breathing, Detection through virtually any material, Ease of mobility over a site, Low-power requirements, little or no maintenance, Unaffected by odors or other bio-sensitivities that can affect detection, Ease of use and deployment, Maximum effectiveness in adverse physical conditions, Maximum effectiveness in minimal time, Intuitive operation requiring minimal training. The disadvantage include; efficiency decrease in noise environment and Short range of operation[141].

7.3 E-Auscultation

7.3.1 Background

A patients heart problem or many other diseases condition is often perceived by the doctor after listening to the heartbeat sound. Even today this method continues to be one of the easiest and common preliminary checkup measure performed by a medical practitioner. This technique is known as auscultation. The skill of auscultation can be achieved only through extensive experience. The heart sounds listened through the stethoscope is source separated to its component signals by the brain. The source separation ability of brain varies from person to person and its effectiveness is affected by the surrounding noises. The inability for performing effective

auscultations can lead to an advice for more costly and time consuming test or can result in wrong diagnosis. The marginalized people from remote village of an under developed country or a developing country finds it difficult to take the advantage of advanced diagnosis methods as time , accessibility and money become critical.

7.3.2 The Methodology

The heart sounds are captured by placing sensors in auscultation area. The captured mixed signals are blind source separated after filtering and preprocessing steps. It is not practical to measure the sensor positions during clinical examination and the mixing system is unknown as the physiques of human beings differ. So blind source separation (BSS) method is a suitable technique to address the problem. In the case of BSS, no information is needed about the source positions or the mixing systems .The low signal to noise ratio makes the problem more difficult[96] [97].

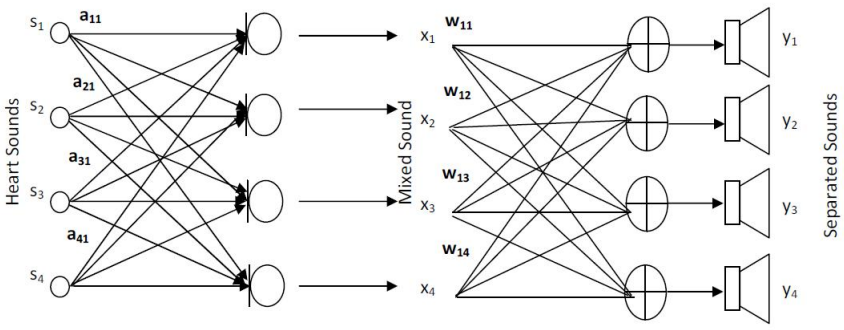

Figure 7.2: Schematic of acquisition and source separation of heartbeat sounds

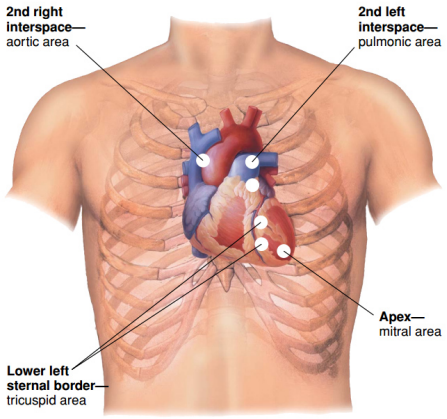

Figure 7.3: Typical auscultation areas [142]

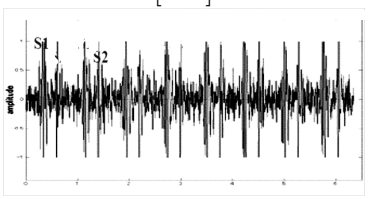

Figure 7.4: A typical heartbeat signal sequence, S1 and S2

Figure (7.3) shows a typical auscultation and figure(7.4) shows the two heart beat sequences, where S1 (Mitral-Tricuspid Valve) and the S2 (Aortic-Pulmonary valve) are clearly visible [143].

A schematic of the arrangement is shown in the figure (7.2). The heartbeat sound signals recorded include mixtures of the various heartbeat sounds and noises . The recorded vibration signals showed a close resemblance with our experimented signals. So our frame work can be best fit for the BSS of heart sounds [96] This idea can be used for making a low cost, easy to use portable medical instrument for clinical practitioners without much deviation from conventional method of auscultation. The people unable to take the advantage of advanced diagnosis methods may find this instrument very useful.

7.4 Fault Detection of Rotating Machinery

The proposed frameworks can be used for the fault diagnosis of rotating machine. The problem due to unbalancing, unnecessary vibrations, bearing fault etc can be easily located and diagnosed using our framework. The sensors are placed at various locations including the machine foundation or machine floors. The captured signals can be processed to predict and localize the fault in many cases. The figure (7.5)shows a signal captured using four sensors at different location of a hydraulic machine rotating at 500 RPM. The figure shows vibration during the gate opening and smooth operation and sudden stoppage of the machine. By analyzing the spectrogram of separated signals we can predict the nature and spot of the fault.

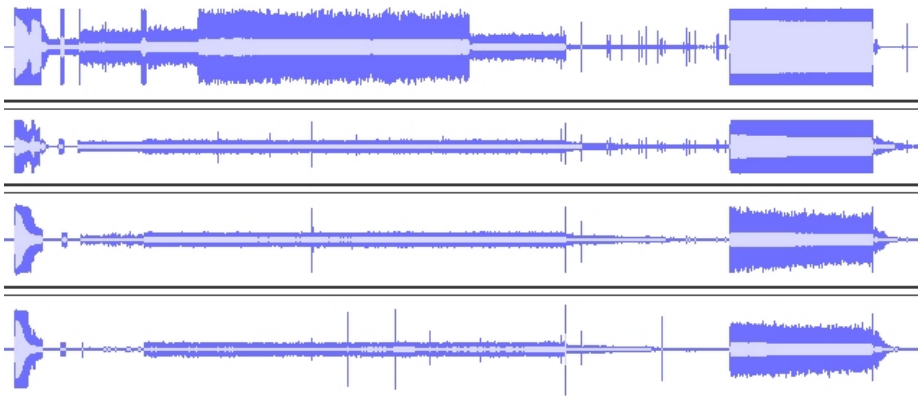

Figure 7.5: Vibration captured from rotating hydraulic machine using the instrument prototype

7.5 Other Applications

Modified version of our proposed frame works can be used for the following applications[2] [4].

7.5.1 Seismological Data Processing

The method can be extended to use in seismological methods like seismic refraction survey or seismological reflection methods for the analysis geographical structure or to analyze seismic waves produced by earth quake, landslides etc.

7.5.2 Biomedical Signal Processing

Methods to separate brain activity from artifacts using ICA is a blistering topic of research during last decades.

7.5.3 Telecommunications

Various successful studies were conducted for using blind separation techniques in the separation of the users own signal from the interfering other users signals in Code-Division Multiple Access (CDMA) mobile communications.

7.5.4 Multi Sensor Signal Processing

Multi-sensor data often presents complementary information about the region surveyed and data fusion provides an effective method to enable comparison, interpretation and analysis of such data.

Chapter 8

Conclusion and Future Direction

The research work described in the thesis focused on the Blind Source Separation (BSS) of Ground Borne Vibrations(GBV). The BSS of GBV signals refers to the task of estimating the signals produced by the individual vibration sources and are propagated through the ground. The captured signals are complex mixtures of the individual sources. These signals have intrinsic reverberation, delayed mixing etc. These necessitated new frameworks for effective source separation of the GBV signals. To solve the blind source separation problems, a quite large selection of techniques are available in the scientific literature, each of them possesses its own features, advantages and limitations. The work described in the thesis.

- *Studied blind source separation of signals and proposed new frameworks for effective blind source separation of Ground Borne Vibrations and proved the superiority of our methods*

- *Studied and identified suitable models for the propagation of GBVs.*

- *Proposed and developed a system,instrument prototype and procedure for field data collection for the evaluation of the frameworks.*

- *Recommended specific targeted technologies based on BSS of GBVs.*

Contributions

We studied and identified appropriate models for vibration sources, suitable models for propagation for ground borne vibration. These models were validated and justified. Algorithms based on second order statistics and higher order statistics were studied. Various frameworks for the BSS of GBVs were presented, evaluated and compared. The dominance of the new frame works were discussed in the thesis. The superiority of the proposed methods was established on the real world data. We considered semi-analytical approach of wave propagation and seismic convolution model for wave propagation through the ground. The research works presented the extensions of BSS algorithm based on a semi analytical approach considering the near field problem and far field problems. The modified algorithm WASOBI-DECONV, SYMHITE-DECONV and FastICA-DECONV and SYMWHITE-WASOBI were presented and the effectiveness of these algorithms for real world data were established.

All proposed frameworks were evaluated against benchmarked and real world data. A complete analysis and comparison of the various frameworks were included in the thesis. When evaluating the performance of the algorithm in this thesis, our focus is mainly on the quality of separation and discussion on computation efficiency was mostly superficial. A new method for field data collection which is very similar to seismic refraction method

was presented. We demonstrated the new prototype for the capture and processing of GBV.

The new applications were identified by the authors namely a life saving system and heartbeat source separation method was included in the thesis. The post processing optimization using Kalman filter or Wiener filter remains as open problems.

Bibliography

[1] T. W. Lee. Independent component analysis: Theory and applications. Kluwer Academic Publishers , ISBN 0 7923 8261 7, 1998.

[2] J. C. Rajapakse, A. Cichocki and Sanchez. Independent component analysis and beyond in brain imaging: EEG, MEG, FMRI, and PET. pages 404 – 412. ICONIP 02. Proceedings of the 9th International Conference on Neural Information Processing, 2002.

[3] C. Jutten and J. Karhunen. Advances in blind source separation (BSS) and independent component analysis (ICA) for nonlinear mixtures. *International Journal of Neural Systems*, 14(5):267–292, October 2004.

[4] Ulrik Kjem, Michael Syskind Pedersen, Jan Larsen and Lucas C. Parra. Survey of convolutive blind source separation methods. In *Springer Handbook on Speech Processing and Speech Communication*. 2007.

[5] Jean-Franc and Ois Cardoso. Blind signal separation: Statistical principles. In *Proceedings of the IEEE Special issue on blind identification and estimation*, pages 2009–2025. IEEE, 1998.

[6] Aapo Hyvarinen and Erkki Oja. Independent component analysis: A tutorial. http://www.cis.hut.fi/projects/ica.

[7] James V. Stone. In *Independent Component Analysis: A Tutorial Introduction*, volume ISBN: 9780262257244, pages 1–200. The MIT Press, Cambridge, 2004.

[8] Ewing W.M., W.S.Jardetzky, Press F. In *Elastic Waves in Layered Media*, pages 380–400. McGraw-Hill Book Co, NY, 1957.

[9] Seth Stein and Michael Wysession. In *An Introduction to Seismology, Earthquakes, and Earth Structure*. Wiley-Blackwell ISBN: 978-1-4443-1131-0, April 2009.

[10] A. Hyvrinen, J. Karhunen and E. Oja. In *Independent Component Analysis*. John Wiley Sons, NY, 2001.

[11] T. W. Lee, A. J. Bell and R. Orglmeister. Blind source separation of real world signals. *Neural Networks*, 4:2129–2134, 1997.

[12] Krishna Kumar M, Pramod K V, Geethu R S. A low cost scheme for tracking the lives buried in landslides. *IJCA*, pages 44–49, 2011.

[13] L.Wang, N.Kitaoka and S.Nakagawa. Distant-talking speech recognition based on spectral subtraction by multi-channel LMS algorithm. *IEICE Trans. Information and Systems*, E94-D(3):659–667, Mar. 2011.

[14] Arie Yeredor. Blind Separation of Gaussian Sources via Second-Order Statistics with Asymptotically Optimal Weighting. *IEEE Signal Processing Letters*, 7:197–199, JUL 2000.

[15] Kyohei Odani, Longbiao Wang and Atsuhiko Kai. Blind Dereverberation Based on Generalized Spectral Subtraction by Multi-channel LMS Algorithm. In *APSIPA ASC*. APSIPA ASC, 2011.

[16] Andrzej Cichocki, Stanisaw Osowski, Krzysztof Siwek. Prewhitening algorithms of signals in the presence of white noise. In *VI International Workshop Computational Problems of Electrical Engineering*, pages 205–208. Zakopane, 2004.

[17] A. Hyvarinen. Fast and robust fixed-point algorithms for independent component analysis. *IEEE Transactions on Neural Networks*, 10:626–634, 1999.

[18] http://www.bsp.brain.riken.jp.

[19] J. Hrault, C. Jutten, and B. Ans. Detection de grandeure primitives dans un message composite par une architechture de calul neuromimetique un apprentissage on supervise. In *GRETSI*. Nice, France, 1985.

[20] K. Pearson. On lines and planes of closest fit to systems of points in space. *Phil.Mag.*, 6(2):559–572, 1901.

[21] H. Hotelling. Analysis of a complex of statistical variables into principle components. *Journal of Educ. Psychol*, 24:498–520, 1933.

[22] H. Hotelling. Simplified calculation of principal components. *Psychometrika*, 1:27–35, 1931.

[23] I.T.Jolliffe. In *Principal Component Analysis*. Springer-Verlag New York Inc, 2nd edition, 2002.

[24] R. W. Preisendorfer. In *Principal Component Analysis in Meteorology and Oceanography*. Elsevier Science Publishing Co, 1988.

[25] C. Spearman. General intelligence: objectively determined and measured. *American Journal of Psychology*, 15:201–293, 1904.

[26] H. H. Harman. In *Modern Factor Analysis*. University of Chicago Press, 2nd edition, 1985.

[27] M. Kendall. In *Multivariate analysis*. Griffin, London, 1975.

[28] A. Webb. In *Statistical Pattern Recognition*. Arnold, 1999.

[29] E. E. Cureton and R. B. DAgostino. In *Factor Analysis: An Applied Approach*. Lawrence Erlbaum Associates Publishers, 1983.

[30] D. B. Rowe. In *Multivariate Bayesian Statistics:Models for Source Separation and Signal Unmixing*. Chapman and Hall, 2003.

[31] J. H. Friedman and J. W. Tukey. A projection pursuit algorithm for exploratory data analysis. *IEEE Transaction of Computers*, c-23(9):881–890, 1974.

[32] P. J. Huber. Projection pursuit. *The Annals of Statistics*, 13(2):435–475, 1985.

[33] J. H. Friedman. Exploratory projection pursuit. *Journal of the American Statistical Association*, 82(397):249–266, 1987.

[34] M. C. Jones and R. Sibson. What is projection pursuit? *Journal of the Royal Statistical Society*, Serial A:150:1–36, 1987.

[35] Abdelhamid Mekaoui, El-Mehdi Hamzaoui, Rajaa Cherkaoui, El Moursli. Application of Blind Source Separation Algorithms to the Preamplifierś Output Signals of an HPGe Detector Used in Gamma-Ray Spectrometry. *Adv. Studies in Theoretical Physics*, 8(9):393–399, 2014.

[36] Botond Sandor Kirei, Marina Dana Topa, Irina Muresan, Ioana Homana, Norbert Toma. Blind source separation for convolutive mixtures with neural networks. *Advances in Electrical and Computer Engineering*, 11(1):63–68, 2011.

[37] Banu Gnel, Hseyin Hacihabibo Glu, Ahmet M. Kondoz. Acoustic Source Separation of Convolutive Mixtures Based on Intensity Vector Statistics . *IEEE Transactions On Audio, Speech, And Language Processing*, 16(4):748–755, May 2008.

[38] Eran Doron, Arie Yeredor, Petr Tichavsk. Cramr-Rao-Induced Bound for Blind Separation of Stationary Parametric Gaussian Sources. *IEEE Signal Processing Letters*, 14(6), June 2007.

[39] German Gomez-Herrero, Zbynek Koldovsky, Petr Tichavsky, Karen Egiazarian. A fast algorithm for blind separation of non-gaussian and time-correlated signals. In *15th European Signal Processing Conference (EUSIPCO 2007)*. EURASIP, Sep 2007.

[40] Herbert Buchner, Robert Aichner, Walter Kellermann. A generalization of blind source separation algorithms for convolutive mixtures based on second-order statistics. *IEEE Transactions On Speech And Audio Processing*, 13(1):120–134, January 2005.

[41] Seungjin Choi, Andrzej Cichocki, Hyung-Min Park, Soo-Young Lee. Blind Source Separation and Independent Component Analysis: A Review. *Neural Information Processing - Letters and Reviews*, 6(1), January 2005.

[42] A.Sergio , Cruces-Alvarez, Andrzej Cichocki, Shun-Ichi Amari. On a New Blind Signal Extraction Algorithm: Different Criteria and Stability Analysis. *IEEE Signal Processing Letters*, 9(8):233–236, August 2002.

[43] Seungjin Choi, Andrzej Cichocki, Adel Beloucharni. Second Order Nonstationary Source Separation. *Journal of VLSI Signal Processing*, pages 1–13.

[44] Yan Li, David Powers , James Peach. Comparison of blind source separation algorithms. *Advances in Neural Networks and Applications*, 1:18–21, 2000.

[45] Abdelhamid Mekaoui, El-Mehdi Hamzaoui, Rajaa Cherkaoui El Moursli. Blind Source Separation of HPGe Output Signals: A New Pulse Pile-up Correction Method. *Adv. Studies in Theoretical. Physics*, 8(16):681–688, 2014.

[46] Ali Mansour, Mitsuru Kawamoto , Noboru Ohnishi. A Survey of the Performance Indexes of ICA Algorithms. In *International Conference Modeling, Identification, and Control*, 2002.

[47] J. F. Cardoso and Antoine Souloumiac. Blind beamforming for non gaussian signals. *Journal of IEEE Proceedings-F*, 140(6):362–370, 1993.

[48] M. Gaeta and J.L. Lacoume. Source separation without prior knowledge: the maximum likelihood solution. In *EUSIPCO90*, pages 621–624, 1990.

[49] D.-T. Pham and P Garrat. Blind separation of mixtures of independent sources through a quasi-maximum likelihood approach. *IEEE Transaction on Signal Processing*, 45(7):1712–1725, 1997.

[50] A. J. Bell and T. J. Sejnowski. An information maximization approach to blind separation and blind deconvolution. *Neural Computation*, 7:1129–1159, 1995.

[51] C. Douglas, A. Cichocki, H. H. Yang S.Amari, S. Multichannel blind deconvolution and equalization using the natural gradient. In *IEEE International Workshop on Wireless Communication, Paris*, pages 101–104. IEEE, 1997.

[52] Andrzej Cichocki and Shun ichi Amari. Adaptive blind signal and image processing. John Wiley, Chichester, UK, 2003.

[53] J. F. Cardoso and B. H. Laheld. Equivariant adaptive source separation. *Transactions on Signal Processing*, 44(12):3017–3030, 1996.

[54] A. Mansour, N. Ohnishi and C. G. Puntonet. Blind multiuser separation of instantaneous mixture algorithm based on geometric concepts. *Signal Processing*, 82:1155–1175, 2002.

[55] Adel Belouchrani, Karim Abed-Meraim, Jean-Francois Cardoso and Eric Moulines. A blind source separation technique using second-order statistics. *IEEE Transactions On Signal Processing*, 45(2):434–444, February 1997.

[56] S. Choi and A. Cichocki. Blind separation of nonstationary sources in noisy mixtures. *Electronics Letters*, 36:848–849, 2000.

[57] Kenneth Ball, Nima Bigdely-Shamlo, Tim Mullen, Kay Robbins. PWC-ICA: A Method for Stationary Ordered Blind Source Separation with Application to EEG . *Computational Intelligence and Neuroscience*, Article ID 9754813:1–20, 2016.

[58] Ganesh R. Naik and Dinesh K Kumar. An overview of independent component analysis and its applications. *Informatica 35*, pages 63–81, 2011.

[59] Edited by P. Comon and C. Jutten. In *Handbook of Blind Source Separation Independent Component Analysis and Applications*. Elsevier-ISBN: 978-0-12-374726-6, First edition 2010.

[60] Aapo Hyvarinen, Pavan Ramkumar, Lauri Parkkonen, Riitta Hari. Independent component analysis of short-time Fourier transforms for spontaneous EEG/MEG analysis. *Neuroimage*, 49(1):257–271, 2010.

[61] Scott C. Douglas, Hiroshi Sawada and Shoji Makino. A Spatio-Temporal Fastica Algorithm For Separating Convolutive Mixtures. In *ICASSP 2005*, pages 165–168. IEEE, 2005.

[62] M. Ungureanu, C. Bigan, R. Strungaru, V. Lazarescu. Independent Component Analysis Applied in Biomedical Signal Processing. *Measurement Science Review*, 4(2), 2004.

[63] Tzyy-Ping Jung, Scott Makeig, Te-Won Lee, Martin J. McKeown, Glen Brown , Anthony J. Bell , Terrence J. Sejnowski. Independent component analysis of biomedical signals. In *Proceedings of the 2nd International Workshop on Independent Component Analysis and Blind Signal Separation*, pages 633–644, 2000.

[64] Shwartz S., Zibulevsky M., Schechner Y.Y , Puntonet C.G.and Prieto A. (eds). ICA Using Kernel Entropy Estimation with N(logN) Complexity. In *Independent Component Analysis and Blind Signal Separation-Lecture Notes in Computer Science*. Springer, 2004.

[65] Hyvarinen, J. Karhunen and E. Oja. Independent component analysis:algorithms and applications. *Neural Network*, 13:411–430, May 2000.

[66] L. Tong, G. Xu and T. Kailath. Blind identification and equalization based on second-order statistics: A time domain approach. *IEEE Trans. Information Theory*, 40:340–349., 1994.

[67] R. Pan and C. L. Nikias. The complex cepstrum of higher order cumulants and nonminimum phase identification. *IEEE Transaction on Acoustics, Speech and Signal Processing*, 36:186–205, 1988.

[68] D. Hatzinakos and C. L. Nikias. Blind deconvolution using a tricepstrum based algorithm. *IEEE Trans. on Communication*, COM-39:669–682, 1991.

[69] D. N. Godard. Self-recovering equalization and carrier tracking in a two dimensional data communication systems. *IEEE Transaction on Communication*, 28:1867–1875, 1980.

[70] J. R. Treichler and B.G. Agee. A new approach to multipath correction of constant modulus signals. *IEEE Transaction on Acoustics, Speech and Signal Processing*, 31:459–471, 1983.

[71] Y. Sato. Two extensional applications of the zero-forcing equalization method. *IEEE transactions on Communication*, COM-23:684–687, 1975.

[72] J.-Y. Lee and A. K. Nandi. Extraction of impacting signals using blind deconvolution. *Journal of Sound and Vibration*, 232(5), 2000.

[73] V. Capdevielle, C. Servire and J L Lacoume. Blind separation of wide band sources: application to rotating machine signals. In *EUSIPCO96*, pages 2085–2088, 1996.

[74] Ye Hongxian, Li Wenchang, Hu Xiaoping. A blind source separation method for convolved mixtures by non-stationary vibration signals. *International Journal On Smart Sensing And Intelligent Systems*, 6(3):974–992, 2013.

[75] G.S Aglietti, Z. Zhang, G Richardson. Disturbance sources modeling for analysis of structure- borne micro-vibration. In *Thematic Conference on Computational Methods in Structural Dynamics and Earthquake Engineering*. Corfu, Greece, May 2011.

[76] Theodor D. Popescu. Blind separation of vibration signals and source change detection Application to machine monitoring. *Applied Mathematical Modelling*, 34:3408–3421, 2010.

[77] Peter W. Tse, J. Y. Zhang, X. J. Wang. Blind Source Separation and Blind Equalization Algorithms for Mechanical Signal Separation and Identification. *Journal of Vibration and Control*, 12(4):395–423, 2006.

[78] J. Antoni. Blind separation of vibration components: Principles and demonstrations. *Mechanical Systems and Signal Processing*, 19:1166–1180, 2005.

[79] J. D. Achenbach. In *Wave Propagation in Elastic Solids*. New York: Elsevier, 1984.

[80] I. A Viktorov. Rayleigh and Lamb Waves. In *Physical Theory and Applications*. Plenum Press, New York, 1967.

[81] B. Engdahl, R. Kind, P. Bormann(Ed.). Seismic wave propagation and earth models. In *New Manual of Seismological Observatory Practice 2 (NMSOP2)*. eo Forschungs Zentrum GFZ, 2012.

[82] Jack Dankowski. Vibration considerations when planning a facility. pages 1–18. Fabreeka International, United States of America, 2001.

[83] J. Cardona, J. Romeu, R. Arcos, A. Balastegui. A Ground-Borne Vibration Assessment Model For Rail Systems At-Grade. In *Internoise 2010*, pages 1–10. Lisbon, Portugal, 2010.

[84] Y B Yang, H H Hung. In *Wave Propagation For Train-Induced Vibrations - A Finite/Infinite Element Approach*. World Scientific Publishing Co., JUN 2009.

[85] Giuseppe Cabras, Roberto Carniel, Joachim Wassermann. Blind Source Separation: An Application to the Mt. Merapi Volcano . *Fluctuation and Noise Letters*, 4(3):249–260, 2008.

[86] Guy G. Drijkoningen, Frederik Rademakers, Evert C. Slob, Jacob T. Fokkema. A new elastic model for ground coupling of geophones with spikes. *Geophysics*, 71(2):9–17, March-April 2006.

[87] Michael L. Oelze, Jr.William D. Obrien and Robert G. Darmody. Measurement of Attenuation and Speed of Sound in Soils. *Soil Sci. Soc. Am. J*, 66:788–796, 2002.

[88] Hermann Brugger, Markus Falk. Analysis of Avalanche Safety Equipment for Backcountry Skiers . In *JAHRBUCH 2002*. Austrian Association for Alpine and High Altitude Medicine, 2002.

[89] Longbiao Wang, Kyohei Odani, Atsuhiko Kai. Dereverberation and denoising based on generalized spectral subtraction by multi-channel LMS algorithm using a small-scale microphone array . *Journal on Advances in Signal Processing*, 12:1–11, 2012.

[90] Seiichi Nakagawa Longbiao Wang, Kyohei Odani, Atsuhiko Kai, Norihide Kitaoka. Dereverberation Based on Spectral Subtraction by Multi-Channel LMS Algorithm for Hands-Free Speech Recognition. *Modern Speech Recognition Approaches with Case Studies*, pages 155–174, 2012.

[91] Saeed V. Vaseghi. Spectral subtraction. In *Advanced Digital Signal Processing and Noise Reduction*. ISBNs: 0-471-62692-9 (Hardback): Second Edition. John Wiley and Sons Ltd, 2000.

[92] Sameer Pawar and Kannan Ramchandran. A robust R-FFAST framework for computing a k-sparse n-length DFT in O(k log n) sample complexity using sparse-graph codes. In *2014 IEEE International Symposium on Information Theory*, 2014.

[93] Shoji Makino, Shoko Araki, Ryo Mukai and Hiroshi Sawada. Audio source separation based on independent component analysis. In *ISCAS 2004*, pages 668–671, 2004.

[94] A. Hyvarinen et al. In *Independent Component Analysis*. John Wiley Sons, New York, 2001.

[95] S.Haykin and Z.Chen. The cocktail party problem. *Neural Computation*, 17:1875–1902, Sep 2005.

[96] Krishna Kumar M, Pramod K V, Geethu R S. Source separation of heartbeat sounds. *MES Journal of Technolgy and Management*, 2:65–71.

[97] Geethu R.S., Sudheesh N.George., Krishna Kumar M. A Proposal for Source Separation of Heartbeat Sounds and Its FPGA Implementation. In *IEEE International Conference on Communication Systems and Network Technologies*, pages 755–758. IEEE, 2012.

[98] Petr Tichavsk, Zbynek Koldovsk and Erkki Oja. Performance Analysis of the FastICA Algorithm and CramrRao Bounds for Linear Independent Component Analysis. *IEEE Transaction on Signal Processing*, 54(4):1189–1198, 2006.

[99] Sarit Shawartz, Michael Zibulevsky, Yoav Y. Schechner. ICA using Kernel entropy estimation with NlogN complexity. In *ICA2004*, pages 422–429. Springer-Verlag, 2004.

[100] Petr Tichavsky, Eran Doron, Arie Yeredor, Jan Nieleson. A computationally affordable implementation of an asymptotically optimal BSS algorithm for AR sources. In *14th European Signal Processing Conference (EUSIPCO 2006)*, pages 4–8, 2006.

[101] Sahar Seifzadeh, Karim Faez, Mahmood Amiri, Mohammad Rezaei. Evaluation of less Common Independent Component Analysis Algorithms for Brain Computer Interface Preprocessing. *IJMEC*, 5(17):2424–2432, 2015.

[102] Dave Davis. Review of Prediction Methods for Ground-Borne Noise due to Construction Activities. In *Proceedings of 20th International Congress on Acoustics, ICA 2010*, pages 23–27. Sydney, Australia, August 2010.

[103] R.D Woods. Screening of surface waves in soils. *J. Soil Mech and Found. Div*, 94(SM 4):951–979, 1968.

[104] Hugh E. M. Hunt, Mohammed F, M. Hussein Edited by Malcolm J. Crocker. Ground-borne vibration transmission from road and rail systems: Prediction and control. In *Handbook of Noise and Vibration Control*, pages 1458–1469. John Wiley Sons, Inc, 2007.

[105] M.A. Biot. Theory of propagation of elastic waves in a fluid saturated porous solid I Low-frequency range. *J. Acoust. Soc. Am*, 28:168–178, 1956a.

[106] M.A. Biot. Theory of propagation of elastic waves in a fluid saturated porous solid II High-frequency range. *J. Acoust. Soc. Am*, 28:168–178, 1956b.

[107] G.F. Miller and H.Pursey. On the partition of energy between elastic waves in semi-infinite solids. volume 203–Series A, pages 56–69, 1955.

[108] Shuji Tamara. Camparison of body and Rayleigh wave displacements generated by a vertical point force on a layered elastic medium. In *Eleventh world conference on earthquake engineering*, pages 1–8. Elsevier Science Ltd., 1996.

[109] G.F.Weissmann and R.R. Hart. Damping Capacity of Some Granular Soils. Number 305, pages 45–54. ASTM STP, 1961.

[110] Mehdi Bahrekazemi. In *Train-Induced ground Vibration and its prediction*. PhD Thesis, Royal Institute of Technology, 2004.

[111] Chiong Ching Lai, Sven Erik Nordholm, Yee Hong Leung. In *A Study into the Design of Steerable Microphone Arrays*, pages 7–17. Springer, 2017.

[112] E Doron, A Yeredor P Tichavsk, Z Koldovsk and G Gmez-Herrero. Blind signal separation by combining two ICA algorithms: HOS-based EFICA and time structure-based WASOBI. In *Signal Processing Conference*, pages 1–5, 2006.

[113] T. Chen S. Amari and A. Cichocki. Non-holonomic constraints in learning blind source separation. *Progress in Connectionist-Based Information Systems, Eds. N. Kasabov, ICONIP-97*, pages 633–636, 1997.

[114] Linda Mthembu and Tshilidzi marwala. A note on the separability index. University of the Witwatersrand, Johannesburg.

[115] Andrew Walsh. Application of supervised and unsupervised learning to analysis of the arterial pressure pulse. In *PhD thesis*. Graduate School of Biomedical Engineering University of New South Wales, 2006.

[116] Enders A. Robinson. Seismic time-invariant convolutional model. *Geophysics*, 50(12):2742–2751, 1985.

[117] John P Wolf. Foundation Vibration analysis using simple physical model . In *ISBN 0-13-010711-5*. Prentice Hall, 1994.

[118] Guang-Yuan Gao, Jian Song, Un yang. Identifying boundary between near field and far field in ground vibration caused by surface loading. *Journal of Central South University*, 21(8):3284–3294, 2014.

[119] Raoul Saggini. In *The Mechanical Vibration; Therapeutic Effects and Applications*, pages 109–111. Bentham books, 2017.

[120] A. Jin, Q., T.Schultz , Waibel. Far-field speaker recognition . *IEEE Transations on Audio, Speech, and Language Processing*, 15:2023–2032, 2007.

[121] Dong-Soo Kim, Jin-Sun Lee. Propagation and attenuation characteristics of various ground vibrations. *Soil Dynamics and Earthquake Engineering*, 19:115–126, 2000.

[122] Jones and Stokes. In *Transportation- and construction-induced vibration guidance manual*. California Department of Transportation, Noise, Vibration, and Hazardous, 2004.

[123] Davis Gray and Ralph Jones. In *The Sound Reinforcement Handbook*. Yamaha International Corporation, 1989.

[124] Iain Fergusson: https://iainisbald.wordpress.com.

[125] Saeed V. Vaseghi. In *SPECTRAL SUBTRACTION, Advanced Digital Signal Processing and Noise Reduction*, pages 334–354. 2nd ed.,John Wiley Sons Ltd, 2000.

[126] K. Lebart, J. M. Boucher, P.N. Denbigh. A new method based on spectral subtraction for speech dereverbration. *Acoustica*, 87:359–366, 2001.

[127] Sameer Pawar, Kannan Ramachandran. FFAST: An Algorithm for Computing an Exactly k-Sparse DFT in O(k log k) Time. *IEEE Trans. Information Theory*, 64(1):429–450, 2017.

[128] Emmanuel Vincent, Remi Gribonval, Cedric Fevotte. Performance measurement in blind audio source separation. *IEEE Transaction on Audio, Speech, and Language Processing*, 14(4):1462–1469, 2006.

[129] Yan Li, David Powers, James Peach. Comparison of blind source separation algorithms. In *Advances in Neural Networks and Applications*, pages 18–21. Mastorakis, 2000.

[130] Petr Tichavsky, Zbynek Koldovsky, Arie Yeredor, German Gomez-Herrero, Eran Doron. A Hybrid Technique for Blind Separation of Non-Gaussian and Time-Correlated Sources Using a Multicomponent Approach. *IEEE Transaction on Neural Networks*, 19:421431, 2008.

[131] D.H. Griffiths and R.F. King. In *Applied Geophysics for geologists and Engineers-The Element of Geophysical Prospecting*. Pergamon press, 1981.

[132] Philip Kearey, Michael Brooks, Ian Hill. In *An Introduction to Geophysical Exploration*, volume 3 ed. Black Well Science, 2002.

[133] EO-Miners Project; www.eo-miners.eu.

[134] Data Sheet of MiniSense 100 Vibration Sensor.

[135] R.N. Iyenegar. In *Elements of Mechanical Vibration*. I.K. International Publishing House, 2010.

[136] Data Sheet of Linear Technology LTC 624X CMOS OP amp.

[137] Data sheet of MAYA44 USB External card.

[138] Siwek, T. Tanaka, Anh Huy Phan A. Cichocki, S. Amari, K and R. Zdunek. ICALAB MATLAB Toolbox Ver. 3 for signal processing.

[139] Geethu R S, Krishna Kumar M, Sudhish N George. A Proposal for source separation of low level vibration signals and its FPGA Implementation. In *IEEE International Conference on VLSI Systems, Architecture, Technology and Applications (VLSI-SATA 2015)*. IEEE, 2015.

[140] Krishna Kumar M., Geethu R.S , Pramod K. V. Performance of Source Separation Algorithm on Ground Borne Low Level Vibration Signals. *Hydel Journal*, 60(1):48–54, 2014.

[141] Krishna Kumar M., Geethu R S, Pramod K V. Source separation of ground borne low level vibration signals using statistical methods. In *International Conference on Advances in Computing, Communication and Information Science*, pages 389–403. Elsevier Publications, 2014.

[142] L Tom Hsiung. Perspectives on Hematology, Health Care, and The Profession of Pharmacy. 2016.

[143] B Bates. The cardiovascular system. In *A Guide to Physical Examination and History Taking, 9 ed.* 2005.

Index